HYDRAULICS AND GEOLOGY RELATED TO BEACH RESTORATION IN LEE COUNTY, FL.

july 1981

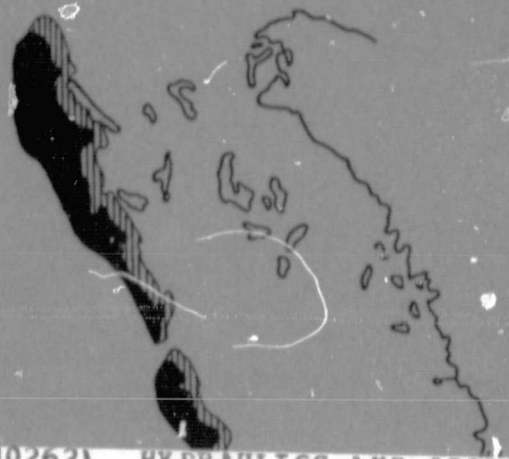

Trevor Winton
H. Kelly Brooks
Janet Degner
Byron Ruth

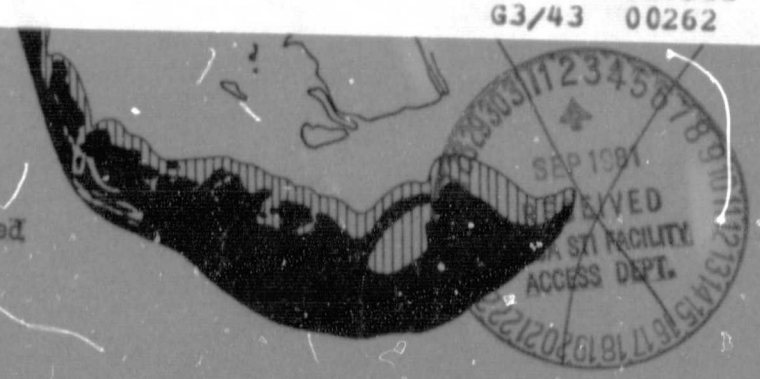

Remote Sensing Applications Laboratory
Department of Civil Engineering
University of Florida, Gainesville, Florida

July 1981

HYDRAULICS AND GEOLOGY RELATED TO BEACH RESTORATION IN LEE COUNTY, FLORIDA

Trevor Winton
H. Kelly Brooks
Janet Degner
Byron Ruth

Remote Sensing Applications Laboratory
Department of Civil Engineering
University of Florida, Gainesville, Florida

ACKNOWLEDGEMENT

This study was conducted under the sponsorship of the National Aeronautics and Space Administration. Their support is gratefully acknowledged.

Thanks is extended to the members of the Captiva Erosion Prevention District and commissioners of Captiva Island who provided the initial impetus for this study.

Sincere thanks goes to Dexter Bender and his associates, Hans Wilson and Mark Chiappino for providing information, equipment and assistance throughout the study.

Thanks is also extended to the Department of Coastal and Oceanographic Engineering for their help and use of their equipment.

The Remote Sensing Applications Laboratory would also like to thank the people of Captiva for their hospitality and cooperation.

TABLE OF CONTENTS

LIST OF FIGURES

APPENDIX FIGURES

CHAPTER I

INTRODUCTION
1.1 Background

Captiva Island is part of a barrier island chain that has historically been the most dynamic and changeable segment of the Florida coastline. The island has genetic and hydrodynamic relationships to the adjacent youthful islands, to the Gulf of Mexico, and to Pine Island Sound. This report is based upon technical studies made to establish the interrelationship in this segment of the coastal system. The findings are being submitted to the board members of the Captiva Erosion Prevention District to help in the formulation of a sand conservation and beach management program.

Captiva Island is one of four islands in the Lee County barrier chain. This chain extends for some thirty miles along Florida's southwest coast. These islands: Cayo Costa (La Costa), North Captiva, Captiva and Sanibel are the seaward boundary of Pine Island Sound. (Figure 1.1) A large inlet, Boca Grand Pass, isolates the barriers and the associated littoral drift system in the surf zone at the northern extremity and San Carlos Bay separates Sanibel Island from the mainland at the southeastern end. The chain is unusual in that the three northern islands face the Gulf of Mexico, whereas Sanibel arches eastward. The directional trend of the northern islands is about 18° west of north. The eastern extremity of the beach at Sanibel trends to the northeast.

It is not adequate to simply recognize that Captiva Island has experienced severe shoreline retreat. This has long been an established fact. The extent of the erosion up to 1978-79 is illustrated in Figure 1.2. The northern portion of Captiva Island experienced a shoreline retreat of over 700 feet between 1888 and 1944. Adjustments are still taking place. Some are seasonal and cyclic, others are trends established over longer periods of time.

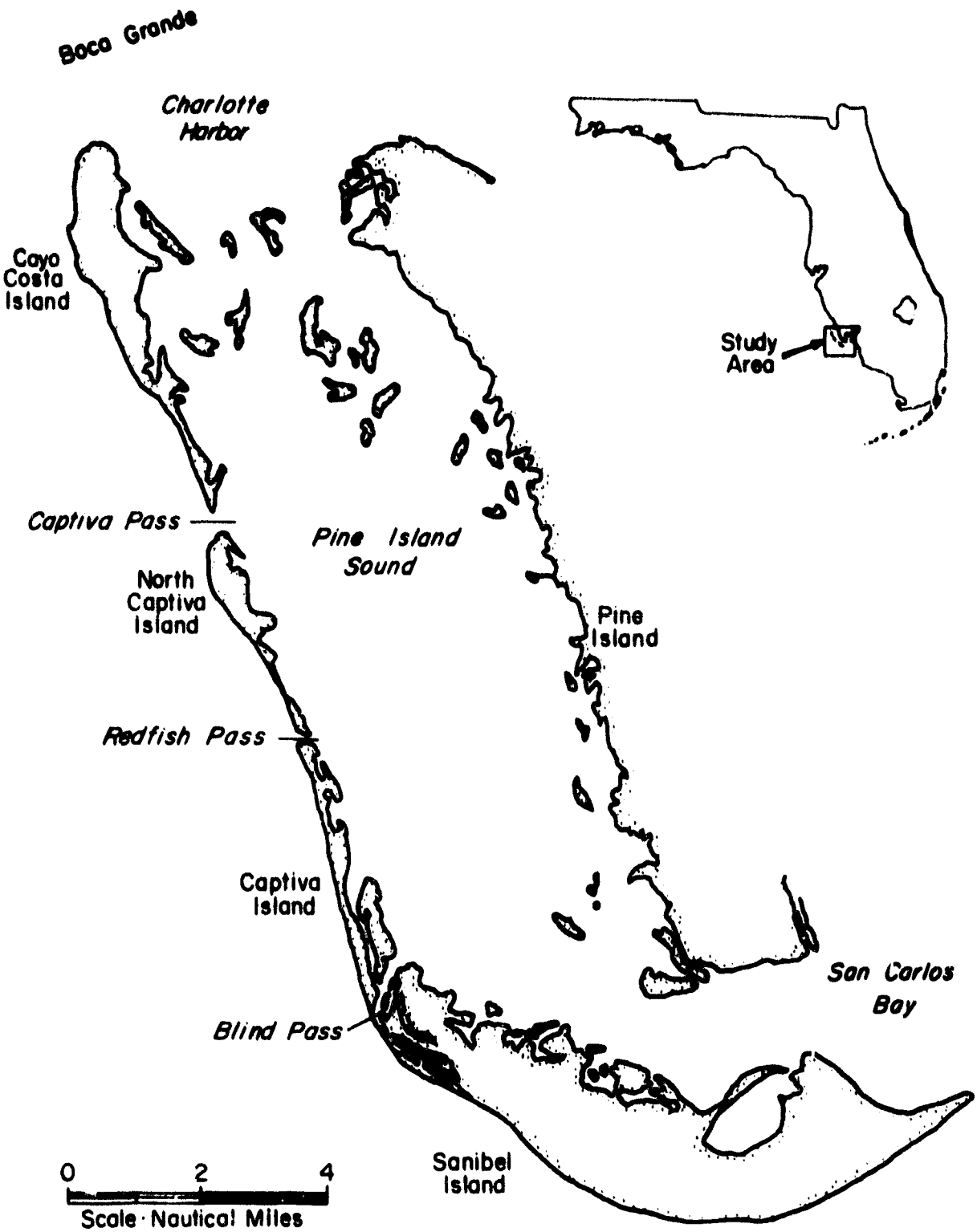

Figure I.1 Location Map of Study Area

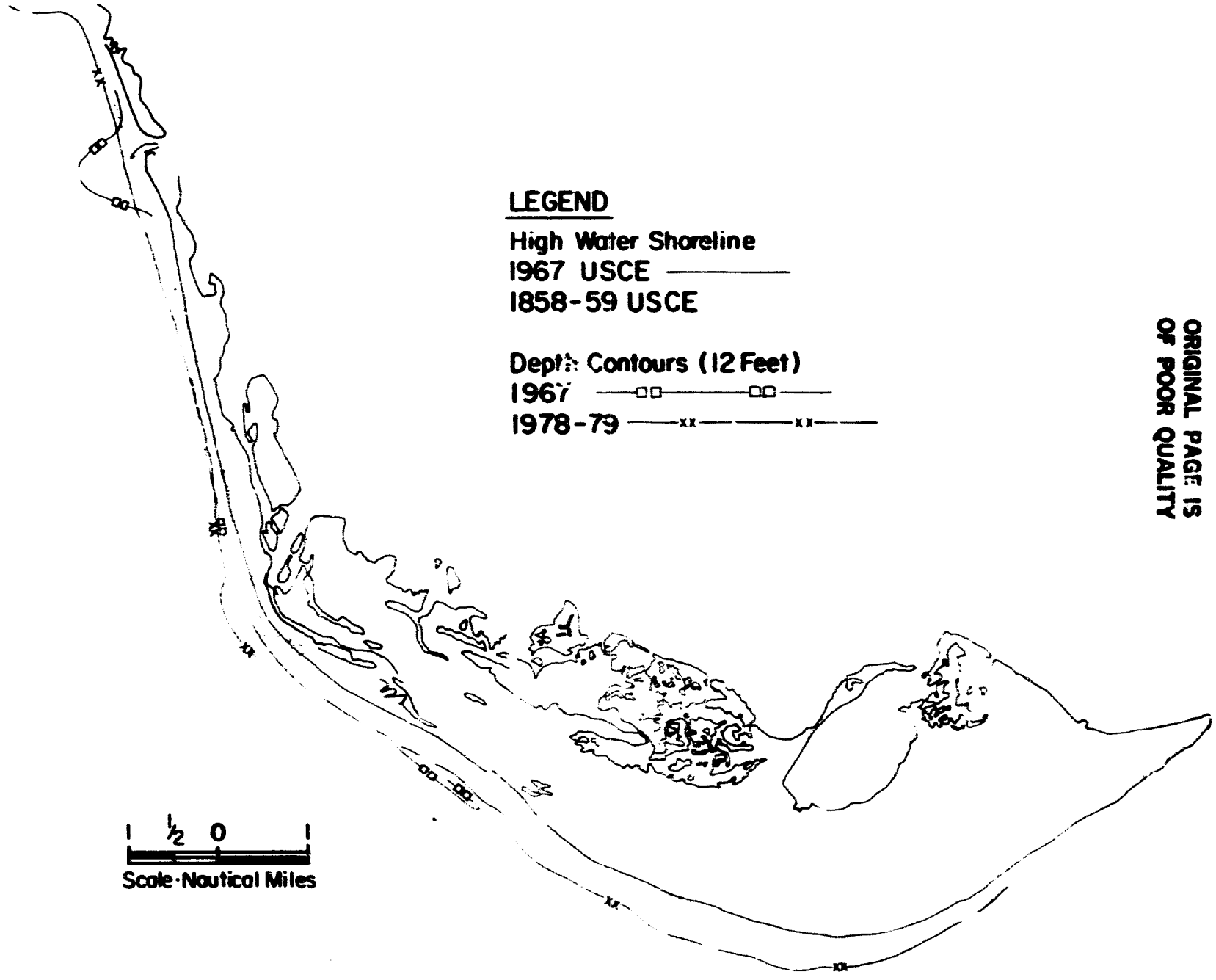

ORIGINAL PAGE IS
OF POOR QUALITY

Figure 1.2 Evolution of Northern Lee County Shoreline (U.S. Army Corps of Engineers)

Since the inception in 1958 of the Captiva Erosion Prevention District, the commissioners have been aware that the ultimate solution to the erosion problems would be an artificial beach restoration project. The history of failures in the attempts to use less expensive, local static structures is comprehensively reviewed in a report prepared in 1971 (C.E.P.C., 1971).

The erosion problem on Captiva Island is due to a deficit in the sand budget of the littoral drift system; a system with losses due to attrition of the particles and mass losses into the lagoons, to offshore, and to lateral transport. The U.S. Army Corps of Engineers (1969) estimated that 100,000 cubic yards of sand are eroded from the beach system of Captiva Island each year. The Coastal and Oceanographic Engineering Laboratory (C.O.E.), (1974, p. 85) estimated that the annual losses by southeastward transport past Blind Pass is 115,000 cubic yards per year. Silberman, 1980, documented that the beach of Sanibel Island does not receive all of the sand carried southward from Captiva. Approximately 4.548×10^6 cubic yards (3.477×10^6 cubic meters) is unaccounted for, and since Blind Pass is now closed, "This amount of sediment must have moved offshore."

Field experiments conducted by C.O.E. (1974, p. 50) have shown that there is a northward flow of the water in the swash channel at the surf zone at the northern end of Captiva and that this littoral current is extremely strong during rising tide. Water and sediment are being fed into the strong tidal current in Redfish Pass. Sand losses from the northern beach at Captiva are largely lost to the inner and outer tidal shoals. This is estimated by C.O.E. (1974, p. 88) to be 85,000 cubic yards annually. The tremendous accumulations of sand at Redfish Pass (Figure 1.2) since its origin in 1926 have come about at the expense of erosion of both North Captiva and Captiva islands.

It was with these facts in mind, and full knowledge that the limited attempts in beach nourishment in 1962 (7,000 cu. yds.), 1963 (50,000 cu. yds.) and 1965 (50,000 cu. yds.) were ineffective, that this study was undertaken. Of special concern was the effect that reopening Blind Pass would have, and the placement of sediment retaining structures in the surf zone at the northern and southern limits of the Captiva beach system.

The problem was approached from a different prospective than previous studies. A study of the geology of the islands has contributed to knowledge of the origin and dynamic changes that have occurred, and through hydraulic modeling we have been able to predict changes that will occur by reopening and stabilization of Blind Pass. The information we have developed is supportive of the previous work of the U.S. Army Corps of Engineers and the Coastal and Oceanographic Engineering Laboratory.

Our conclusions are, that, if the island is to be stabilized, beach nourishment with proper amounts and particle size is a necessity and that jetties adequate to restrict lateral and offshore losses are essential. Hydrologic modeling showed that reopening Blind Pass would have minimal effects on the passes to the north and south. The increased interchange and improved flushing of water in Pine Island Sound, brought about by reopening Blind Pass, would improve the environmental conditions in the sound with no adverse effects on the beach system. Stabilization of Blind Pass would slow the accretion of Sanibel Island and some adjustments in the vicinity of the reopened, stabilized pass would occur.

1.2 The Geologic History of the Islands

Without going into technical detail, the ensuing discussion presents the dynamic history of the Lee County barrier islands. Because the four islands

have been largely isolated from lateral coastal sources of sand and from adjacent littoral drift systems, they ideally serve as a model to test the hypotheses for the origin of barrier islands. Barrier island formation resulting from onshore sediment transport was discussed by de Beaumont (1845), Johnson (1918) and Shepard (1960) while lateral transport was studied by Gilbert (1885) and engulfment by Hoyt (1967).

Missimer (1973), Brooks (1973) and Riggs (1976) concluded that the Lee County chain originated at a time of rising sea level due to onshore transportation of sediment, as Shepard (1960) proposed for the barrier islands of the Texas Gulf coast. There is no doubt that Sanibel has also benefited from the littoral drift system, as proposed by Gilbert.

Throughout its history, Sanibel Island has been different. Sanibel has been a place of persistent deposition, as shown by the accreted beach ridge sets. It has gained mass, not only from onshore transportation of quartz sand and sea shells, but also it has been the predominant repository of the sediment in the prevailing southward littoral drift system. Sanibel is larger, broader and much more stable than the other islands. It is also the only island in the Lee County barrier chain that has previously received adequate geologic study (Missimer, 1973; Riggs, 1976; and Silberman, 1980).

Brooks (1973) emphasized that 30 to 50 percent of the compositional mass of the Lee County barriers above sea level is sea shells. No doubt that this component of the sediment was derived from an offshore source. A study of the heavy minerals associated with the clastic quartz sand proves it also had an offshore source (Ceryak, 1980).

The impression obtained from the known erosional characteristics of the beaches during the 1940 and 1950's suggests that a rising sea level results in accelerated erosion (per Brunn, 1962). It could be that both of the Captiva

islands are experiencing adjustment in relationship to the 1926 opening of Redfish Pass. It is possible that the known accelerated rise in mean sea level during the 1940's and 50's contributed to the rapidity of the adjustment. No doubt, the slow aging and final demise of Blind Pass (Figure 1.3) during the last few centuries has contributed to sediment bypassing and the recent rapid growth of Sanibel Island.

It could also be true that in the history of the Gulf coast barrier islands, after the offshore source of sediment above surf base is depleted by onshore transport, that the same wave system responsible for building the barrier islands then destroys them. We do not pretend to predict the future but we all should be aware that Pleistocene barrier island systems have been preserved and constitute the formations of the Atlantic side of peninsular Florida. No such relics are preserved on the Gulf side. If past history is of value in predicting the future, the reader is free to speculate on the ultimate fate of the Lee County barrier islands.

Assuming that the reader is only marginally interested in theory and in the long range speculation of future events, we will discuss the greater, more immediate concern: the facts relating to the history of change of the Lee County barriers. The origin and evolution of this real estate can be determined by studying the sediments, their composition, internal structures, and mass relationships.

The relative chronological relationship of the depositional events on each island can be readily interpreted by study of aerial photographs. The establishment of the time of origin of the delineated beach ridge sets (in years) can then be established by radiometric dating of the unstable Carbon 14, which is a component of the sea shells ($CaCO_3$).

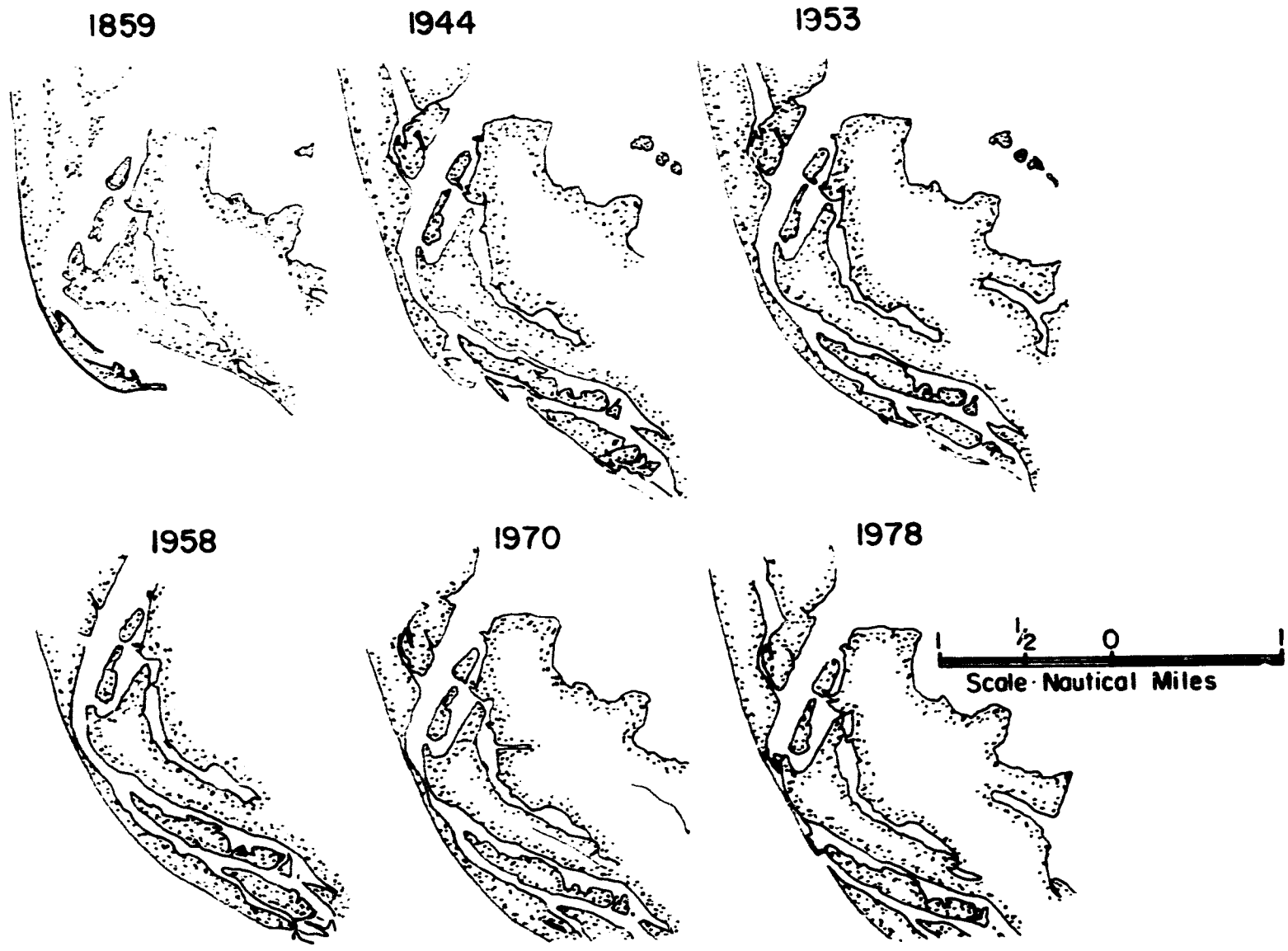

Figure 13 Changes in Blind Pass between 1859 and 1978.

There are problems in using sea shells for dating purposes because of the possibility of reworking. The radiometric dates herein reported,(Appendix A) were on shells that were very carefully selected for freshness, and exhibited no signs of alteration and abrasion. Only species living in the aeriated surf zone and the immediate offshore zone were included in the samples submitted to Geochron Laboratories for analysis.

The use of aerial photographs to show the relationships of the beach ridge sets is essential in establishing the accretionary history of the islands. Remote sensing techniques furnish productive and reliable results.

The accretionary history of the islands is evident by the patterns of the increments displayed on the aerial photographic mosaics presented in Figures 1.4 and 1.5 . Note that the Pine Island Sound side of all the islands, and especially Cayo Costa and Sanibel, are more densely vegetated. Also note that beach ridge sets can be seen within and underlying mangroves on the sound side of Sanibel Island.

The fact that the terrestrial vegetation cover on barrier islands evolves, and that there is a succession with antiquity, has long been a recognized fact. Herwitz (1977), a botanist, recently interpreted the geological history of Cayo Costa Island on vegetative criteria alone. This is a dangerous practice. The only way to establish detailed chronological relationship of beach ridge sets is to dig pits and thereby obtain data on the sediment. These data provide the basis for interpreting the genesis of the sedimentary masses.

A few well placed test pits were dug by H. K. Brooks at sites selected after the study of aerial photographs; the aerial photographs and the test pits have provided the data upon which this report is based.

Figure 1.4 Aerial Photo Mosaic of Cayo Costa Island and North Captiva Island (ASCS photography, 1944)

Figure 1.5 Aerial Photo Mosaic of Captiva Island and Sanibel Island (ASCS photography, 1944)

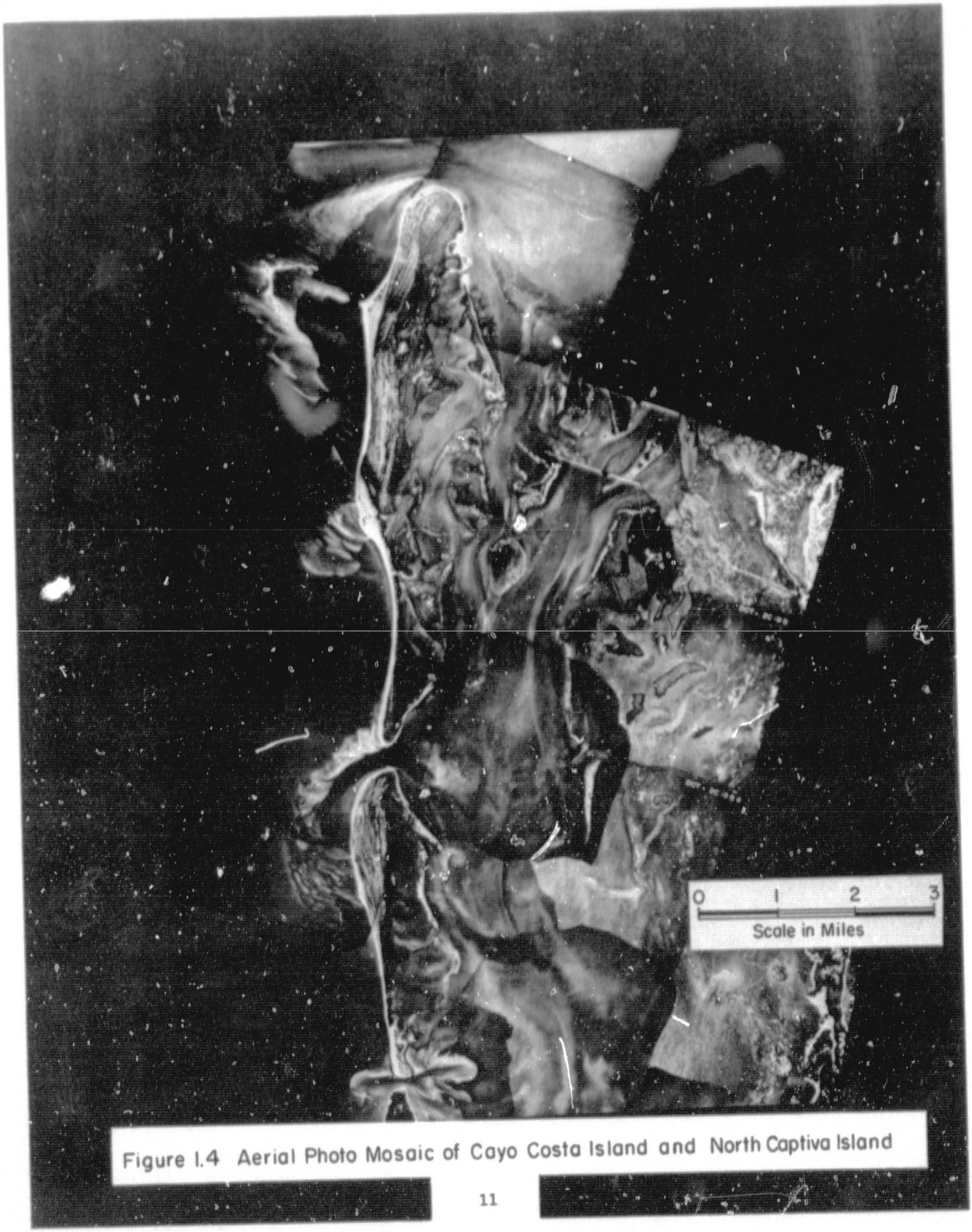

Figure I.4 Aerial Photo Mosaic of Cayo Costa Island and North Captiva Island

Figure 1.5 Aerial Photo Mosaic of Captiva Island and Sanibel Island

The "absolute" chronology in "Carbon 14 years" is based upon radiometric analysis. Missimer (1973) established the geologic history of Sanibel Island in a similar manner. Our results confirm the previous interpretation of the depositional history of Sanibel Island with few minor changes. Most significantly, we now have proof that the Captiva islands have been the site of shifting sands and that no subaerial portion of them is of great antiquity.

The shell content and texture of the beach ridges constituting the upland portions of the islands are different than that on the present low energy fore beach and back beaches, especially for the three islands facing the Gulf of Mexico. There is a general increase in the elevation of the upland ridges from the Pine Island Sound side to the Gulf side on all of the islands. This is correlated to the general rise in sea level during the accretionary history.

The highest ridges are located back of the present beach system and rise to an elevation of eight feet plus on the three northern islands. Again, Sanibel is different with the highest being at the northern end near Wulfert. Here, elevations of ten feet occur. The central and eastern portions of Sanibel form a basin. The highest ridges are four to five feet high and are immediately landward of the active beach system.

The internal sedimentary structure of the upland ridges are those produced by runup and overtopping. The higher the ridge, the coarser the texture. The greater the shell content in any particular set of ridges is the correlation proving a surf energy relationship. Missimer (1973) interpreted the variation in ridge set height as due to fluctuation of sea level superimposed upon the acknowledged worldwide rising trend.

The fact that contemporaneous ridges in the central and southern portions of Sanibel do not show a corresponding increase in height demonstrates that his (Missimer, 1973) hypothesis of higher sea level intervals cannot be the

controlling factor. Because of the consistent correlation of height, texture, and shell content, we believe that the changes in the surf energy environment, reflected by the depositional history, is predominently due to weather changes. The high surf energy, run up, and overtopping that produced the ridges represent periods of storminess in the Gulf of Mexico. In evaluating the stormy episode hypothesis, one should keep in mind that the predicted 50 year storm tide for Captiva Island is plus 12 feet.

The chronology of events recorded in the sediments of the four barrier islands was established by 32 radiocarbon dates taken from test pits dug to or below ground water level. Location of these samples, those taken by Missimer (1973), and Stapor and Mathews (1980) appear on Figures 1.6 and 1.7. These figures also illustrate the beach ridge patterns visible on the aerial mosaics. Some of the samples were from paleo beach face deposits and other from overwash. These and pertinent C 14 dates obtained by Missimer, Stapor and Mathews have been utilized in the preparation of the map showing the ages of the beach ridge sets (Figures 1.8 and 1.9).

Though the island chain arose sometime before 4,000 years ago, Sanibel is the only island to retain a relatively unchanged relic of the original emerged island. The fact that this beach ridge set is now submerged and underlies a mangrove forest is proof that sea level has risen. These ancient deposits of sand and shell have all the characteristics of beach ridges. The islands, as a barrier chain, appear to have emerged from the sea by the building up of a linear offshore shoal. All of the test boring sites of which we are aware, both onshore and offshore, prove that the islands were constructed upon 15 to 20 feet of silty, clayey sand with some shell; the same type of deposit that now exists in the offshore sedimentary environment.

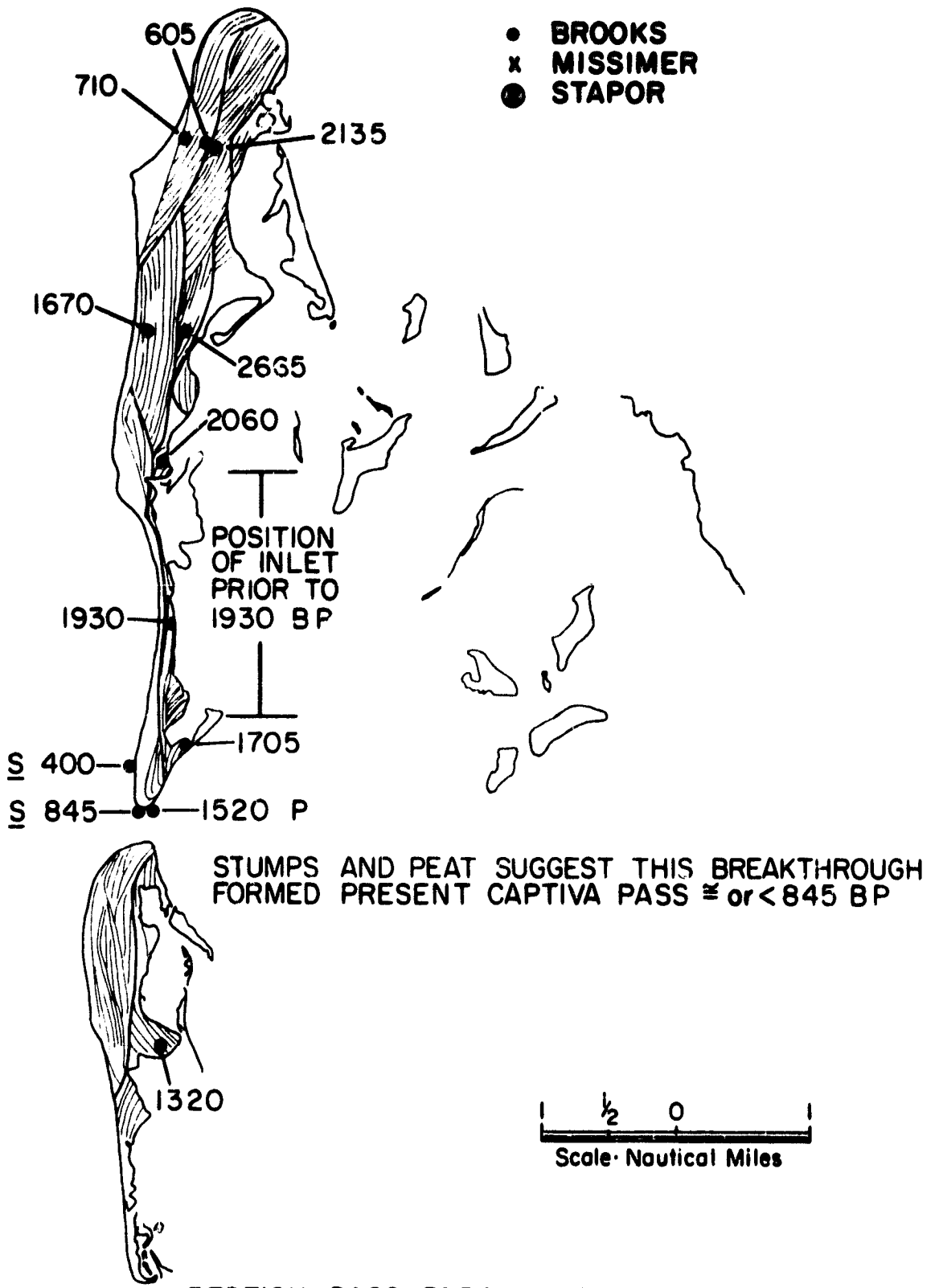

Figure 1.6 Beach Ridge Sets with Carbon 14 Sample Location and Dates for Cayo Costa Island and North Captiva Island

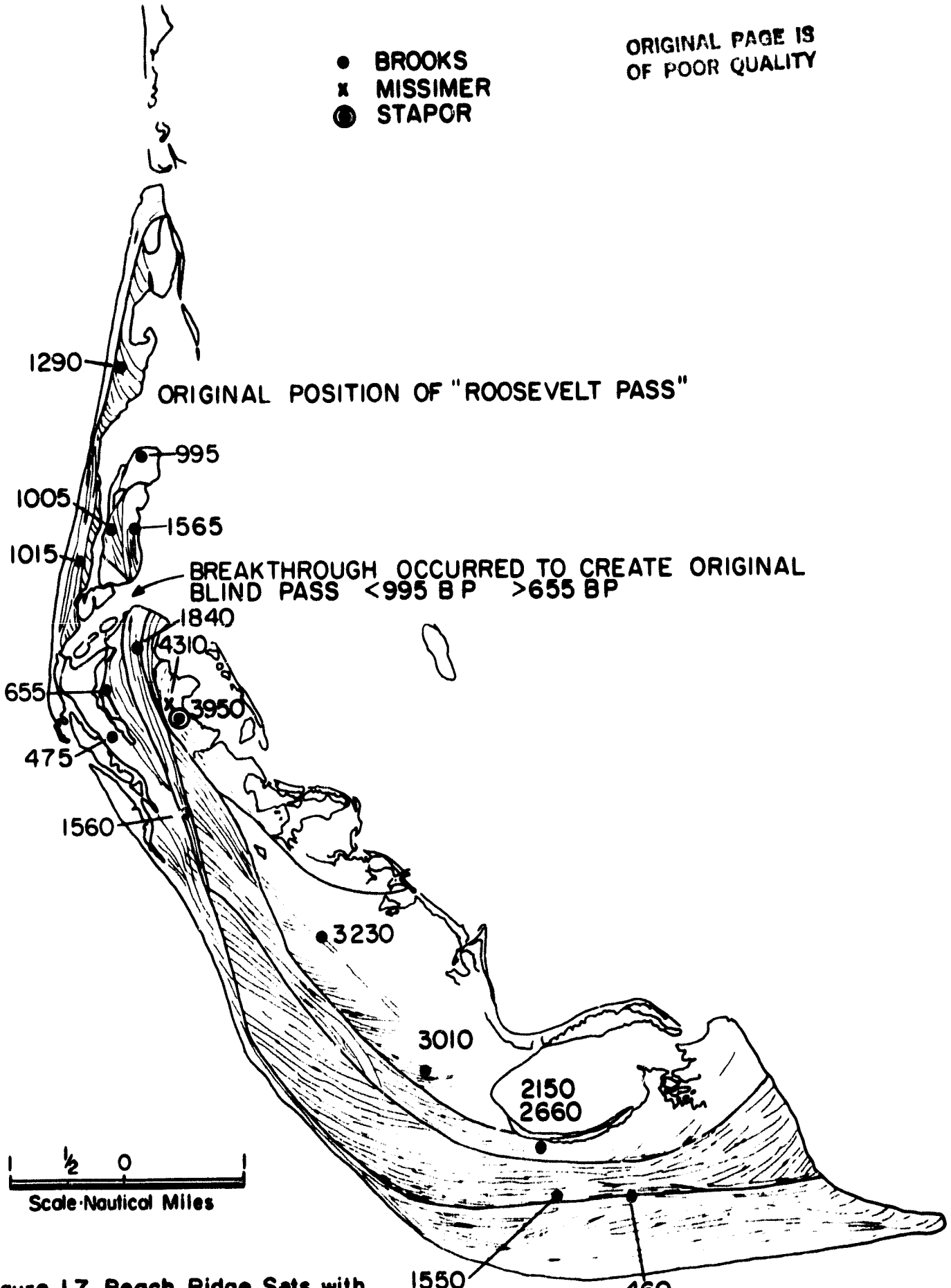

Figure 1.7 Beach Ridge Sets with Carbon 14 Sample Location and Dates for Captiva Island and Sanibel Island

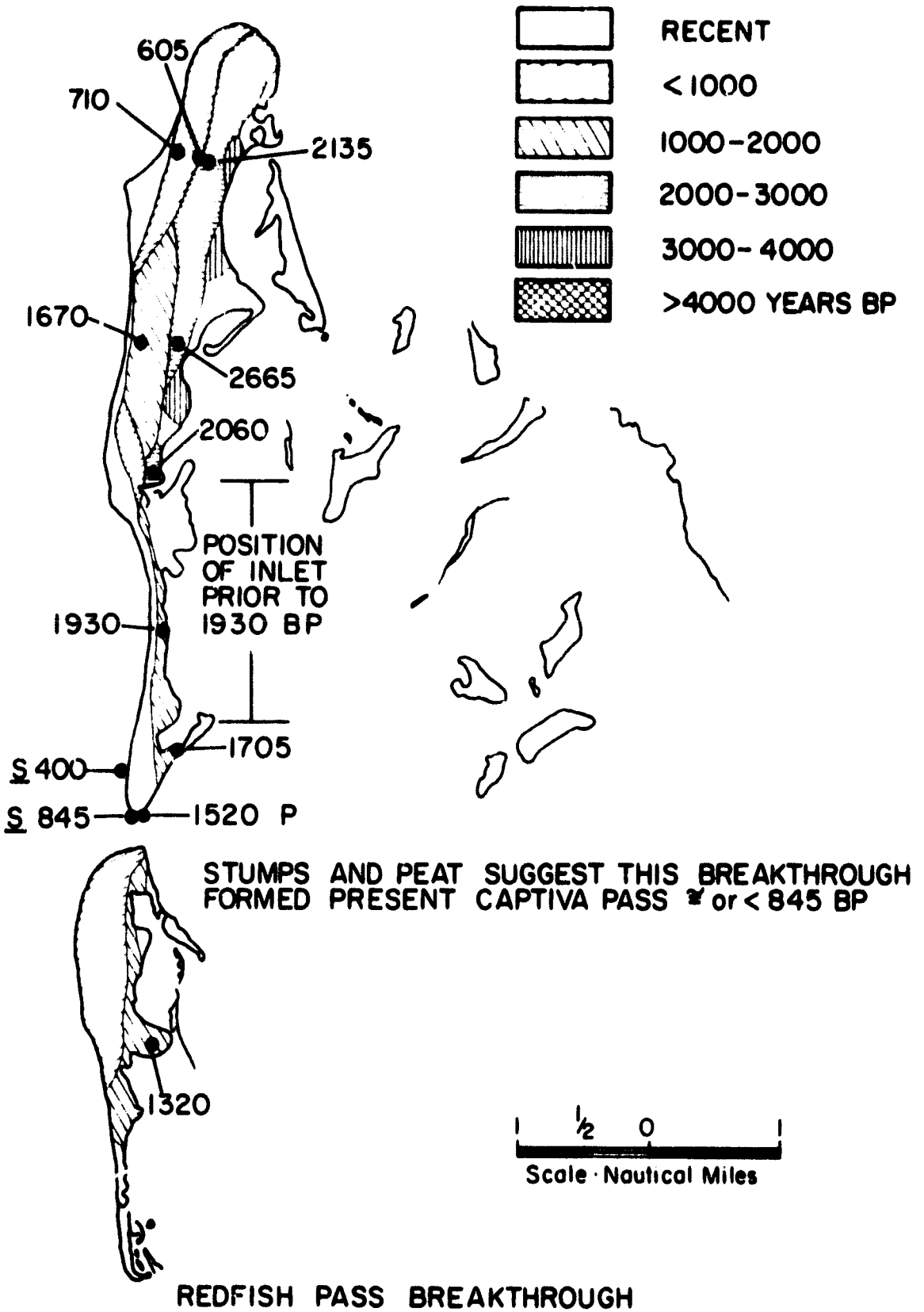

Figure 1.8 Ages of Beach Ridge Sets with Sample Locations and Dates for Cayo Costa Island and North Captiva Island

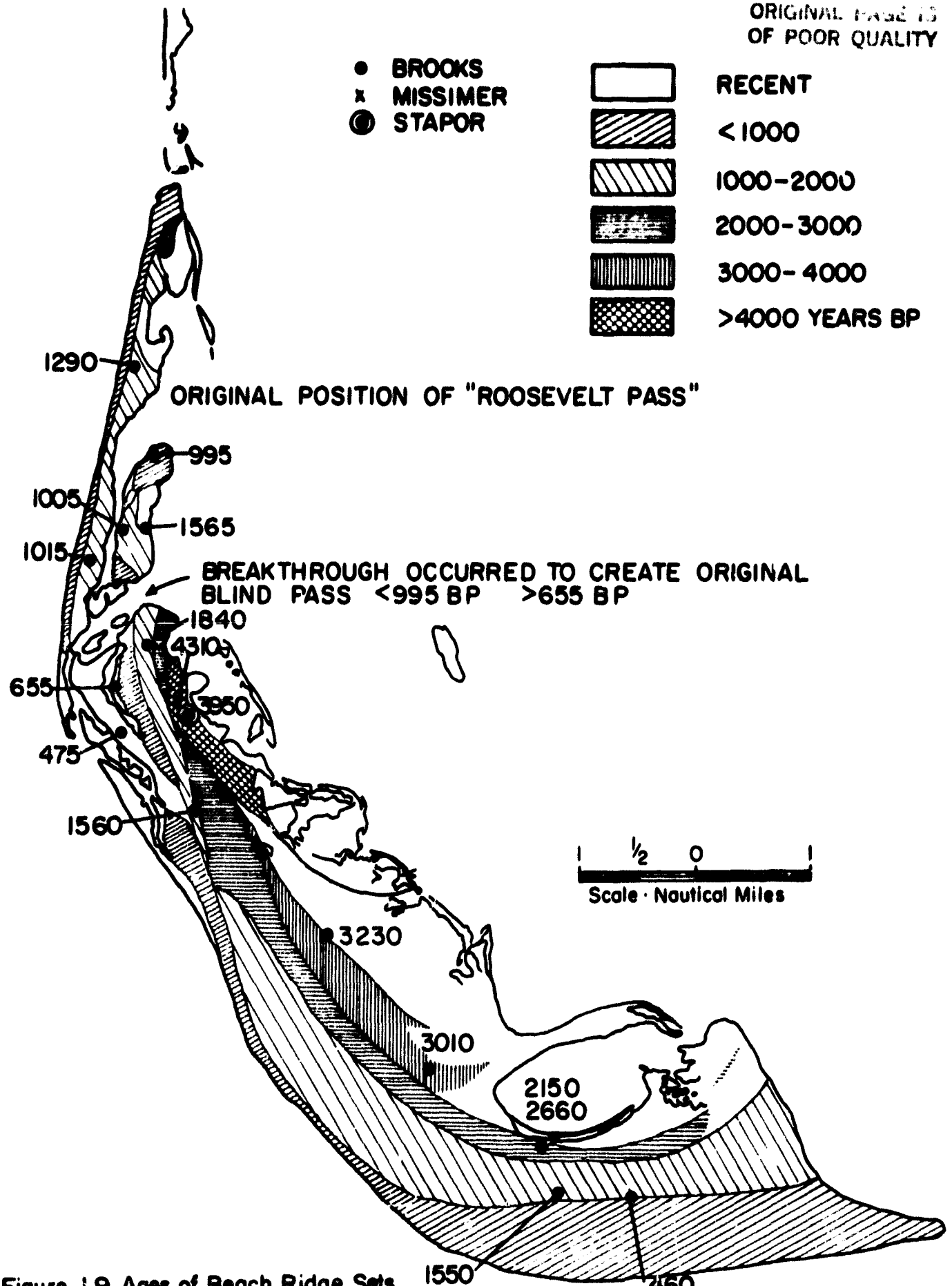

Figure 1.9 Ages of Beach Ridge Sets with Sample Locations and Dates for Captiva Island and Sanibel Island

More than one half of Sanibel Island has originated in the last 2,000 years, i.e., since the time of Christ. Cayo Costa, at the north end of the Lee County chain, is the only other island with relics of anticedent evolutionary stages. The exact age of the oldest beach ridge set on Cayo Costa is now known, but it is certainly older than 2,650 years. Older dates, published by Stapor and Mathews (1980) were obtained for specimens collected from apparently the same deposit that we have dated as being only 1520 $\pm$ 130 years B.P.

Beach ridge deposits over mud and mangrove peat deposits near the present south end of Cayo Costa demonstrate that a large inlet existed at this position prior to 1930 years before present (B.P.) i.e. 20 A.D.

With reference to the map, Figure 1.2 and Figures 1.6 through 1.9, both of the Captiva islands have originated as a series of spits from an ancestral island or islands that no longer exist.

Buck Island, now separated from Captiva by Roosevelt Channel and from Sanibel by Blind Pass was once the northern portion of Sanibel Island. Because of a spit that built southward during the interval from about 1500 to 1000 years ago, the mouth of a pass, hereafter referred to as Roosevelt Pass, migrated southward and the tidal inlet channel became restricted. Roosevelt Channel is all that remains of the large pass that was at the position of Captiva Island. The spit that resulted in the closing of Roosevelt Pass now constitutes the greater part of Captiva Island. From information now available, it would appear that the ancestral Roosevelt Pass "died" between 990 (1040 A.D.) and 650 (1300 A.D.) years ago with the breakthrough of Blind Pass. Severe erosion was experienced at the northern end of Sanibel for a period of time after the Blind Pass breakthrough. By 650

(1350 A.D.) years ago accretion began. The period of erosion of Sanibel Island related to the original breakthrough of Blind Pass was for an interval of 50 to 200 years thereafter.

Captiva Island is not just another Florida barrier island. Steps planned to stabilize it must take this fact into account. There will be special problems, and any steps taken must be of the proper magnitude to overcome the natural coastal processes.

Captiva Island arose as a spit during the Dark Ages of European history. Such narrow spits are notable for their instability. Based upon what we know about the origin and evolution of the island, and taking into consideration that there is now a deficit of sand in the littoral drift system, we must conclude that artificial beach nourishment with adequate sediment retaining structures at the passes are essential if Captiva Island is to be preserved in its present configuration.

CHAPTER II

NUMERICAL TIDAL MODEL

2.1 Introduction

The purpose of this numerical model is to provide a means of realistically representing the hydraulics of Pine Island Sound and any changes that would occur due to the reopening of Blind Pass.

The model has been modified from an earlier model (Mehta & Brooks, 1973) to calculate: 1) the tidal response of Pine Island Sound to the astronomical tides in the Gulf of Mexico, and 2) the resulting flows and the average velocity of each flow through each of the inlets which connect Pine Island Sound to the Gulf of Mexico (i.e., Blind Pass, Redfish Pass, Captiva Pass, and the northern and southern model boundaries of Pine Island Sound).

Tidal variations, referenced to the tide at the southern model boundary of Pine Island Sound, are given at the outside of each inlet. The flows through each of these inlets are calculated by knowing the water surface elevation adjacent to these inlets inside Pine Island Sound, and hence, the water surface slope across the inlets.

Pine Island Sound was divided into nine segments (Fig. 2.1), within which the hydraulic parameters were considered to be constant, especially the depth of water. The tidal variation within each segment was determined, in a sequential manner, by calculating the mass transfer of water from one segment into another. Initially, these volumes result from the flows through the inlets. The net flows into each (segment) were divided by the water surface area of that segment, thus giving the change in water surface elevation. Together with the continual flow through the inlets, the different water elevations between adjacent

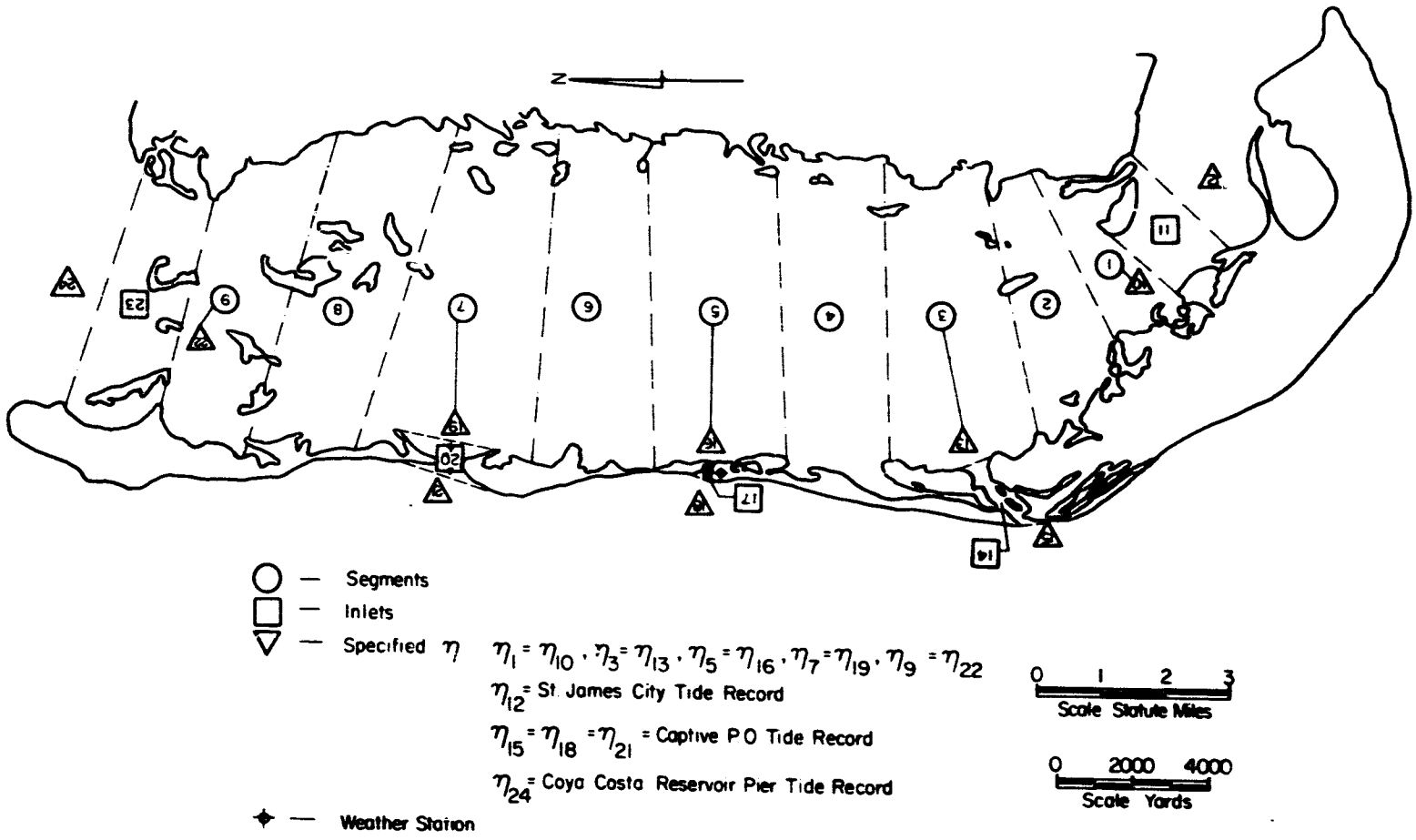

Figure 2.1 Nine Segments of Pine Island Sound Representing Constant Hydraulic Parameters.

segments gave rise to flows from one segment into another, which in turn gave rise to further differences between the water surface elevations of adjacent segments, which in turn gave rise to new flows, etc., etc.

The model begins with the tidal variations for MSL equal to zero for all segments. Hence, this initial condition must have, for a short time after start up, some effect on the flows through the inlets and from one segment into another. Consequently, a simple sinusoidal tide, with appropriate phase lags at each inlet, was used to represent the tide at the outside of each inlet so that the time could be found when the amplitude of the predicted tide reaches a maximum constant value.

A two phase study was conducted; 1) to calibrate the numerical tidal model; and 2) to evaluate the effect of opening Blind Pass. In the initial calibration phase, Blind Pass was closed (as it is presently found) and field data collected during the study was used to assess the validity of and/or modify the numerical model, accordingly. Once its validity was established, Blind Pass was reopened in the model and the hydraulics of this pass, together with its effect on the tide in Pine Island Sound, and the flows through each of the other four passes were investigated. A computer program listing of the model is presented in Appendix B.

2.2 Governing Differential Equations

The differential equations governing the flow in bay systems are the depth integrated equations of motion and continuity.

2.2.1 *Equation of Motion*

The vertically integrated differential equation of motion can be written for the center line flow direction in a semilinearized form as:

$$\frac{\partial q}{\partial t} = - g D \frac{\partial n}{\partial x} + \frac{1}{\rho} [\tau_\eta - \tau_b] \qquad (2.1)$$

in which

q = discharge per unit width in the x direction

t = time

g = gravitational constant

D = tidal depth = $h + \eta$

h = depth, referred to mean sea level

η = tide displacement above mean sea level due to astronomical, wind, and barometric tides

x = horizontal distance coordinate aligned with bay axis

ρ = mass density of water

τ_η = wind stress in x direction of air interface

τ_b = frictional stress on bottom of water column

The quantities τ_η and τ_b can be expressed as:

$$\tau_\eta = C_f \rho_a U^2 \cos \beta \qquad (2.2)$$

and

$$\tau_b = \frac{\rho f \, q|q|}{8D^2} \qquad (2.3)$$

in which

C_f = wind stress coefficient

and when

$$= \begin{cases} 0.0013, & U < 7.20 \text{ m/s} \\ 0.0013 + 0.00295 \left(1.0 - \frac{7.20}{U}\right)^2 & U > 7.20 \text{ m/s} \end{cases} \qquad (2.4)$$

ρ_a = mass density of air

U = wind speed at 10 m reference elevation

β = angle of a wind vector relative to the bay axis

f = Darcy-Weisbach friction factor

Note: During the calibration and running phases of the model, the effects of wind stress on the air/water interface will be ignored.

2.2.2 *Equation of Continuity*

The equation in one dimension can be expressed as:

$$\frac{\partial \eta}{\partial t} + \frac{\partial q}{\partial x} = \frac{q_R}{w} \tag{2.5}$$

in which the right hand side represents the effect of runoff,

q_R = runoff in cubic meters/sec per meter of bay length

w = width of segment considered.

2.3 Finite Difference Equations

In order to employ Equations (2.1) and (2.5) for realistic geometries and Gulf tides, it is necessary to cast these equations into finite difference form. The time- and space-staggered procedure is used in which the equation of motion is applied between midpoints of adjacent segments (i.e., across a segment boundary) at full time steps, Δt, and the equation of continuity is applied for each segment at half time step increments.

2.3.1 *Finite Difference Form of the Equation of Motion*

Equation (2.1) can be expressed in finite difference form for the total flow, Q_n, onto the nth segment, as:

$$Q_n' = \frac{Q_n + \frac{\overline{w}}{\rho}\overline{\tau}_n - \overline{wD}\, g\, (\eta_n - \eta_{n-1}) \times \frac{\Delta t}{\Delta x}}{1 + \frac{\overline{w}\, \Delta t\, f\, |Q_n|}{8\, (\overline{Dw})^2}} \tag{2.6}$$

in which the over barred quantities represent averages based on the nth and (n-1)th segments. The primed quantities, e.g. Q', indicate the value at time, t + Δt, whereas unprimed quantities are known from calculation at time, t, and w is the width of the bay segment. See Figure 2.2 for the variable representations and Figure 2.3 for the numerical model representation of the area of concern.

2.3.2 *Finite Difference Equation of Continuity*

Equation (2.5) can be written in finite difference form as:

$$\eta_n' = \eta_n + \frac{\Delta t}{\Delta x}\frac{1}{w_n}(Q_n - Q_{n-1}) + \frac{q_{R_n}\,\Delta t}{w_n} \qquad (2.7)$$

where the primes indicate the unknown quantities as before and the terms on the right hand side are known from calculations at previous time steps.

2.4 Boundary Conditions

The boundary conditions for this problem are the flows through the inlets and may be expressed, for example, for Redfish Pass as:

$$Q_{17}' = \frac{A_C\sqrt{2g\,|\eta_{16} - \eta_{18}|}\;\text{sign}\,(\eta_{16} - \eta_{18})}{\sqrt{K_{en} + K_{ex} + f1/4R}} \qquad (2.8)$$

in which

A_C = cross-sectional flow area of Redfish Pass

Q_{17} = flow from Pine Island Sound through Redfish Pass into the Gulf of Mexico

η_{16} = Pine Island Sound tide at the inside of Redfish Pass

η_{18} = Gulf tide at the outside of Redfish Pass

K_{en} = entrance loss coefficient

K_{ex} = exit loss coefficient

Variables Represented at
Segment Midpoints
η, h, τ

Variables Represented at
Segment Junctions
Q

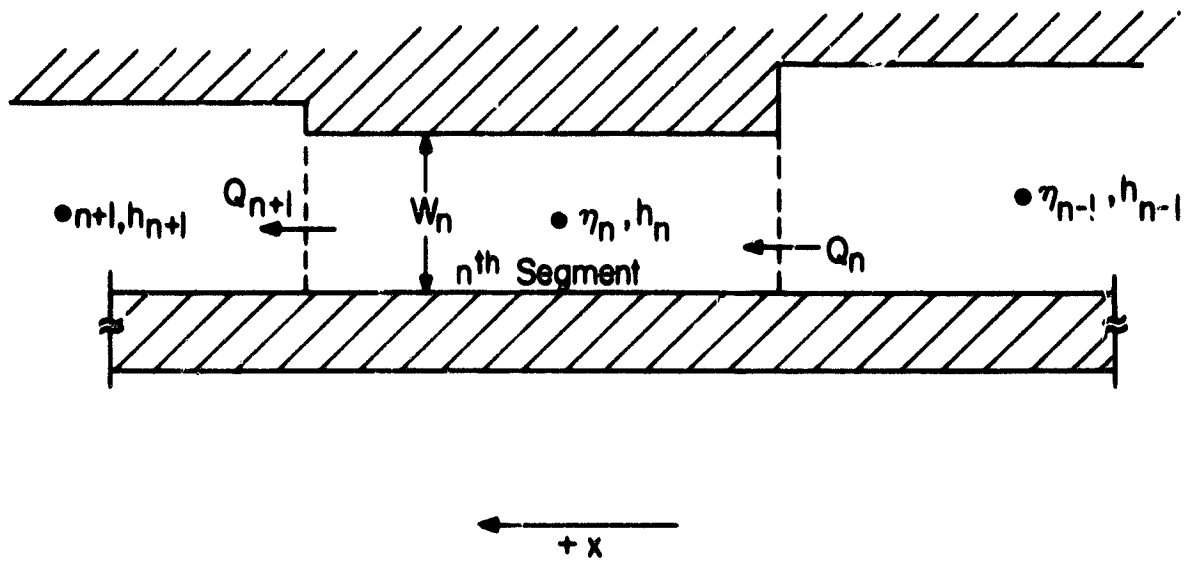

Figure 2.2 Illustration of Bay Segment Representation

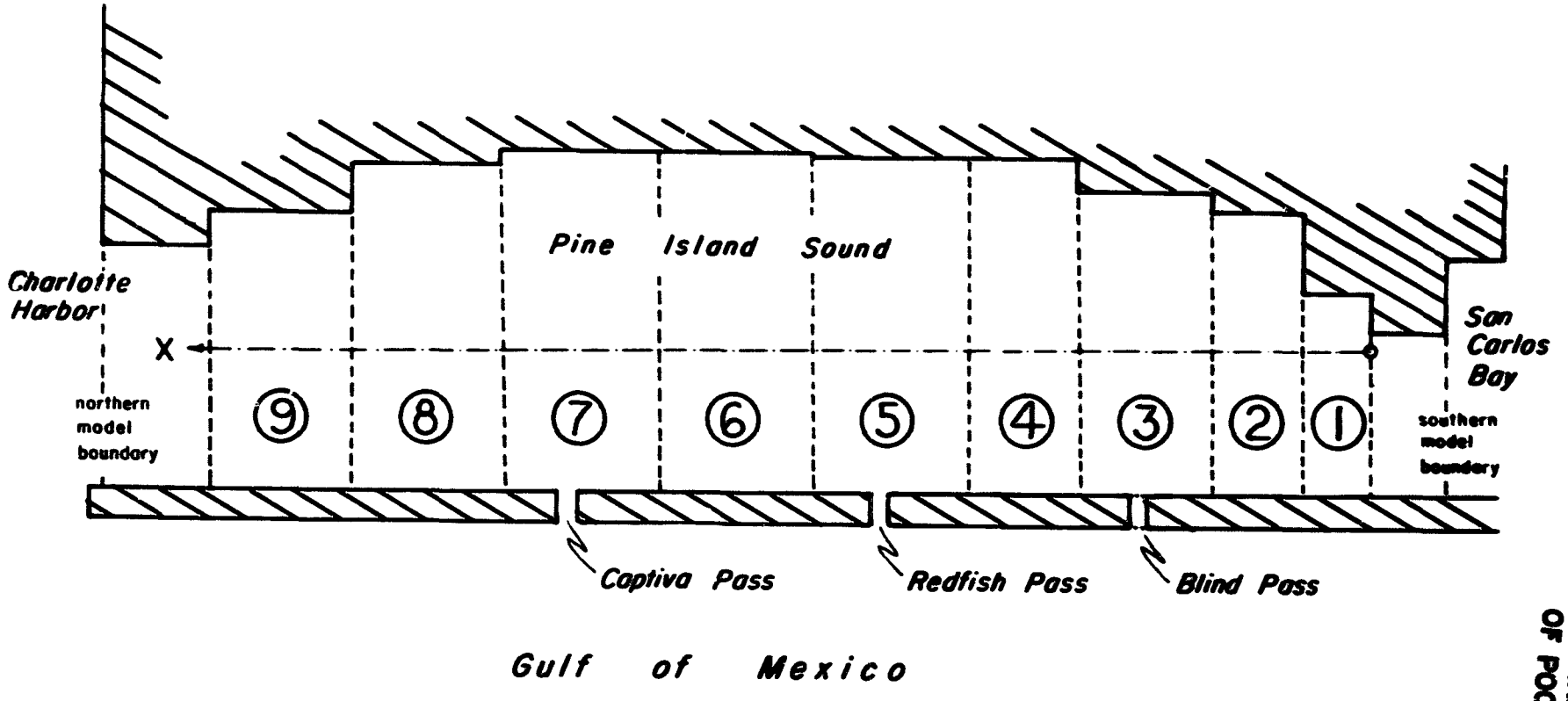

Figure 2.3 Schematization of Pine Island Sound and Gulf of Mexico System

$$R = \text{hydraulic radius of inlet} = \frac{A_c}{W + 2h + \eta_{16} + \eta_{18}}$$

w = equivalent width of Redfish Pass

h = equivalent depth of Redfish Pass (relative to mean sea level)

L = equivalent length of Redfish Pass

An expression similar to Equation (2.8) applies for Captiva Pass, Blind Pass, and the northern and southern model boundaries of Pine Island Sound. The location of the numerical subscripts used within the model are as shown in Figure 2.1. As stated previously, complete listing of the computer model and list of symbols used within the model can be found in Appendix B.

CHAPTER III

FIELD DATA AND ANALYSIS

3.1 Tidal Measurements

3.1.1 *Field Data*

To measure the spatial and temporal distribution of the astronomical tide propagation through the inlets and through Pine Island Sound, six Leupold and Stevens type tide gauges were installed in June 1978. Five of these were installed within Pine Island Sound, as shown in Figure 3.1, and the sixth installed on the tip of a groin, midway along the Gulf shore of Captiva Island.

The elevations of the tide gauges with respect to the 1929 Sea Level Datum, now referred to as the National Geodetic Vertical Datum (NGVD), were found and subsequently corrected (Piccolo, 1976) to the 1965 Mean Low Water by the following factors[1]:

St. James City	MLW = NGVD - 0.32 m
Captiva Island - Blind Pass	MLW = NGVD - 0.40 m
Captiva Island - Midway, Bayside	MLW = NGVD - 0.25 m
Captiva Island - Redfish Pass	MLW = NGVD - 0.03 m
Pine Island Sound - Charlotte Harbor	MLW = NGVD - 0.23 m

The gauges were installed with "4-day" clocks. They were serviced twice a week which included replacing the chart paper through mid December, at which time the gauges were removed and the tide stations disassembled.

3.1.2 *Data Analysis*

The data, collected twice weekly from each of the six stations, was in the form of a smooth curve traced out on chart paper. To ensure that there was no slippage between the steel float tape and the tide gauge pulley, the water level, relative to the instrument, was read both prior

---

1 Mr. W. D. Bender, Captive Erosion Prevention District, personal communication.

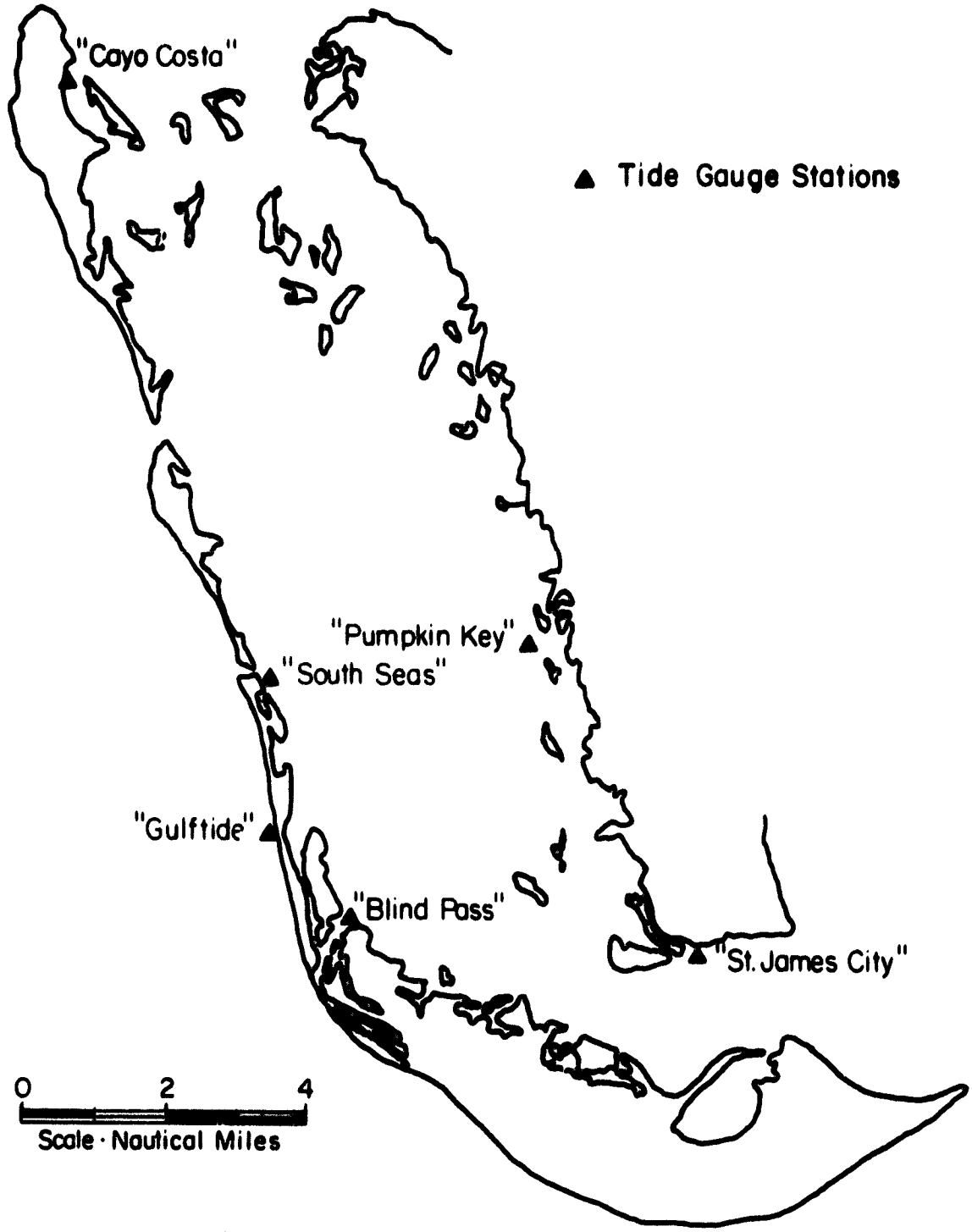

Figure 3. Location and Name of Tide Gauge Stations

to and upon replacement of the chart paper. The time that the chart paper was exchanged was marked down so that each chart could be checked for its accuracy and cogency.

Doubtful records (fouling by marine organisms occasionally blocked or partially blocked the orifice to the stilling well) were rejected. Valid data was digitized at two hour intervals, assembled into continuous time and water surface elevation data arrays, and stored within the computer facilities of the Northeast Regional Data Center at the University of Florida. These two-dimensional time/elevation arrays were then reduced to one (a time series vector of the water surface height relative to MSL) and then harmonic analysis was performed on the array.

The premises upon which the harmonic analysis of tides is founded are the following:

1. The resultant tide at any point is composed of a finite number of constituents, each with its own periodicity, phase angle and amplitude, and
2. The constituents are each simple harmonic in time and are independent values.

These premises may be formulated as:

$$\eta_r = a_0 + \sum_{i=1}^{N} a_i \cos\left(\frac{2\pi t}{T_i} - \delta_i\right) \qquad (3.1)$$

where η_r is the resultant tidal variation at a particular locality at time, t, and is composed of N constituents. The amplitude, phase, and period of the i^{th} constituent are a_i, δ_i, and T_i, respectively, and the displacement from the reference datum to the mean water level is a_0.

The periods of the important constituents are determined from a knowledge of the earth, moon, and sun system which cause the tide producing forces. Tables listing the important tidal constituents and their respective periods are presented in Schureman (1940). Although, in most cases the measured tide can be represented with reasonable accuracy if about ten constituents are considered (Ippen, 1966), 16 constitutents were utilized in the analysis due to the "mixed" nature of the tides in the Pine Island Sound region.

The time of start and end dates of the largest continuous tidal record for each tide station, and the principal constituents used together with their respective periods are presented in Tables 3.1 and 3.2. Tabulated results of the harmonic analysis for each station are contained in Tables 3.3 - 3.8. Graphical displays of the reconstructed tide for the period October 24, to November 1, 1978, for each station (except Blind Pass) are shown in Figures 3.2 - 3.6.

The sea slope across Pine Island Sound was computed by comparing the tidal records from the "South Seas" and "Pumpkin Key" tide stations. The average value of the absolute slope between the two stations over a nine day period was 0.079 m. This value, when compared to the average tidal range of approximately 0.50 m for the same time period, is insignificant, and so, water surface cross slopes will be ignored in the subsequent analysis.

3.2 Hydrographic Surveys

3.2.1 *Inlet Bathymetry*

During October 1978, the cross sections and bathymetry of the Gulf and bay shoals associated with both Redfish and Captiva passes were

Table 3.1 Time, Length, and Start and End Dates of the Longest Continuous Tidal Record Collected at Each Tide Station

Tide Station	Time of Longest Continuous Record (hrs)	Date of Start of Longest Record	Date of End of Longest Record
Gulftide	796	10/18/78	11/23/78
South Seas	1062	10/18/78	12/02/78
St. James City	1080	9/30/78	11/20/78
Blind Pass	1058	8/24/78	10/10/78
Coya Costa	1064	10/18/78	12/02/78
Pumpkin Key	2018	9/19/78	12/02/78

Table 3.2 Major Harmonic Constituents Used in Tidal Analysis

Constituent	Symbol	Period (hrs)	Constituent	Symbol	Period (hrs)
Principle Lunar	M_2	12.421	Composite Lunar	M_1	24.833
Principle Solar	S_2	12.000	Diurnal	J_1	23.099
Larger Lunar Elliptic	N_2	12.658	Diurnal	Q_1	26.868
Lunisolar	K_1	23.934	Composite Solar	L_2	12.191
Principle Lunar	O_1	25.819	Long Period	M_{tm}	219.191
Principle Solar	P_1	24.066	Lunar Fortnightly	M_f	327.869
Lunisolar	K_2	11.967	Lunisolar synodic Fortnightly	M_{sf}	354.365
Semidiurnal	ν_2	12.626	Lunar Monthly	M_m	661.230

Table 3.3 Harmonic Analysis Results for "Gulftide" Tide Station

Amplitude a_i (m)	Angular Velocity (deg/solar hr)	Period T_i (solar hrs)	Phase δ_i (degrees)
0.1869	28.9841	12.421	77.8219
0.1001	30.0000	12.000	99.6483
0.0299	28.4397	12.658	194.7250
0.0528	15.0411	23.934	185.8221
0.1079	13.9430	25.819	115.1912
0.0601	14.9589	24.066	132.1366
0.1351	30.0821	11.967	342.0671
0.0157	28.5126	12.626	145.0242
0.0082	14.4967	24.833	248.4851
0.0088	15.5854	23.099	238.9296
0.0298	13.3987	26.868	221.5013
0.0461	29.5289	12.191	140.3845
0.0539	1.6424	219.191	62.4574
0.0578	1.0980	327.869	81.6405
0.0090	1.0159	354.365	225.0921
0.0161	0.5444	661.230	193.1122

a_0 = 0.1756 m

Table 3.4 Harmonic Analysis Results for "South Seas" Tide Station

Amplitude a_i (m)	Angular Velocity (deg/solar hr)	Period T_i (solar hrs)	Phase δ_i (degrees)
0.1719	28.9841	12.421	106.6122
0.0703	30.0000	12.000	56.1490
0.0197	28.4397	12.658	312.5256
0.0848	15.0411	23.934	229.1151
0.0928	13.9430	25.819	131.4091
0.0747	14.9589	24.066	113.8363
0.0173	30.0821	11.967	286.1309
0.0412	28.5126	12.626	214.2384
0.0079	14.4967	24.833	354.3335
0.0042	15.5854	23.099	191.0508
0.0220	13.3987	26.868	244.9655
0.0172	29.5289	12.191	172.5199
0.0520	1.6424	219.191	65.9714
0.0351	1.0980	327.869	106.3389
0.0359	1.0159	354.365	236.3255
0.0157	0.5444	661.230	207.5721

a_0 = 0.2161 m

Table 3.5 Harmonic Analysis Results for "St. James City" Tide Station

Amplitude a_i (m)	Angular Velocity (deg/solar hr)	Period T_i (solar hrs)	Phase δ_i (degrees)
0.1965	28.9841	12.421	248.8228
0.1626	30.0000	12.000	283.8420
0.2816	28.4397	12.658	138.1712
0.0653	15.0411	23.934	178.6380
0.0768	13.9430	25.819	329.3757
0.0629	14.9589	24.066	57.4832
0.1005	30.0821	11.967	155.1988
0.2775	28.5126	12.626	355.9224
0.0106	14.4967	24.833	110.1599
0.0096	15.5854	23.099	339.0046
0.0172	13.3987	26.868	214.5224
0.0122	29.5289	12.191	257.4768
0.0470	1.6424	219.191	84.3383
0.0419	1.0980	327.869	323.7251
0.0282	1.0159	354.365	109.7659
0.0209	0.5444	661.230	44.3093

a_0 = 0.2398 m

Table 3.6 Harmonic Analysis Results for "Blind Pass" Tide Station

Amplitude a_i (m)	Angular Velocity (deg/solar hr)	Period T_i (solar hrs)	Phase δ_i (degrees)
0.1925	28.9841	12.421	265.2305
0.0886	30.0000	12.000	170.2067
0.1457	28.4397	12.658	129.2080
0.0363	15.0411	23.934	324.7966
0.1033	13.9430	25.819	201.6792
0.0419	14.9589	24.066	246.1249
0.0404	30.0821	11.967	71.3185
0.1535	28.5126	12.626	358.7432
0.0220	14.4967	24.833	167.8727
0.0105	15.5854	23.099	206.3855
0.0140	13.3987	26.868	331.7178
0.0257	29.5289	12.191	257.4165
0.0126	1.6424	219.191	276.5144
0.0298	1.0980	327.869	336.1199
0.0090	1.0159	354.365	103.0673
0.0334	0.5444	661.230	193.0418

a_0 = 0.2781 m

Table 3.7 Harmonic Analysis Results for "Coya Costa" Tide Station

Amplitude a_i (m)	Angular Velocity (deg/solar hr)	Period T_i (solar hrs)	Phase δ_i (degrees)
0.1156	28.9841	12.421	98.5081
0.0811	30.0000	12.000	45.3995
0.0573	28.4397	12.658	288.5349
0.0861	15.0411	23.934	236.0377
0.0820	13.9430	25.819	125.0145
0.0838	14.9589	24.066	108.6996
0.0441	30.0821	11.967	268.5476
0.0745	28.5126	12.626	157.4006
0.0086	14.4967	24.833	295.8311
0.0018	15.5854	23.099	33.4601
0.0157	13.3987	26.868	219.2867
0.0125	29.5289	12.191	132.3917
0.0553	1.6424	219.191	64.0319
0.0616	1.0980	327.869	126.8128
0.0598	1.0159	354.365	267.9661
0.0199	0.5444	661.230	221.7917

a_0 = 0.2369 m

Table 3.8 Harmonic Analysis Results for "Pumpkin Key" Tide Station

Amplitude a_i (m)	Angular Velocity (deg/solar hr)	Period T_i (solar hrs)	Phase δ_i (degrees)
0.1744	28.9841	12.421	257.1814
0.0850	30.0000	12.000	208.5735
0.0505	28.4397	12.658	10.6014
0.0928	15.0411	23.934	329.8096
0.0867	13.9430	25.819	182.8130
0.0609	14.9589	24.066	162.7971
0.0331	30.0821	11.967	138.7372
0.0406	28.1526	12.626	262.9060
0.0072	14.4967	24.833	145.6895
0.0060	15.5854	23.099	287.8303
0.0137	13.3987	26.868	299.3713
0.0105	29.5289	12.191	294.4321
0.0422	1.6424	219.191	165.5211
0.0237	1.0980	327.869	220.6792
0.0357	1.0159	354.365	297.2253
0.0235	0.5444	661.230	197.0435

a_0 = 0.2344 m

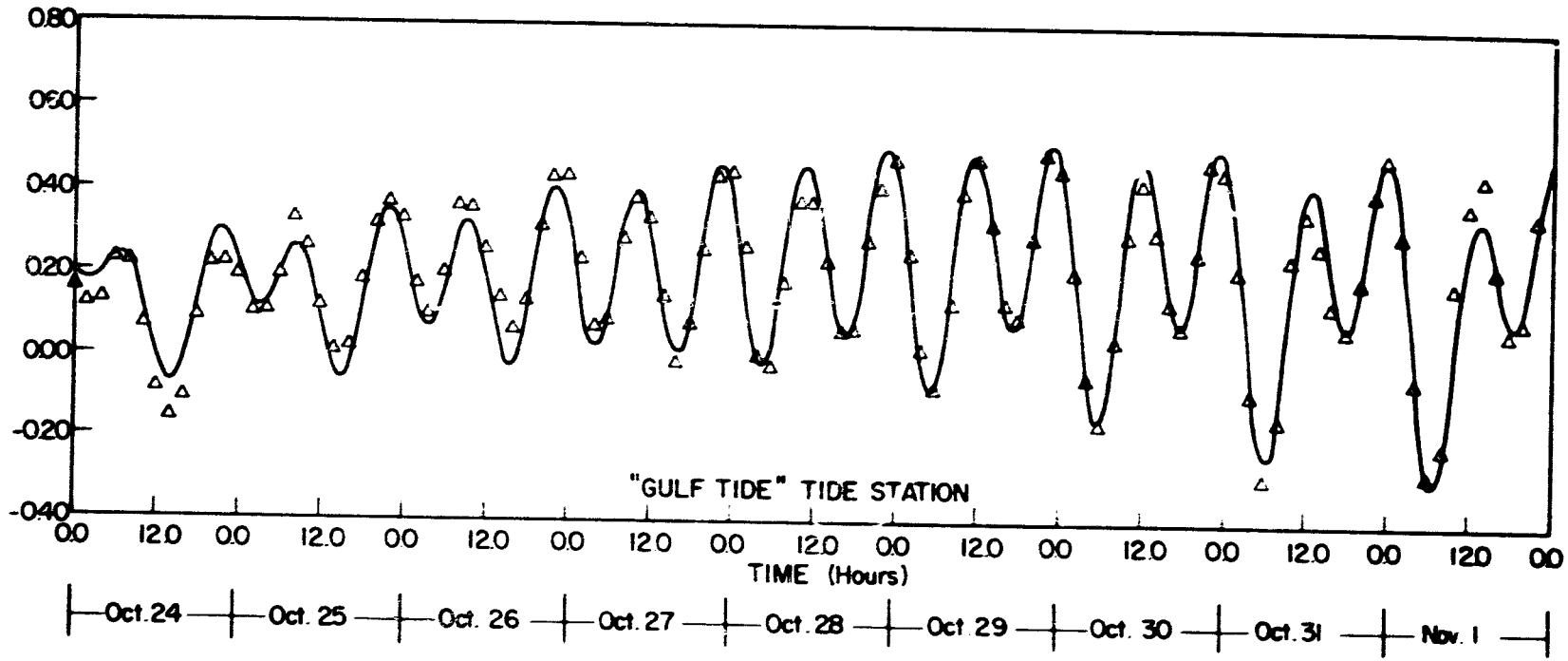

Figure 3.2 Graphical Display of the Reconstructed Tide for the Period October 24 to November 1, 1978 for the "Gulf Tide" Tide Station.

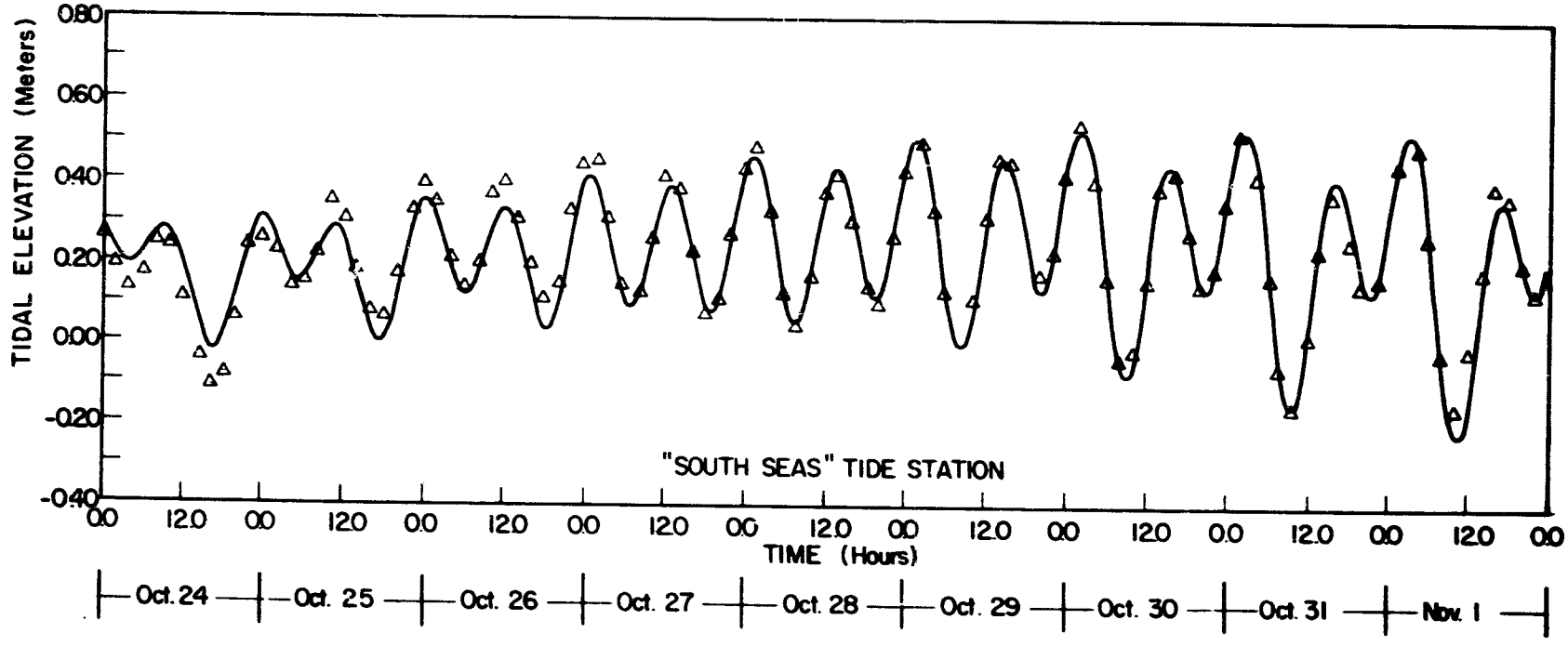

Figure 3.3 Graphical Display of the Reconstructed Tide for the Period October 24 to November 1, 1978 for the "South Seas" Tide Station.

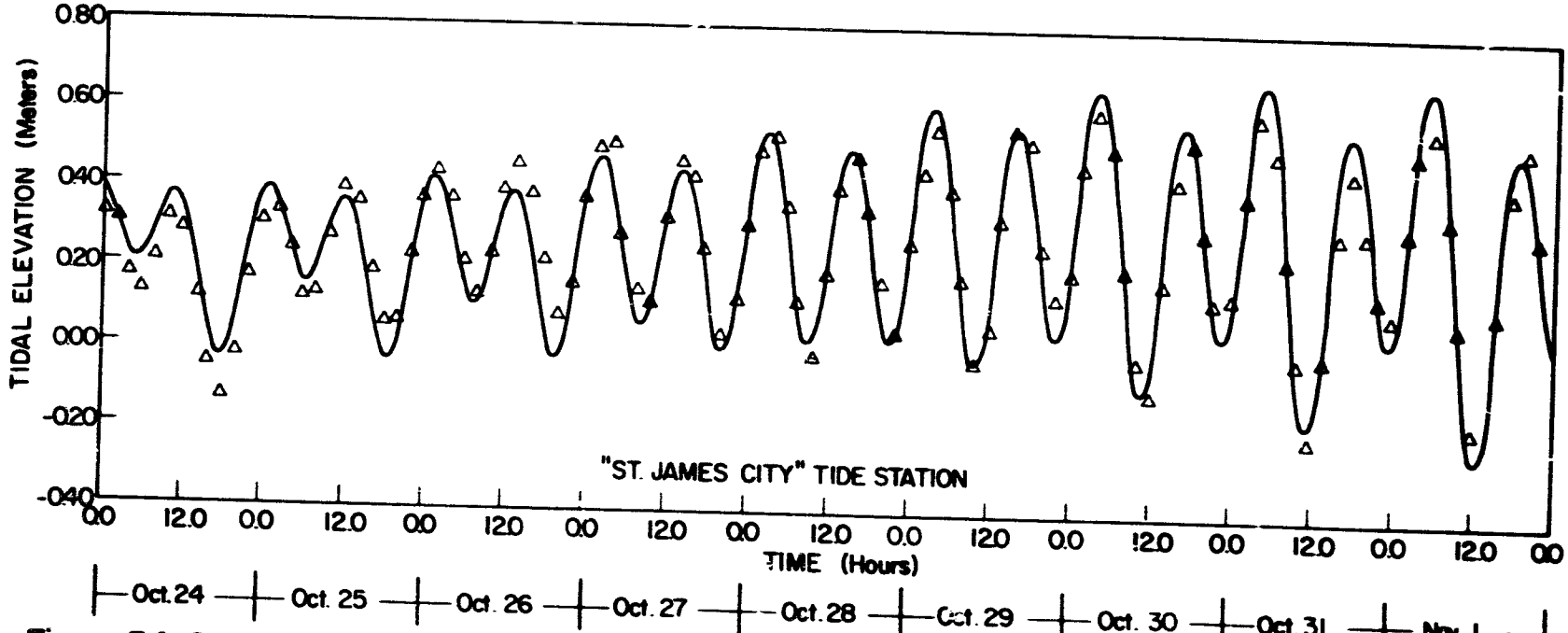

Figure 3.4 Graphical Display of the Reconsiructed Tide for the Period October 24 to November 1, 1978 for the "St. James City" Tide Station.

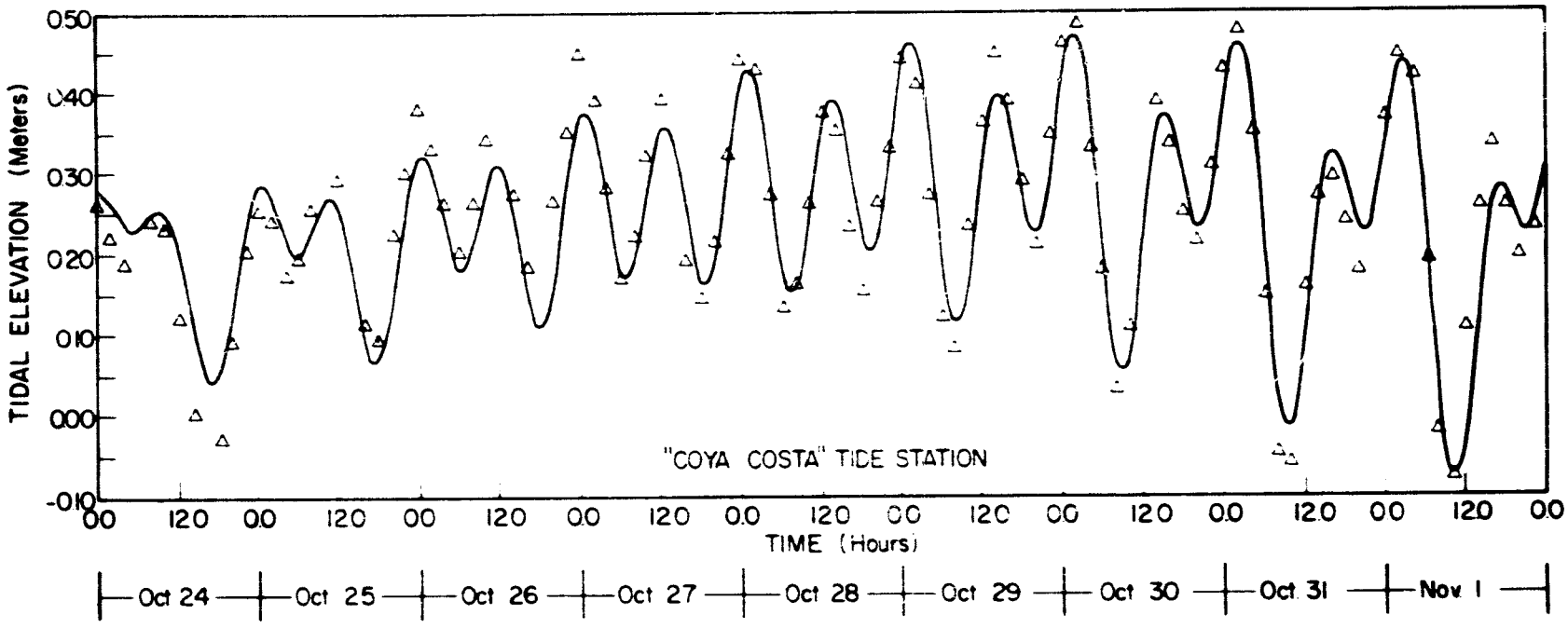

Figure 3.5 Graphical Display of the Reconstructed Tide for the Period October 24 to November 1, 1978 for the "Cayo Costa" Tide Station.

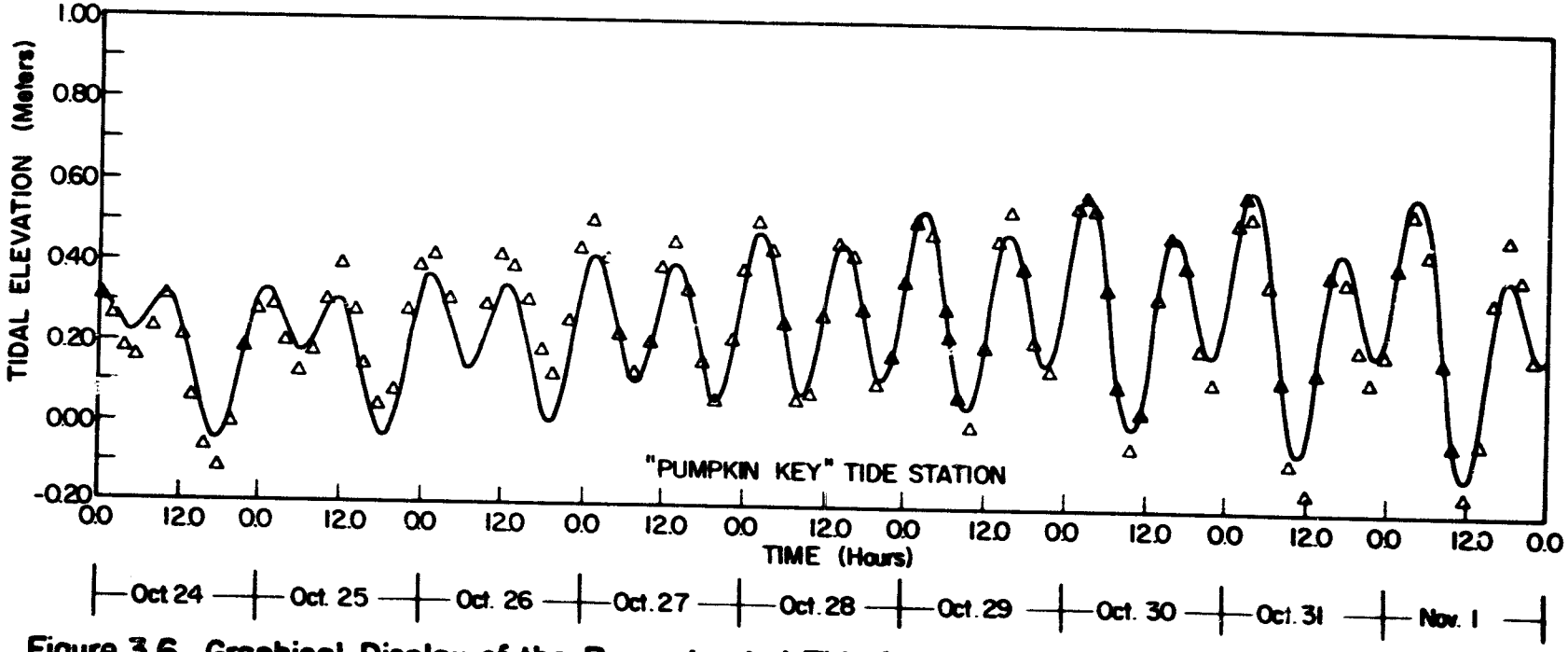

Figure 3.6 Graphical Display of the Reconstructed Tide for the Period October 24 to November 1, 1978 for the "Pumpkin Key" Tide Station.

obtained. A depth recorder was mounted on a boat which traversed across the channel and shoal areas. Within the inlet channel, a transit and two-way radios were used to keep the boat on line and, in part, a range finder was used to mark the distance. Due to the increased traversing distances over the shoals, two transits were used for triangulation fixes to locate the boat's position within the shoal regions.

Once collected, the bathymetric data was corrected for the height of tide during the periods of measurement and then reduced to the 1965 MLW datum. This information was then digitized into X-Y coordinates with an associated depth and then processed by the SYMAP-SYMVU programs at the computing facilities of the Northeast Regional Data Center at the University of Florida. The results of this analysis are shown in Figures 3.7 and 3.8 and in Appendix C. Figures 3.7 and 3.8 show a three-dimensional perspective view of Redfish and Captiva passes, respectively, and Figures C.1 and C.2 show their associated two-dimensional forms. Contour lines, in meter intervals, have been drawn in on Figures C.1 and C.2, providing an excellent bathymetric representation of the two passes.

3.2.2 *General Bathymetry*

Low altitude photography was used to evaluate the depositional and erosional patterns of the islands and associated inlets. LANDSAT imagery, processed on the IMAGE 100 system at NASA-KSC, was used to develop generalized bathymetry in support of the findings of the inlet surveys.

Using the results of the bathymetric surveys as ground truth data, six depth intervals (themes) were developed in the IMAGE 100 analysis.

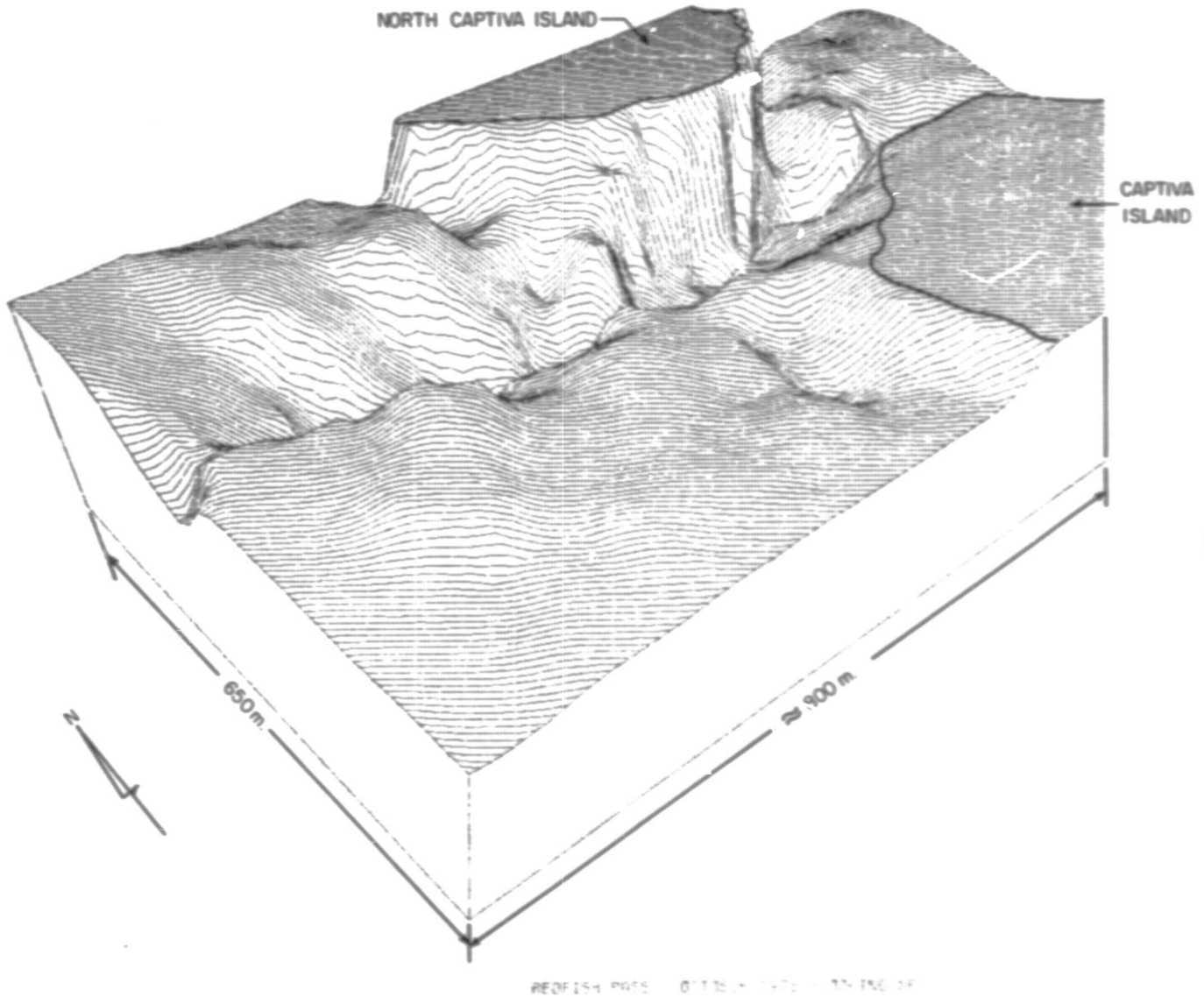

Figure 3.7 SYMVU Three-Dimensional Perspective of Redfish Pass.

Figure 3.8 SYMVU Three-Dimensional Perspective of Captiva Pass.

These were: 0-1 m (grass flats), 0-1 m (sandy bottom), 1-2 m (sand), approximately 3 m, approximately 4 m, and 5-8 m. Each theme was analyzed and recorded separately and then displayed together as is shown in Figure 3.9. Figure 3.10 shows only the 0-1 m (sandy bottom) and the 1-2 m (sand) themes, delineating the shoal systems associated with all inlets. In the bottom left hand section of Figures 3.9 and 3.10 are two "windows", which are digital magnifications of Captiva Pass (bottom left hand corner) and Redfish Pass (bottom middle) and highlight the inlet shoal systems. The depth intervals and their corresponding color themes are given in Table 3.9. By comparing the results displayed in the windows of Figures 3.9 and 3.10 to those from Figures C.1 and C.2 in Appendix C, a very good agreement between the hydrographic survey results and the satellite imagery analysis becomes apparent.

Table 3.9 Color Code for Depth Related Features in Figures 3.9 and 3.10

Color	Depth
grey	land
blue	0-1 m (grass flats)
orange	0-1 m (sandy bottom)
green	1-2 m (sand)
light blue	≈ 3 m
yellow	≈ 4 m
pink	5-8 m
black	unclassified water depths

To determine the water surface area of the nine model segments and the northern and southern model boundaries within Pine Island Sound, LANDSAT imagery data was used instead of conventional planimetry

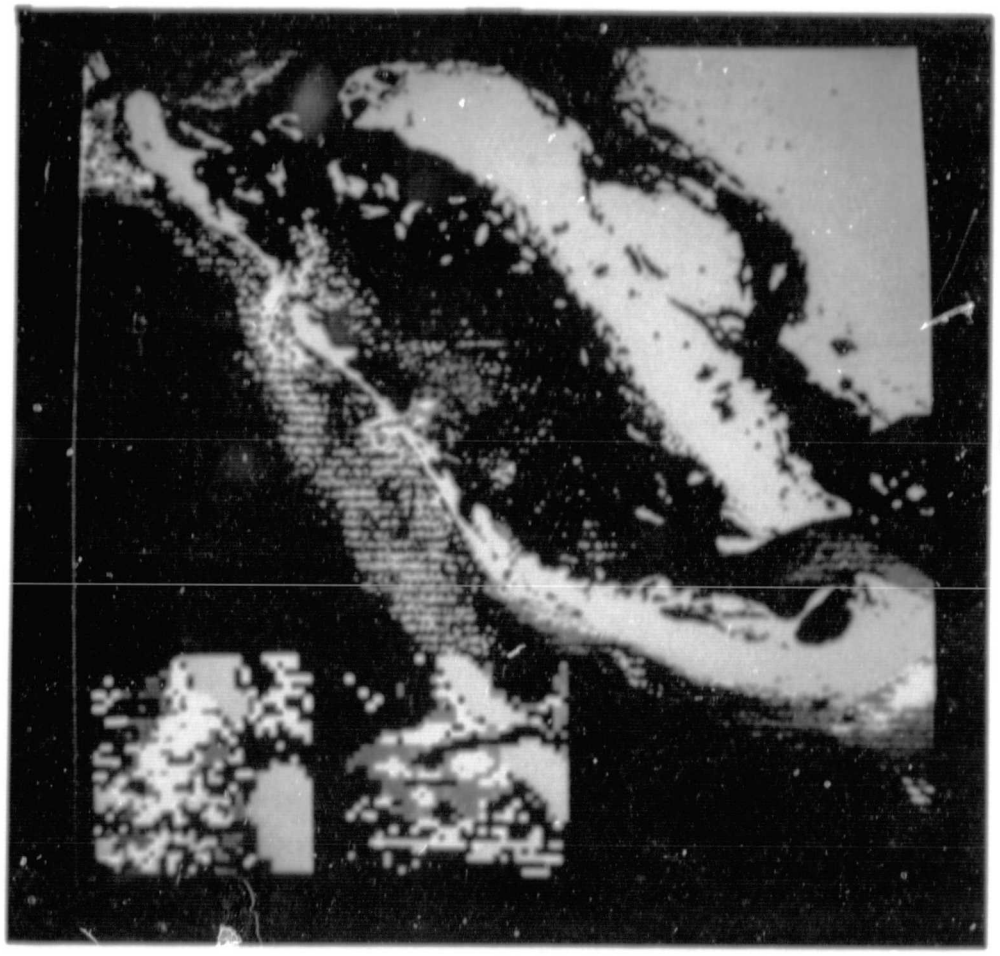

(Skewed image – not geometrically corrected)

Figure 3.9 General Results from LANDSAT Imagery Analysis showing Depth Related Features (see Table 3.9 for legend)

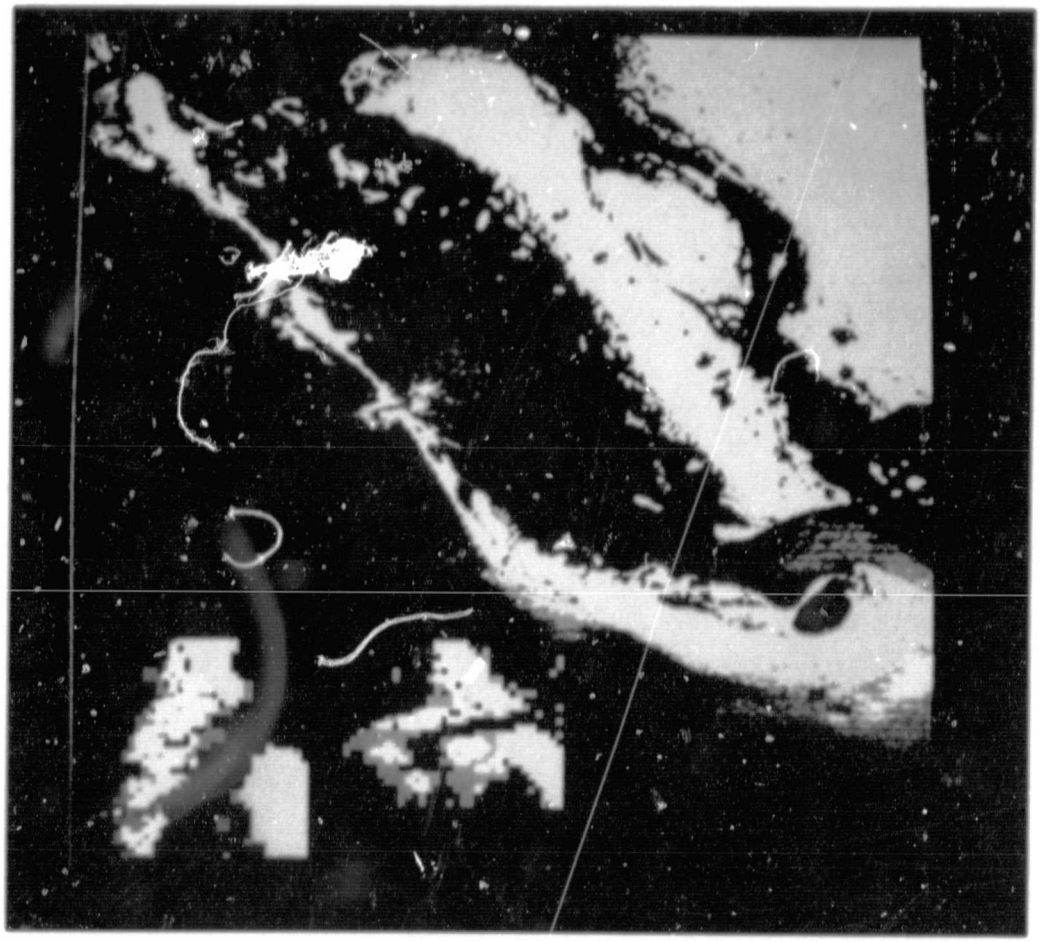

(Skewed image — not geometrically corrected)

Figure 3.10 Results from LANDSAT Imagery Analysis Showing Shoal Systems Associated with the Inlets.

techniques. The irregular shape of the coastline and the large number of islands can be more accurately delineated in considerably less time by the image analysis than by the use of either a planimeter or a conventional digitizer/integrator. The cursor on the color cathode ray tube (CRT) was used to locate the end points of the transect lines (inter-segment borders) and then acreage values were established for water surface areas between the transects and the land boundaries. This information is listed in Table 3.10 and shown in Figure 3.11.

To determine the average depth within each of the segments, each segment was subdivided into four sections. The average depth for each subsection was found from the Nautical Chart 11427, NOAA. These four values were averaged to give the mean depth below MLW 1965 for the entire segment. This data, together with the segment lengths and areas, is contained in Table 3.10.

Table 3.10 Depth, Length and Water Surface Area Values for Model Segments and Boundaries within Pine Island Sound

Segment N^{o}/Inlet	Mean Depth (m)	Mean Length (m)	Water Surface Area (hectares)
Southern Model Boundary	1.7	2065.0	725.3
1	1.0	1950.0	1053.8
2	1.1	1960.0	985.4
3	1.3	2450.0	1684.5
4	1.2	2600.0	2037.4
5	1.6	3300.0	2594.4
6	1.2	2690.0	2122.0
7	0.9	3090.0	2384.0
8	0.8	3050.0	2188.6
9	1.1	2710.0	1673.5
Northern Model Boundary	1.3	1825.0	1003.5

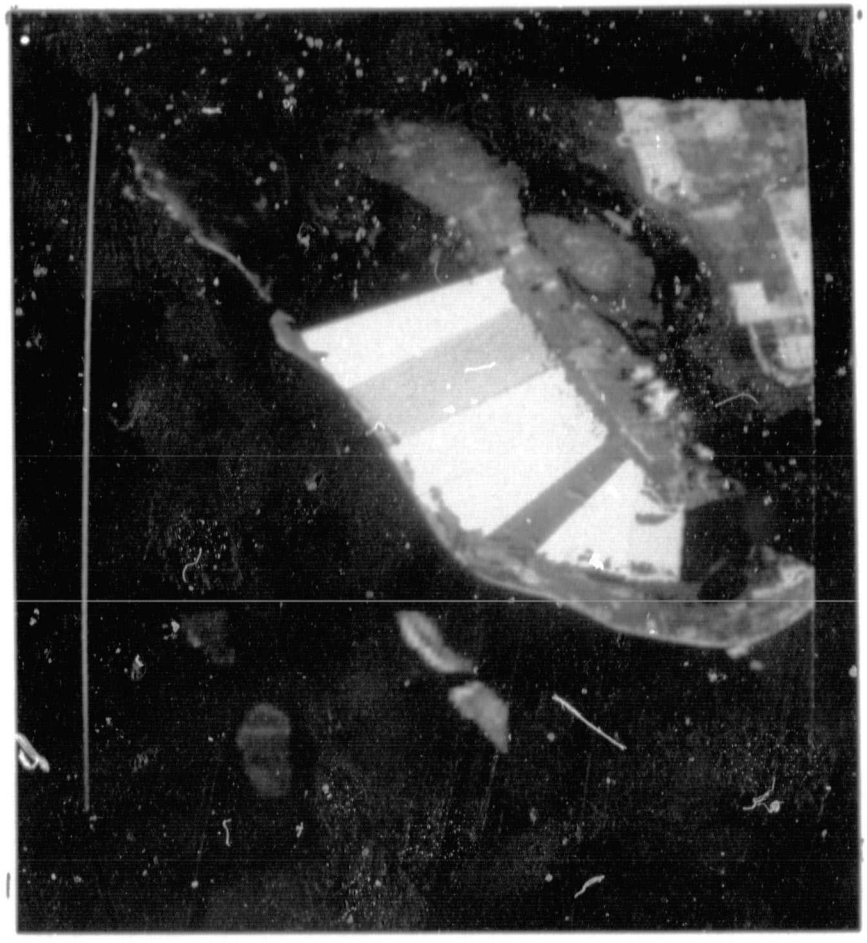

(Skewed image — not geometrically corrected)

Figure 3.11 Resulting Determination of Water Surface Areas within Pine Island Sound by LANDSAT Imagery Analysis.

3.2.3 *Beach Profiles*

Beach profiles, extending from the top of the beach berm out to water depths of 5 to 6 feet, were taken every 330 m (1000 ft) along the northern Gulf shoreline of Captiva Island and at every 33 m along the southern most 330 m of Captiva's coastline. Profiles were taken prior to and just after storm activity during the 15th to 20th of October. However, due to instrument errors, vertical control between all profile base pegs was not accurate. Pre- and post-storm profiles resulted in net changes in the beach profiles, with net erosion occurring along the northern coastline and significant deposition occurring on the northern side of the rock jetty on the southern tip of Captiva Island. Profiles taken along the southern end of Captiva can be found in Appendix D.

3.3 Inlet Flow Measurements

The spatial and temporal distributions of the tide induced flow through Redfish Pass were measured over flood and ebb flows during both spring and neap tidal conditions. From 07:30 to 19:30 on October 25, vertical velocity profiles (Appendix E) were obtained approximately at hourly intervals at six equally spaced locations, labelled Stations A, B, C, D, E, and F, across the throat section of Redfish Pass. Two boats simultaneously obtained the profiles using Ott type current meters with four inch impellers and using hand counters to count the impeller revolutions over a fixed time interval of 30 seconds.

The Ott meters were calibrated prior to field use by comparing results from tests performed in a towing tank, in which the current meters were towed along at a predetermined velocity, to the manufacturer's calibration charts. The results of the comparison were most

satisfactory and so each of the velocity measurements made in Redfish Pass represented an average flow velocity taken over a 30 second interval.

After each profile was obtained, each boat moved to an adjacent station, the position was established by a buoy which had been placed at an earlier time, and monitoring continued. The total time for each boat to shift and to measure three velocity profiles was, on the average, 30 minutes.

On October 31st from 08:00 to 18:45, the velocity distribution for the spring tidal condition was measured. Due to equipment malfunction and personnel shortages, only four stations were monitored, and they were stations B, C, D, and E. During both days the angle of cable deflection from the vertical position was estimated.

It was assumed that a reasonable correction to the vertical position of the current meter, as affected by the flow induced drag, could be made by assuming a linear cable deflection from the surface to the meter. All profiles were adjusted to account for this deflection and then drawn. The average velocity for each profile was obtained by integrating the profile over the depth of flow. Appendix E, contains these profiles together with the value of the average flow velocity.

The spatial distribution across the throat section was determined by plotting the depth-averaged values for each station for every time sampling period. Figures 3.12 and 3.13, respectively, show the spatial and temporal distribution of the flow in Redfish Pass during the 25th and 31st of October 1978. The spatial distributions were subsequently integrated across the width of the inlet to give the cross-sectionally averaged mean velocity, $\bar{u}_a$. Figure 3.14 shows the time changing values of $\bar{u}_a$ for the 10/25/78, 10/30/78 and 10/31/78.

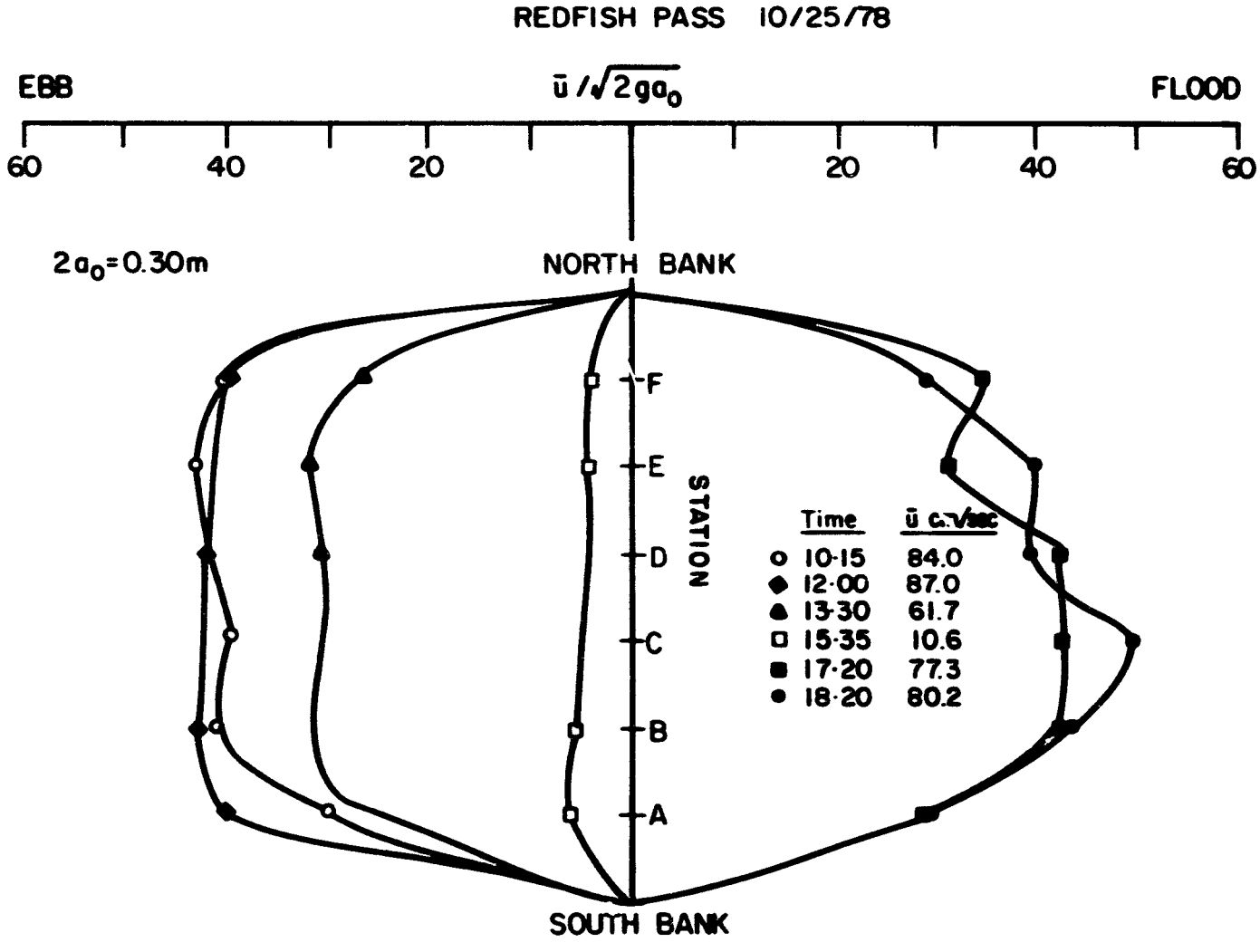

Figure 3.12 Spatial and Temporal Distribution of Flow in Redfish Pass, October 25, 1978.

Figure 3.13 Spatial and Temporal Distribution of Flow in Redfish Pass, October 31, 1978.

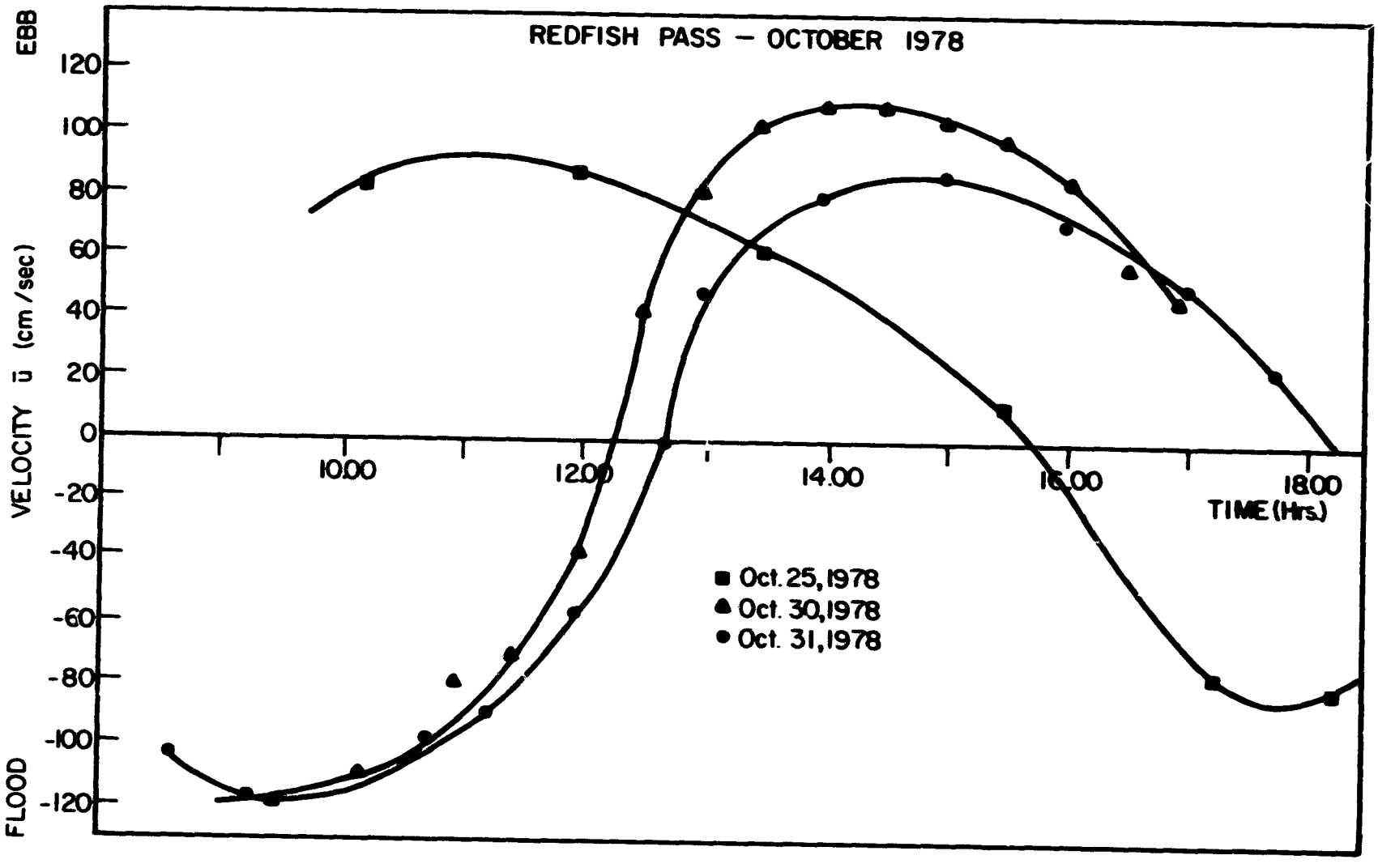

Figure 3.14 Time Distribution Velocity Profile of depth-averaged values for Redfish Pass, October 25, 30, 31, 1978.

To obtain the times of slack water and the maximum ebb and flood velocities in all of the inlets which connect Pine Island Sound to the Gulf of Mexico, velocity profiles were simultaneously recorded during a 12 hour period on October 30, 1978. Ott type current meters with four inch impellers were used to measure the average velocity over a 30 second period at each depth in Redfish and Captiva passes and in the northern model boundary. A Gurley type meter with a direct velocity reading meter, which was recalibrated prior to use, was used in the southern model boundary at St. James City.

The velocity profiles were plotted and the depth-averaged values found by integrating the velocity measurements over the flow depth. The profiles at their depth-averaged values can be found in Appendix E, and the time distribution of the depth-averaged values for each inlet for October 30 is shown in Figure 3. 14 and Figures 3.15 to 3.17.

3.4 Salinity Measurements

Salinity, conductivity, and water temperature profiles were obtained simultaneously with most velocity profiles taken on October 30, 1978, at Captiva Pass and at the northern and southern model boundaries. Salinity profiles were taken at Redfish Pass on October 25th. In the shallower regions, a Beckman Model RS53 Electrodeless Induction Salinometer was placed 30 cm above the current meters. At Redfish and Captiva passes, a Van Doorn water sampling bottle was used to sample water from predetermined depths and the salinometer was then used to measure the salinity of the sampled water.

Two important results come from these measurements. First, the salinity and temperature profiles at each location were constant with

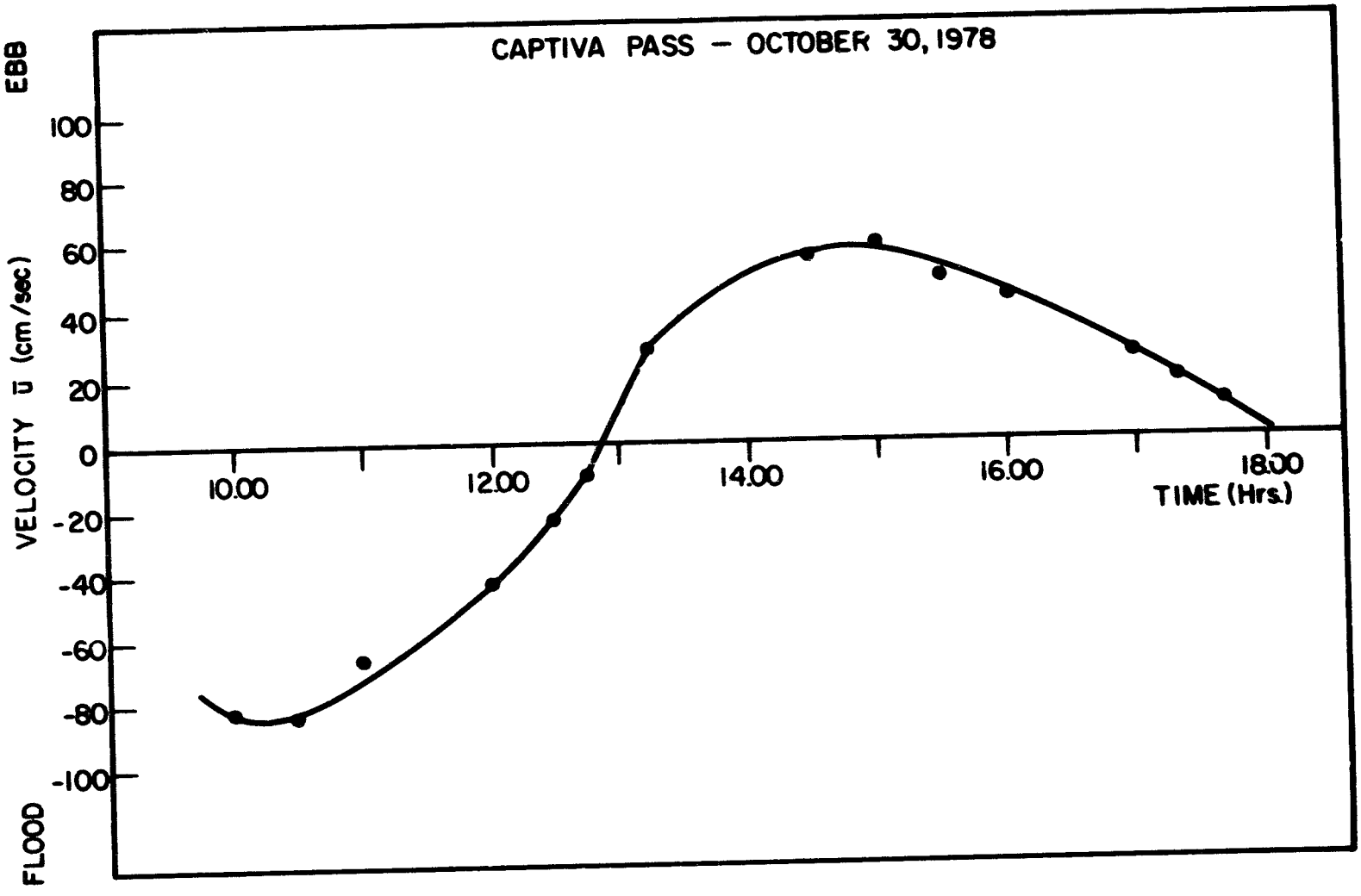

Figure 3.15 Time Distribution Velocity Profile of Depth-Averaged Values for Captiva Pass.

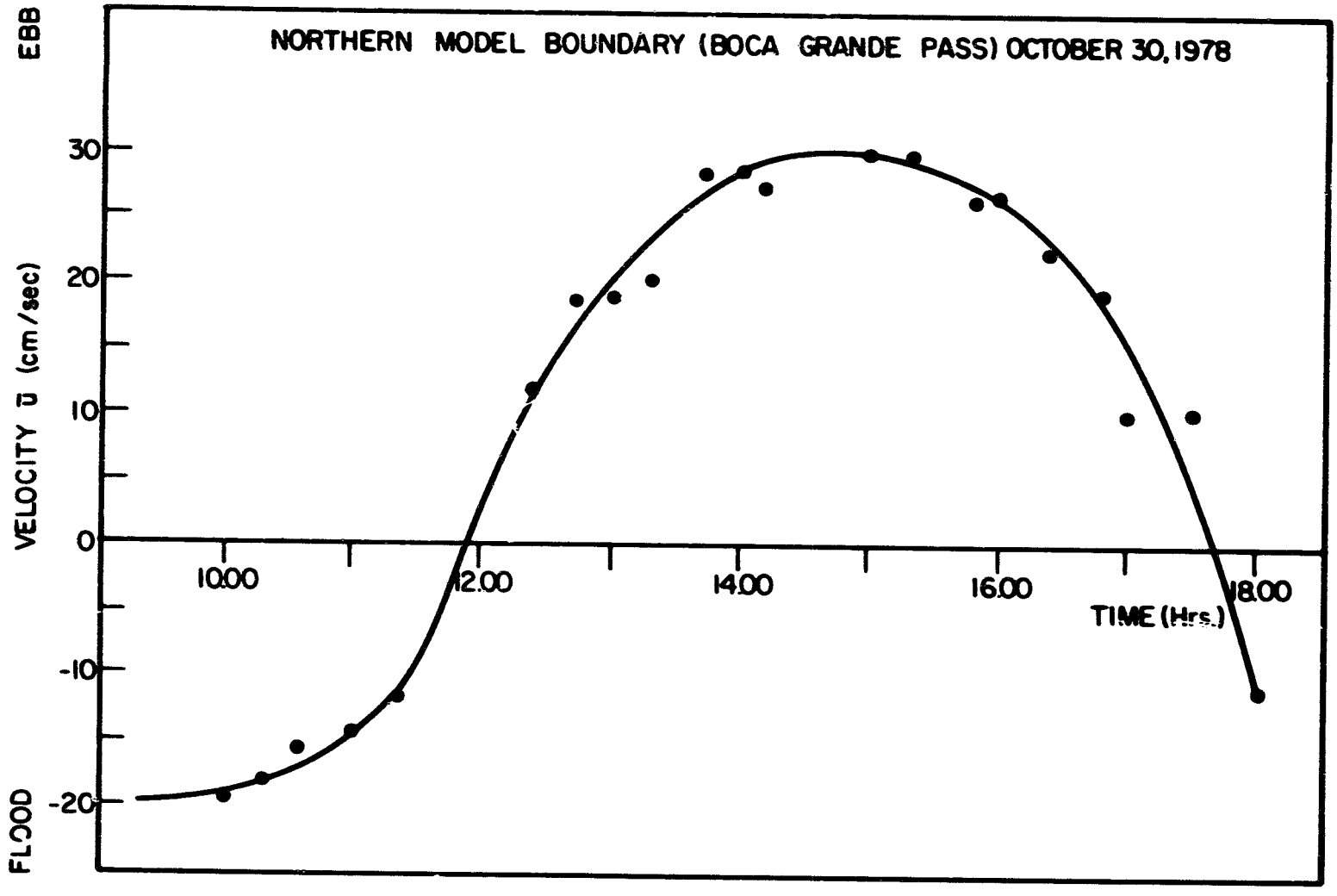

Figure 3.16 Time Distribution Velocity Profile of the Depth-Averaged Values for the Northern Model Boundary.

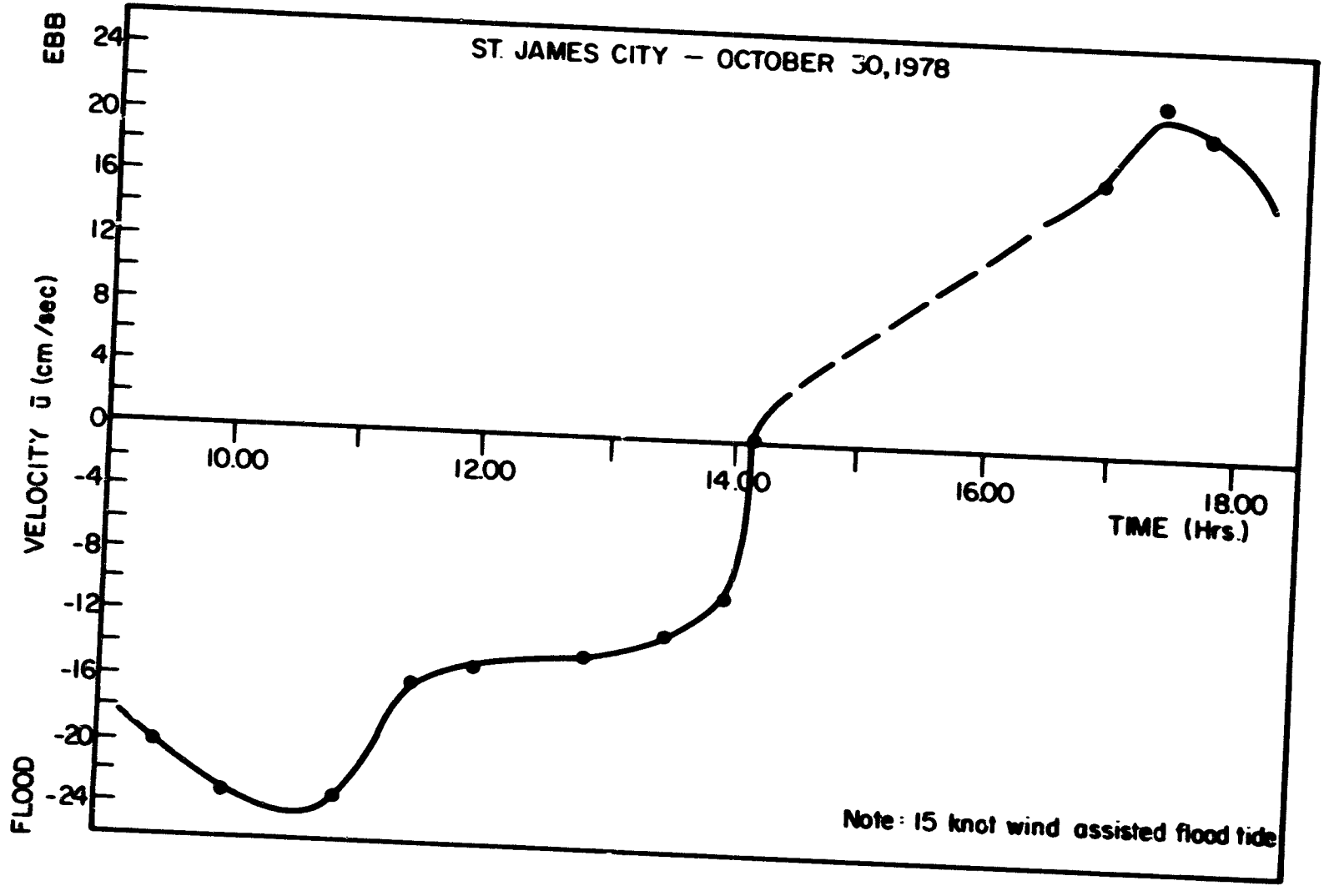

Figure 3.17 Time Distribution Velocity Profile of the Depth-Averaged Values for St. James City.

depth. This indicates that throughout the study period, stratification within the inlets did not exist at the time of measurement and that the water in each inlet can be considered "well mixed". This would be expected in such a shallow bay. The second important observation is that the salinity of the water decreases towards the southern model boundary of Pine Island Sound. This observed trend is consistent with expectation since the Caloosahatchee River discharges into San Carlos Bay, a bay which adjoins the southern end of Pine Island Sound.

A summary of the results of the salinity measurements is contained in Table 3.11, below:

Table 3.11 Time Averaged Salinity Values for the Four Inlets Connecting Pine Island Sound to the Gulf of Mexico

Inlet	Salinity (parts per thousand, ppt)
Northern Model Boundary	35.5 ± 0.9
Captiva Pass	33.0 ± 0.5
Redfish Pass	33.0 ± 0.5
Southern Model Pass	29.3 ± 1.0

3.5 Wind and Wave Data

During the months of October through December 1978, daily LEO observations were made along the Gulf coast of Captiva Island at the "Gulftide" tide station (see Figure 3.1 for location) in order to obtain wave and littoral current data (Balsillie, 1978). The only significant wave activity occurred during the period of November 27th to December 4th and Table 3.12 summarizes the pertinent data collected during that time.

Daily wind roses were established from data collected from the weather station owned and operated by the Captiva Erosion Prevention District. This station is located on the northern tip of Captiva Island.

Table 3.12 LEO Observations along the Gulf Coast of Captiva Island

Day	Time	Wave Height (m)	Wave Period (sec)	Width of Surf Zone (m)	Littoral Drift Direction	Magnitude (m/sec)
10/14	1800	<0.3	-	-	-	-
10/15	1230	1.6-1.9	8.0	30.0	N to S	0.15
10/17	1200	0.6-1.0	6.0	12.0	N to S	0.06
10/19	945	0.6-1.0	5.0	8.0	N to S	0.53
10/20	1200	<0.3	-	-	-	-

3.6 Sediment Data

Sediment cores, each approximately 15 cm long and five cm in diameter, were taken in and around Redfish Pass and its associated shoal system. Percentage shell content and granulometry analyses were performed on these samples and results can be made available upon request from the Coastal and Oceanographic Engineering Archives, Weil Hall, University of Florida, Gainesville, Florida, 32611.

CHAPTER IV

EVALUATION USING THE HYDRODYNAMIC MODEL

4.1 Numerical Model Verification

A simple sinusoidal tide was programmed to determine the time when the effect of the initial conditions become insignificant for the outside of the southern model boundary, Redfish Pass, Captiva Pass, and outside the northern model boundary. The respective phase lags used at each of these inlets were:

southern model boundary,	0.0 hours
Redfish Pass,	-4 hours
Captiva Pass	-3 hours
northern model boundary	-0.5 hours

A plot of the first 76 hours of the tidal variations and of the sinusoidal tide was prepared for two of the segments. After six hours, the maximum amplitude of the tidal response within the two segments remained constant. Therefore, model results were referenced to a time frame which begins six hours after the start of the model test run.

The results from the harmonic analysis of the "Gulftide" and "St. James City" tidal records were used as input data into the model. Phase lags of -0.05, 0.45, and 0.85 hours were applied to the "Gulftide" time record to account for the difference between the time of arrival of high tide at the entrance to Blind Pass, Redfish Pass, and Captiva Pass, respectively, to the time of arrival of high tide at the "Gulftide" tide station. Each tidal record generated by the model was adjusted so that the reconstructed tide at all model boundary locations were identical with the actual tide measured from midnight, October 28th through midnight, October 31st.

Information on the length, depth, and surface area of each of the nine model segments and of the four active inlets, as contained in Sections 3.2.1 and 3.2.2, were fed into the model together with bed frictional resistance factors for each segment and inlet. A time step of 300 seconds (5 min.) was used and each model run lasted for 72 hours. Graphical display of the tidal elevation at the outside of the southern model boundary and Redfish Pass, and at the inside of Blind and Redfish passes, together with a display of the velocities through the southern model boundary, and through Blind, Redfish and Captiva passes, were continuously plotted for the full 72 hours of each test run. Tabulated results of the flow into each segment, tidal elevation of each segment, the flow through each inlet, and the average velocity within each inlet were printed out every 10 minutes for the first 24 hours of each test.

The results from the test runs were compared with the actual tidal data collected at the "Gulftide", "St. James City", "Blind Pass", and "South Seas" tide stations between the 28th to 31st of October. Also, comparisons were made of the times of slack water and maximum velocities through the southern model boundary, Redfish Pass, and Captiva Pass measured during October 30th. Adjustments were made for the frictional resistance factors to achieve a satisfactory agreement between the predicted and measured results. The final values used in the model were:

Inlets: Darcy-Weisbach Friction Factor = 0.05
Model Segments: Darcy-Weisbach Friction Factor = 0.01

Results from the model, together with the appropriate measured data points are shown in Figures 4.1-4.4. Figures 4.1 and 4.2 show the tidal elevation at the outside and inside (TID 5) of Redfish Pass, and at the outside of the southern model boundary ("St. James City", TID 12) and

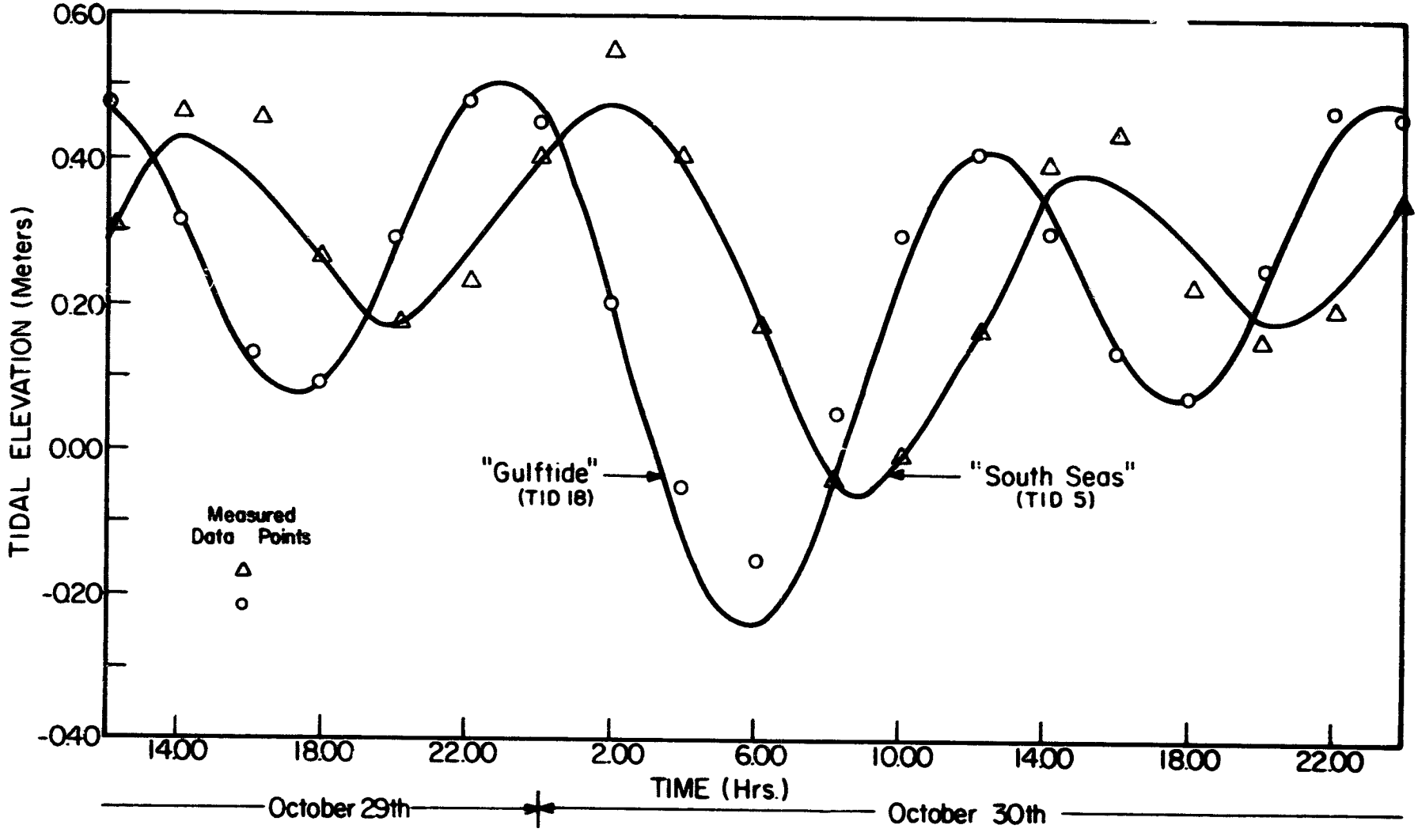

Figure 4.1 Tidal Elevation at the Outside (TID 18) and Inside (TID 5) of Redfish Pass.

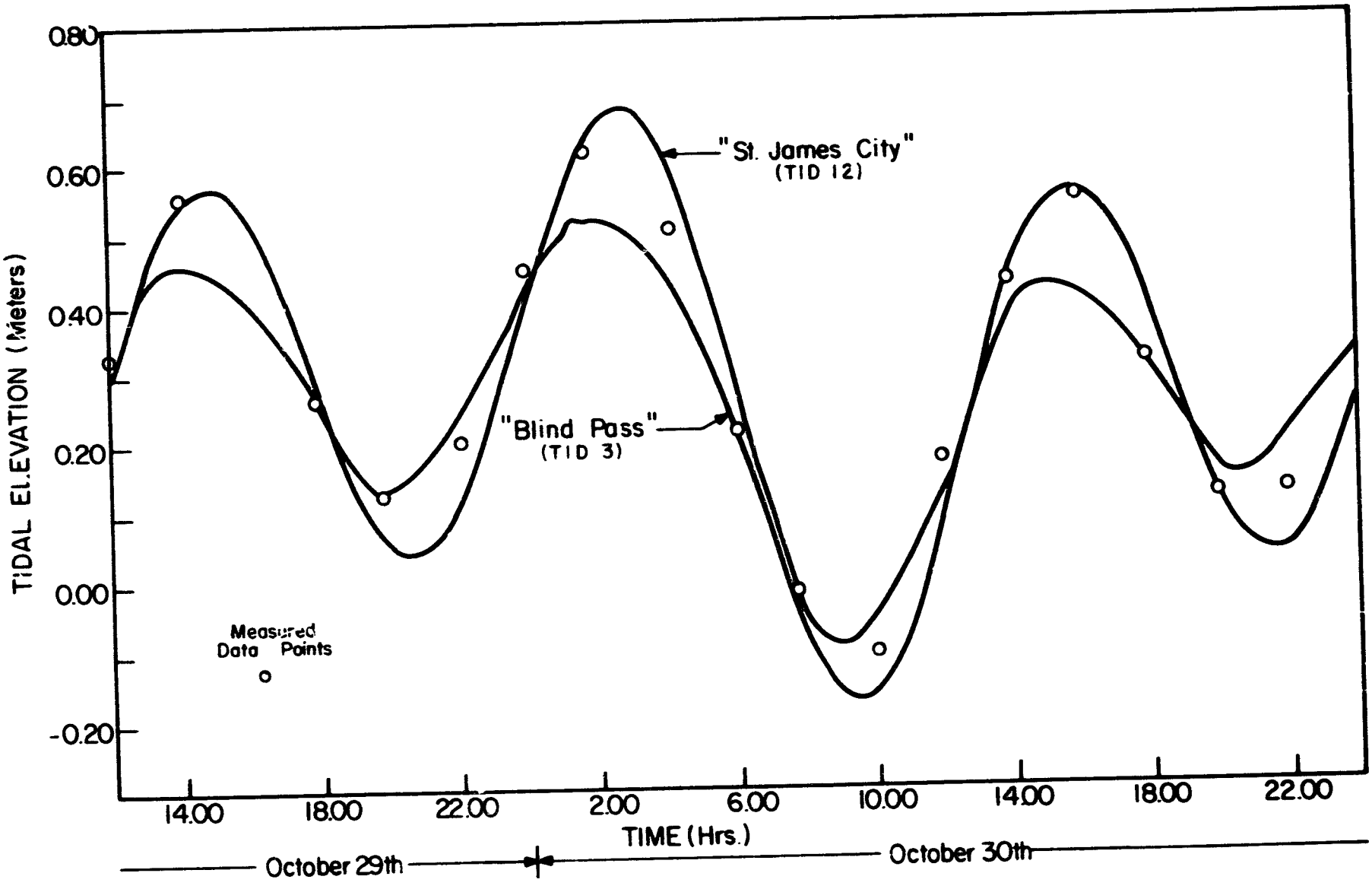

Figure 4.2 Tidal Elevation at the Outside of the Southern Model Boundary (TID 12) and the Inside of Blind Pass (TID 3)

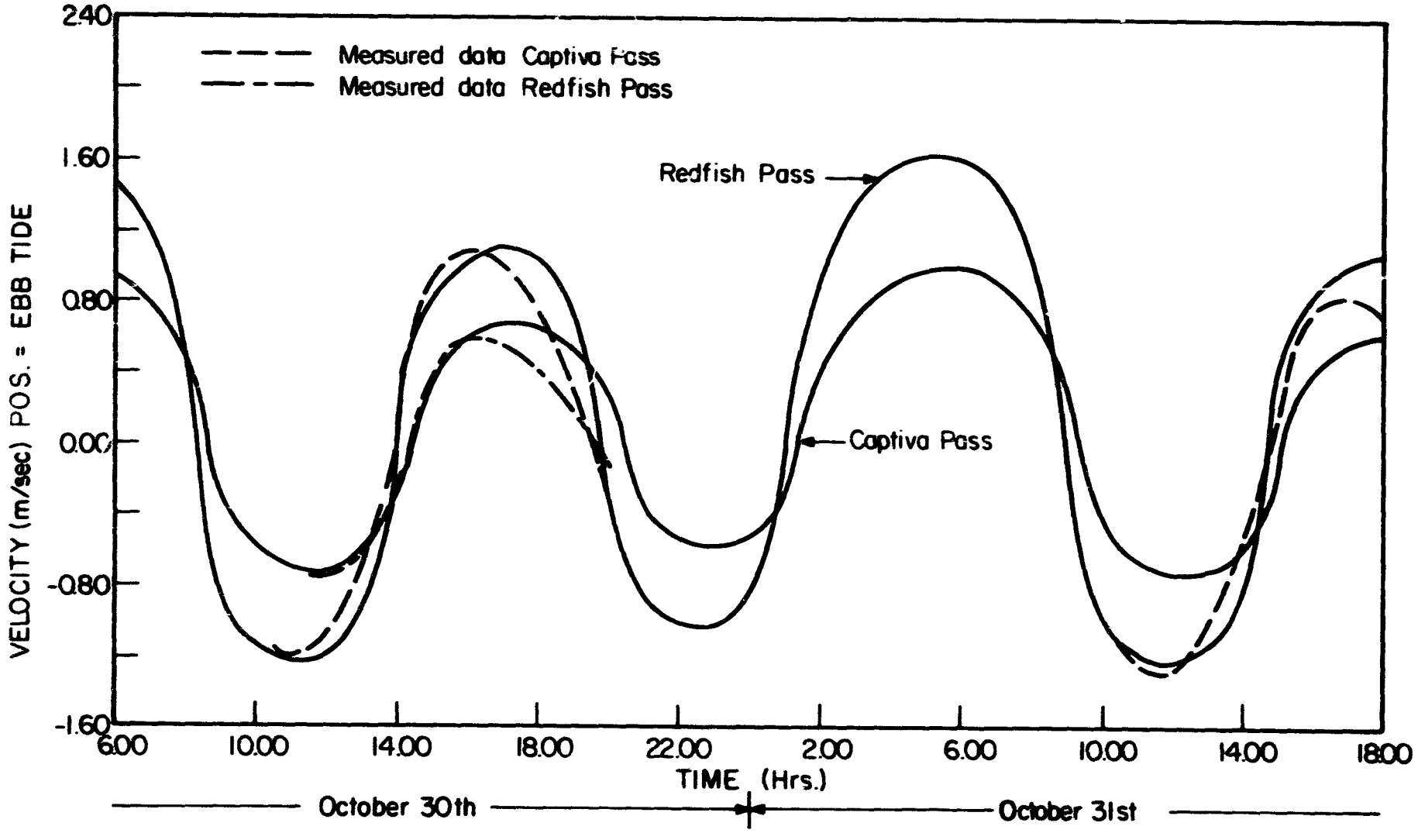

Figure 4.3 Velocities through Redfish Pass and Captiva Pass.

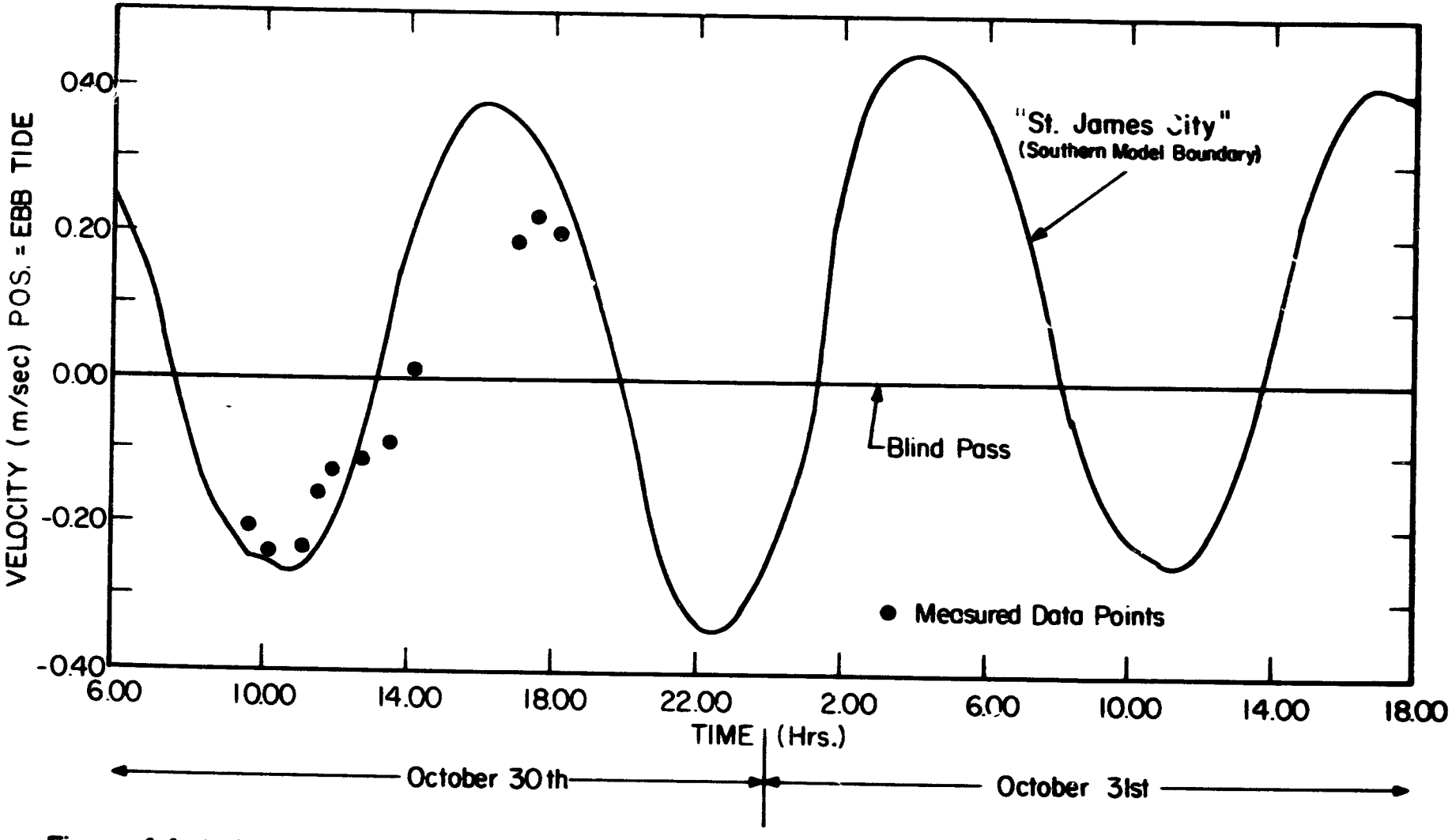

Figure 4.4 Velocities through Blind Pass and the Southern Model Boundary.

inside of Blind Pass (TID 3), respectively. Figures 4.3 and 4.4 show the velocities through Redfish and Captiva passes and through Blind Pass and the southern model boundary, respectively. These figures show that a good agreement between the measured and the predicted values for the computer model has been achieved. Hence, a satisfactory representation of the present day hydrodynamics of the Pine Island Sound and of the flow through the inlets which connect Pine Island Sound to the Gulf of Mexico has been presented in the form of the numerical model.

The model can be used to predict the effects due to the reopening of Blind Pass and other associated events, if it is assumed that the general morphological conditions within Pine Island Sound will not significantly change when alterations are made to the model boundary conditions.

Low altitude photography, together with information from a 1974 survey[2] of Blind Pass, was used to determine the historic channel length and width of the pass from 1966 to 1975. To determine the associated depth for each channel width, use was made of Figures 3.4a and 3.4b in Winton (1979) which are reproduced in this report as Figures 4.5 and 4.6. The basis for these figures comes from Mehta (1976), who plotted the cross-sectional mean depth, d_c, against the width, b_c, at mean water level at the throat section for inlets along the U.S. coastline and for some small scale and model inlets. Mean lines through the data points were drawn in order to indicate the average trend. Galvin (1971) studied the plan form features of 51 inlets located along the east and Gulf coasts of the United States. Width/depth data for inlets not

---

[2] W. D. Bender, Captiva Erosion Prevention District, Personal Communication.

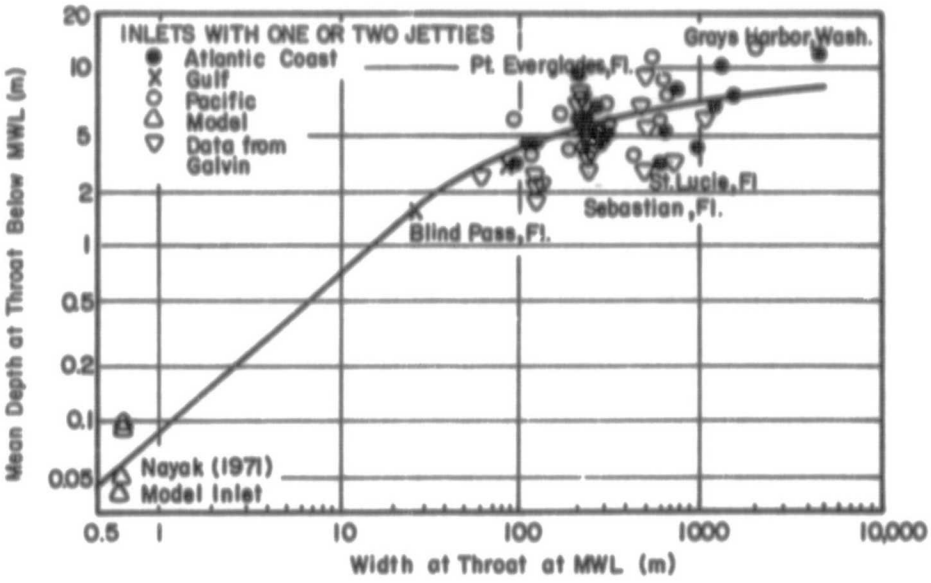

Figure 4.5 Width-Depth Relationship for Several North American Inlets and a Model Inlet. Data for Inlets with One or Two Jetties (Winton, 1979)

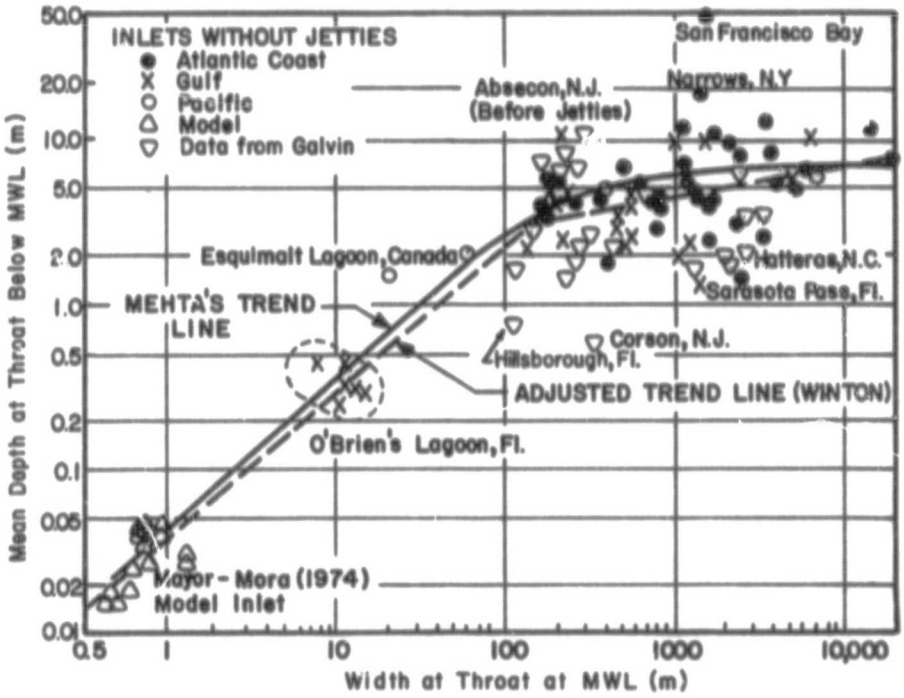

Figure 4.6 Width-Depth Relationship for Several North American Inlets and a Model Inlet. Data for Inlets Without Jetties (Winton, 1979)

already included by Mehta was abstracted from Galvin's report by Winton and, together with data from several inlets along the southwest coast of Florida, were included with the data shown in Figures 4.5 and 4.6. The inclusion of this data required a modification to Mehta's trend line. This new trend line for unimproved inlets can be expressed by the following width/depth ratios:

$$b_c \leq 150 \text{ m} \qquad d_c = 0.038\, b_c^{0.87} \text{ m} \qquad (4.1a)$$

$$b_c > 150 \text{ m} \qquad d_c = 1.164\, b_c^{0.19} \text{ m} \qquad (4.1b)$$

It should be noted that most of the data collected was from established inlets or from inlets with relatively good stability. Bedrock control of the inlet geometry must play some part in determining the width/depth ratio, thus explaining some of the variation as seen in these figures.

The 1974 survey of the entrance to Blind Pass was used to check the width/depth assumptions. The cross section under the bridge, which connects Captiva and Sanibel islands, is shown in Figure 4.7. The surface width at MLW is 64 m and the average depth is 2.08 m, which is deeper than the 1.42m vlaue predicted by Equation 4.1b. However, one reason for this difference is due to the constriction of the width by the bridge abutments (especially the northern abutment) and the consequent increased bottom scour. Consequently, the results shown in Figures 4.5, and 4.6 were used in the model and should be used for the design depths of channel dredging.

4.2 Model Application

The model was then used to evaluate the effect of opening Blind Pass to different channel widths which were varied from 10 m to 400 m. The effect of these changes on the maximum velocity through the other

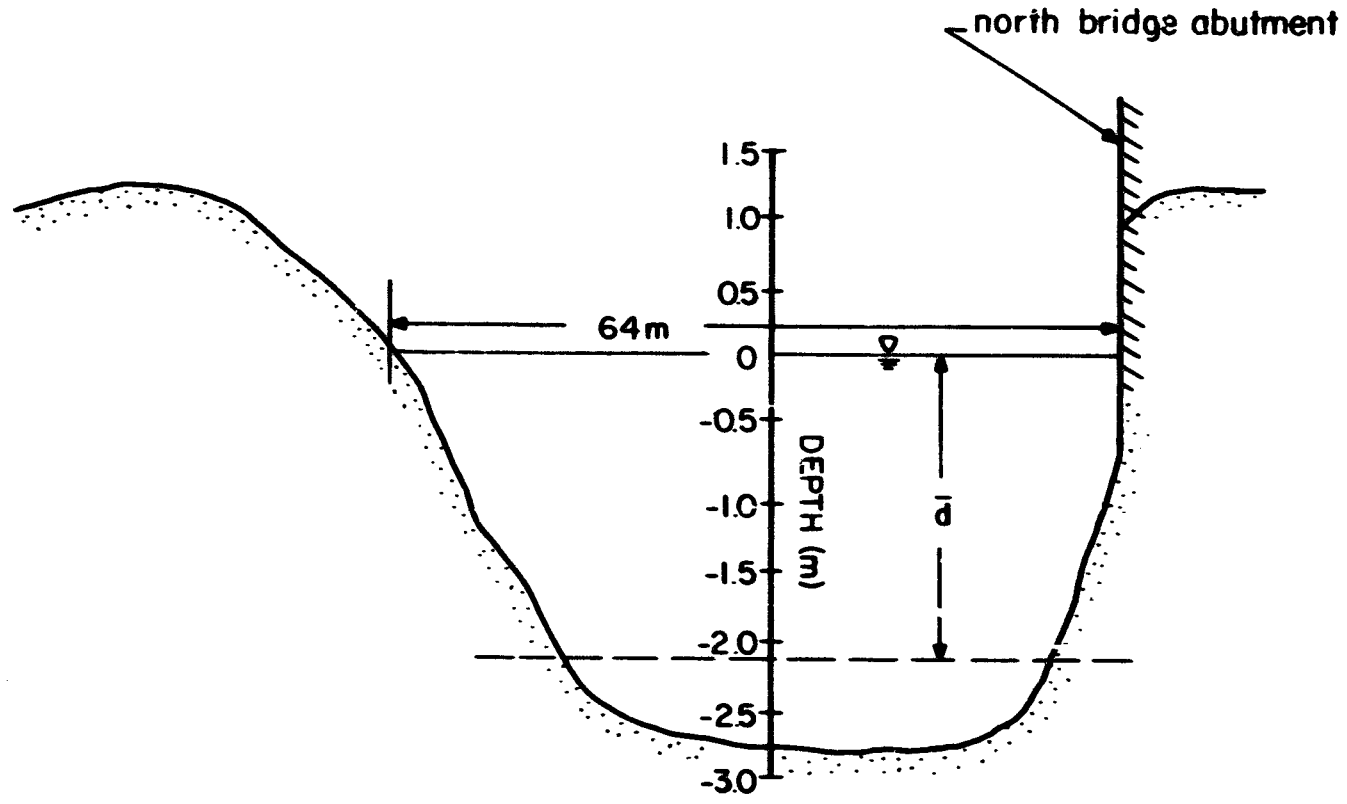

Figure 4.7 1974 Cross-section of the Inlet Channel at the Bridge over Blind Pass.

existing inlets is shown in Table 4.1 and in Figure 4.8. Due to the mixed nature of the tides in the Captiva region, there are up to four different maximum velocities through each inlet per tidal cycle, the maximum of which usually occurred during the spring ebb tide. The average maximum velocity, as shown in Table 4.1 and Figure 4.8, is the average value of the maximum predicted velocities during the spring flood, neap flood, and ebb tidal flows.

Figure 4.8 shows that a significant increase in the cross-sectional area of Blind Pass results in only a slight increase in the maximum spring velocity. At a cross-sectional area of 1400 m^2, the maximum spring velocity is 0.72 m/s, which is only 0.15 m/s greater than (26% increase over) the maximum spring velocity at an area of 28 m^2. The value of the average maximum velocity through Blind Pass increases with the increase in flow area from 0.45 m/s to 0.55 m/s, as the flow area increases from 2.5 to 1500 m^2.

The model was run for three cases of different depth but constant width to test whether an increase in the flow depth would result in a significant increase in the flow velocities. The results, given in Table 4.2, reveal that for a width equal to 75 m, a 66 percent increase in flow depth, results in only a 9 percent increase in the maximum spring velocities.

The reason for the very weak dependence of flow velocities on inlet cross-sectional area and flow depth is due to the fact that the tidal prism through Redfish Pass and through the southern model boundary provide a tidal head difference between the inner and outer ends of Blind Pass, and hence, is the dominant factor which controls the flows through Blind Pass. If Blind Pass was the only tidal inlet connecting

Table 4.1 Effect of Variation of Width and Corresponding Depth of Blind Pass on Maximum Velocities Through Each Inlet

Inlet	Width of Blind Pass (m)	Depth of Blind Pass (m)	Maximum Spring Velocity Through Inlet (m/s)	Average Maximum Velocity Through Inlet (m/s)	% Change In Maximum Spring Velocity From Existing Conditions
Blind Pass	10	0.28	0.57	0.45	---
Redfish Pass			1.60	1.23	-3.0
St. James City			0.42	0.36	+1.0
Captiva Pass			1.00	0.75	-2.0
Blind Pass	25	0.75	0.60	0.48	---
Redfish Pass			1.60	1.23	-3.0
St. James City			0.42	0.36	+1.0
Captiva Pass			1.00	0.75	-2.0
Blind Pass	50	1.10	0.62	0.49	---
Redfish Pass			1.60	1.23	-3.0
St. James City			0.42	0.36	+1.0
Captiva Pass			1.00	0.75	-2.0
Blind Pass	75	1.80	0.65	0.52	---
Redfish Pass			1.60	1.23	-3.0
St. James City			0.42	0.36	+1.0
Captiva Pass			1.00	0.75	-2.0

Table 4.1 (cont.)

Inlet	Width of Blind Pass (m)	Depth of Blind Pass (m)	Maximum Spring Velocity Through Inlet (m/s)	Average Maximum Velocity Through Inlet (m/s)	% Change In Maximum Spring Velocity From Existing Conditions
Blind Pass	100	2.00	0.66	0.52	---
Redfish Pass			1.60	1.23	-3.0
St. James City			0.42	0.36	+1.0
Captiva Pass			1.00	0.75	-2.0
Blind Pass	200	3.00	0.70	0.55	---
Redfish Pass			1.60	1.21	-3.0
St. James City			0.45	0.37	+7.1
Captiva Pass			0.95	0.71	-6.9
Blind Pass	300	3.05	0.70	0.55	---
Redfish Pass			1.57	1.21	-4.9
St. James City			0.45	0.38	+7.1
Captiva Pass			0.99	0.73	-3.0
Blind Pass	400	3.50	0.72	0.56	---
Redfish Pass			1.55	1.18	-6.1
St. James City			0.45	0.39	+7.1
Captiva Pass			0.95	0.74	-6.9

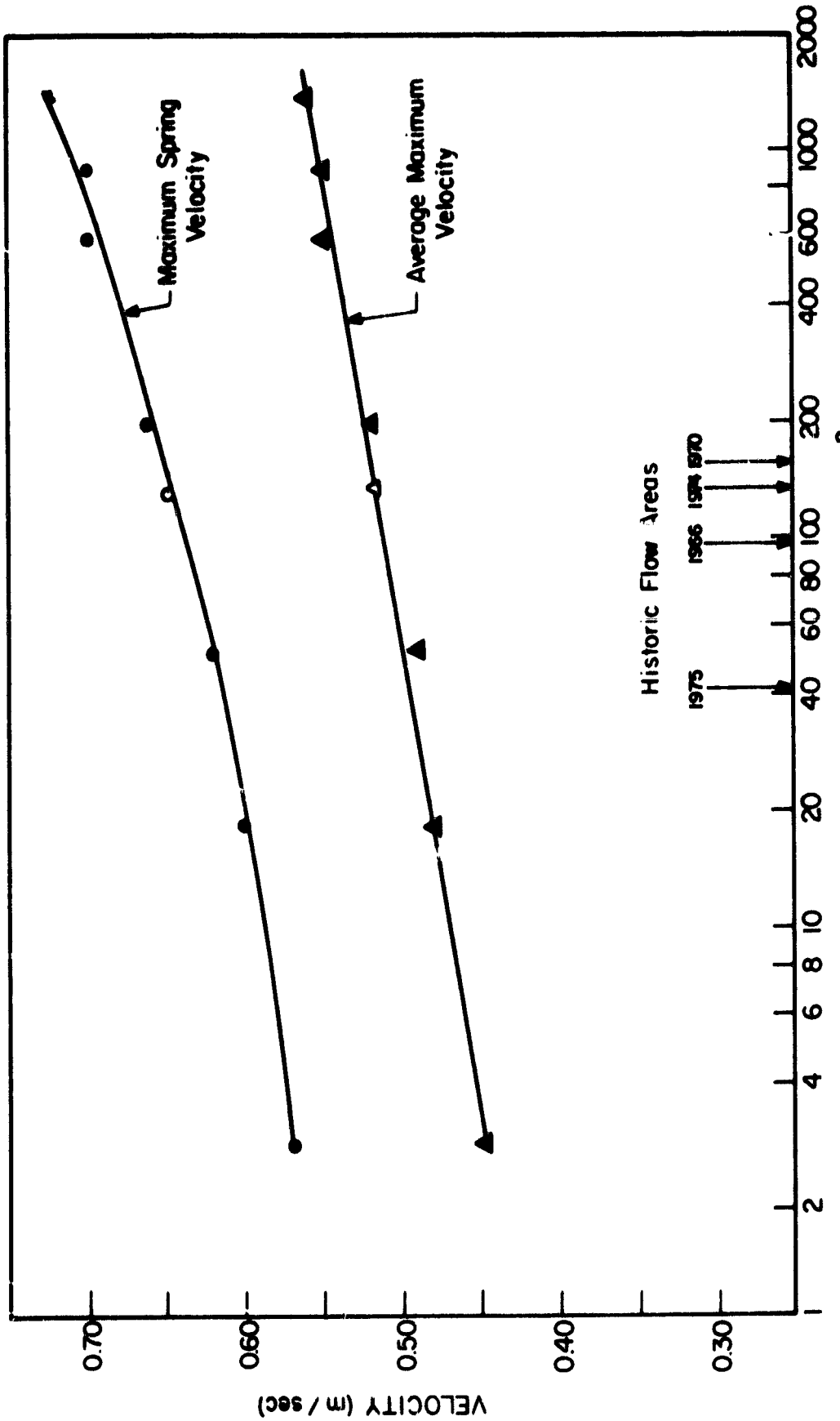

Figure 4.8 Variation of Computed Maximum Velocities through Blind Pass.

Table 4.2 Effect of Variation of Depth of Blind Pass on Maximum Velocities Through Each Inlet

Inlet	Width of Blind Pass (m)	Depth of Blind Pass (m)	Maximum Spring Velocity Through Inlet (m/s)	Average Maximum Velocity Through Inlet (m/s)	% Change In Maximum Spring Velocity From Existing Conditions
Blind Pass	75	1.80	0.65	0.52	---
Redfish Pass	75	1.80	1.60	1.23	-3.0
St. James City	75	1.80	0.42	0.36	+1.0
Captiva Pass	75	1.80	1.00	0.75	-2.0
Blind Pass	75	2.50	0.70	0.55	---
Redfish Pass	75	2.50	1.60	1.23	-3.0
St. James City	75	2.50	0.42	0.36	+1.0
Captiva Pass	75	2.50	1.00	0.75	-2.0
Blind Pass	75	3.00	0.71	0.55	---
Redfish Pass	75	3.00	1.60	1.23	-3.0
St. James City	75	3.00	0.42	0.36	+1.0
Captiva Pass	75	3.00	1.00	0.75	-2.0

Pine Island Sound to the Gulf of Mexico, then a far greater variation of maximum flow velocities with a change in flow area would be expected.

Table 4.1 shows that the effect of the reopening of Blind Pass on the flows through the other existing passes. The greatest percent change in the maximum spring velocities from present flow conditions is a 7.1 percent increase at the southern model boundary. This increase occurs when the cross-sectional area of Blind Pass was chosen to be 1400 m^2. Figure 4.8 shows the estimated or measured flow areas in 1966, 1970, 1974 and 1975. It is obvious that the flow area of 1400 m^2 is significantly larger than these historic flow areas. The maximum percent change in spring velocities through the other inlets for cross-sectional areas of Blind Pass up to approximately 200 m^2 (width = 75 m) are:

southern model boundary	+1%
Redfish Pass	-3%
Captiva Pass	-2%

The effect on the tides within Pine Island Sound due to the reopening of Blind Pass is predicted to be minimal. The greatest predicted changes in the tides behind Blind Pass occurs when the cross-sectional area for Blind Pass is chosen to be 1400 m^2. Under this condition the times of arrival of high and low water are predicted to be 45 minutes to one hour earlier than under present conditions and the tidal amplitude is increased by 0.04 m. The effect on the tides behind Redfish Pass is even less, with the times of arrival of high and low water being 15 to 20 minutes earlier than at present and with an increase of 0.02 m in the tidal amplitude.

The effects on the tides at both locations are significantly less for smaller cross-sectional areas of Blind Pass. The model results

indicate that the effect on the time sequence and amplitude of tides of Pine Island Sound, due to reopening Blind Pass, are negligible. However, there would be water interchange.

During the time of tidal data collection and subsequent analysis, it was noticed that the time of arrival of high and low water at the "St. James City" Station were delayed by approximately four hours with respect to the "Gulftide" station. Since the tidal wave moves generally northward along the southwest Florida coastline, the delay of the arrival times of high water at "St. James City" indicated that significant retardation due to flow constriction must be occurring between "St. James City" and the open waters of the Gulf of Mexico. The major restriction of flow comes from the Punta Rassa-Sanibel Causeway which was constructed in 1963, and which consists of three open piled sections and two very long spoil islands.

The tidal phase lag due to the causeway cannot be accurately estimated with only the data collected in 1978. However, estimates for two hours and four hours were obtained using the model. The results derived from this analysis indicate that the earlier arrival of the tide at "St. James City" causes a slight decrease in the maximum velocities through all of the inlets, except for the southern model boundary, which experienced a slightly greater velocity peak. More data and a more accurate hydrodynamic model of the Pine Island Sound and of San Carlos Bay are needed to confirm or modify these tentative results.

Redfish Pass is a relatively new inlet within the Pine Island Sound system, having opened in 1926 during a severe hurricane. Since then, it has increased in size and in tidal prism, and has trapped extensive

quantities of sand in the associated shoal system both in the Gulf of Mexico and in Pine Island Sound.

The additional tidal prism through Redfish Pass must have some effect on the flow through the adjacent inlets. Therefore, the hydrodynamic model was used to determine the effect with Blind Pass open and Redfish Pass closed. Despite the fact that the morphology and hydrodynamic characteristics of Pine Island Sound and the other inlets have changed since 1926, the model results indicated that the opening of Redfish Pass caused a slight decrease in the flows and in the maximum velocities through Blind and Captiva passes.

4.3 Summary and Conclusions

A computer program was developed to determine tidal effects on the various inlets connecting Pine Island Sound and the Gulf of Mexico. Input included data from field investigations, actual tidal records, inlet dimensions determined from aerial photography and previous studies. These adjustments resulted in a satisfactory representation of the present day hydrodynamics of the area that could accurately predict velocities of flow and tidal elevations.

The model was then used to determine the effects of reopening Blind Pass. Inlet dimensions and flow velocities were varied, yet, these changes did not significantly change the overall tidal response. Redfish Pass has increased in size and tidal prism since its opening in 1926. The effects of closing this pass were also examined by the model and results indicated no significant changes in flows through the other inlets.

In conclusion, the numerical model of Pine Island Sound and its associated inlets has been successfully calibrated with data collected

between June and December, 1978. Assuming that no significant changes from the measured conditions occur within Pine Island Sound, the numerical model predicts that the reopening of Blind Pass has negligible effects on the tides within Pine Island Sound and on the maximum velocities through the existing inlets.

BIBLIOGRAPHY

Balsillie, J. H., 1977, "Prediction of Longshore Transport in the Littoral Zone With and Without The Use of Breaking Wave Angles", in: Coastal Sedimentology, Tanner, W.F., editor, Proceedings of a Symposium on Coastal Research and the Department of Geology, Florida State University, Tallahassee, Florida.

Beaumont, Elie de, 1845, Lecons de Geologie Pratigue, pp. 223-252.

Brooks, H.K., 1973, The physical environment: Geological Oceanography, in: A Summary of Knowledge of the Eastern Gulf of Mexico, The State University System of Florida, Institute of Oceanography, St. Petersburg, Florida, p. 11E/1-11E/48.

Brunn, P., 1962, "Sea Level Rise as a Cause of Shore Erosion", Am. Soc. Civil Engineering Proceedings, Vol. 88, pp 117-130.

Captiva Erosion Prevention Commission, 1971, Beach Erosion Control Report and Recommendations for Captiva Island, Florida, 24 p.

Ceryak, R., 1980, A Mineralogical Analysis of Recent Beach Sands of the Gulf Coast of Florida, in: Southeastern Geological Society Guidebook No. 22, pp. 16-18.

Coastal Engineering Laboratory, 1974, Coastal Engineering Study of Captiva Island, Florida Engineering and Industrial Experiement Station, University of Florida, Gainesville, Florida, 131 p.

Galvin, C.J. and Kohler, R.R., 1971, "Office Study of Inlets - Geometry", Project 042202, Unpublished Data, U.S. Army Corps of Engineers, Coastal Engineering Research Center, Fort Belvoir, Virginia.

Gilbert, G.K., 1885, "Lake Bonneville", U.S. Geol. Survey, Mem. 1, 438 p.

Herwitz, S.R., 1977, Elements of the Cayo Costa Island Ecosystem, Lee County, Florida, New College USF, 4th Annual Conference of the Restoration of Coastal Vegetation in Florida, pp. 152-165.

Hoyt, J.H., 1967, "Barrier Island Formation", Geol. Soc. America, Bulletin 78, pp. 1125-1136.

Ippen, A.T., 1966, Editor, Estuary and Coastline Hydrodynamics, McGraw-Hill, 744 p.

Johnson, D.W., 1919, Shore Processes and Shoreline Development, John Wiley, 584 p.

Mehta, A.J., 1976, "Stability of Some New Zealand Coastal Inlets," New Zealand Journal of Marine and Freshwater Research, Wellington, New Zealand, Letter to the Editor, Vol. 10, No. 4, pp. 737-742.

Mehta, A.J. and Brooks, H.K., 1973, "Mosquito Lagoon Barrier Beach Study", Shore and Beach, Vol. 41, No. 2, pp. 26-34.

Missimer, T.M., 1973, "Growth Rates of Beach Ridges on Sanibel Island, Florida", Trans. G.C.A.G.S., Vol. 23, pp. 383-388.

Piccolo, J., 1976, "A Guide for the Use of Tidal and Geodetic Datum Planes", Unpublished Notes, Hydraulic Laboratory, Department of Civil Engineering, University of Florida, Gainesville, Florida.

Schureman, P., 1940, "Manual of Harmonic Analysis and Prediction of Tides," U.S. Department of Commerce, Coast and Geodetic Survey, Special Publication No. 98, U.S. Government Printing Office.

Shepard, F.P., 1960, "Gulf coast barriers", in Recent Sediments of Northwestern Gulf of Mexico, Am. Assoc. Petrol. Geol., Tulsa, Oklahoma, 394 p.

Silberman, L.Z., 1980, A Sedimentological Study of the Gulf Beaches of Sanibel and Captiva Islands, Florida, Unpublished M.S. Thesis, Florida State University, Tallahassee, Florida, 132 p.

Stapor, F.W. and T. D. Mathews, 1980, C-14 Chronology of Holocene Barrier Islands, Lee County, Florida in W.F. Tanner, "Shorelines Past and Present", Dept. Geol., Florida State University, Tallahassee, Vol. 1, pp. 47-67.

Riggs, S.R., 1976, Beach Geology, in: The Sanibel Report, Editor: John Clark, Washington, D.C., The Conservation Foundation, pp. 229-255.

U.S. Army Corps of Engineers, 1969, Beach Erosion Control Study on Lee County, Florida, Jacksonville District, Jacksonville, Florida, Series No. 60, 41 p.

Winton, T.C., 1979, Long and Short Term Stability of Small Tidal Inlets, M.S. Thesis, University of Florida, Gainesville, Florida, UFL/COEL-79/006.

APPENDIX A

The following Carbon 14 dates were obtained on materials sampled by H. K. Brooks, 1971 and 1978. Test pits were dug and materials for dating were carefully selected on the basis of freshness, color and absence of wear. The surf clam, Spisula was used in most cases because, during storms, these shells are thrown up on the beach in great quantities. Where not obtainable or where there was evidence of reworking, shells of Chione cancellata, the barred venus, was used Some sites were checked by two analyses. In every case, the date plotted on Figures and are the youngest dates. For this report, the half life of 5570 years has been chosen. The samples analyzed by Geochron Laboratories, Cambridge Massachusetts (GX-XXXX) were C 13 corrected. The previous samples, dated by Gakushuin University, Tokyo, Japan (GAK-XXXX), are uncorrected dates. B.P. (Before Present) is 1950.

Laboratory No.	Sample description and location	Carbon 14 years B.P.
GX-6085	Shell, Spisula, north end Cayo Costa, depth 3-5 ft., 26° 41' N, 82° 14.9' W.	2135 ± 125
GX-6086	Shell, Spisula, north end Cayo Costa depth 3-6 ft., 26° 41' N, 82° 15' W.	605 ± 125
GX-6087	Shell, Spisula, highest beach ridge, north end Cayo Costa, depth 3.5 ft., 26° 41' N, 82° 15.2' W.	710 ± 120
GX-6088	Shell, Spisula, east side Buck Island 2-3 ft. depth, 26° 30.1 N, 82° 10.8' W.	1565 ± 120
GX-6089	Shell, Spisula, west side Buck Island 2-3.5 ft. depth, 26° 31' N, 82° 10.9' W.	1005 ± 145
GX-6090	Shell, Spisula, near Murdock Bayou, Cayo Costa, 2 ft. depth, 26° 38.1 N, 82° 13.9' W.	1930 ± 125

GX-6091	Shell, Spisula, low beach ridge east of mangroves, Captiva Pass, Cayo Costa, 26° 37' N, 82° 13.3 W.	1705 ± 135
GX-6092	Shell, Spisula, in mangrove peat, Captiva Pass, depth 1 ft., 26° 36.6' N, 82° 13.5'W	1520 ± 130
GX-6093	Mangrove peat, probably contaminated by younger roots, same as GX-6092.	845 ± 130
GX-6094	Red mangrove stump in place on fore beach, south end Cayo Costa, 26° 37'N, 82° 13.5'W	400 ± 120
GX-6095	Shell, Spisula, near Murdock Bayou, Cayo Costa, 26° 39' N, 82° 14.4' W.	2060 ± 135
GX-6096	Shell, Spisula, southwest of Old Wave Mound, Cayo Costa, 26° 39.3 N, 82° 14.4 W.	2665 ± 130
GX-6097	Shell, Spisula, Gulf side, Cayo Costa, depth 2 ft., 26° 40.3' N, 82° 15.2 W.	1670 ± 100
GX-6098	Shell, Spisula, east of road on Wulfert Ridge, Sanibel, depth 2.5 ft., 26° 29.3 N, 82° 13.3' W.	1840 ± 120
GX-6099	Shell, Chione, probably reworked, same as above.	2380 ± 130
GX-6100	Shell, Chione, east of Dinkens Bayou, Sanibel, depth 2 ft., 26° 28.8 N, 82° 10.2' W.	655 ± 115
GX-6101	Shell, Chione, 0.8 mi. S.E. Wulfert, Sanibel, depth 2 ft., 26° 28.5' N, 82° 11.0' W.	475 ± 135
GX-6102	Shell, Spisula, reworked, same as above.	725 ± 100
GX-6103	Shell, Chione, back of city hall, Sanibel, depth 2.5 ft., 26° 26' N, 82° 4.4' W.	1550 ± 130
GX-6105	Shell, Chione, low ridges in mangrove swamp, Sanibel, 26° 27.8' N, 82° 9' W.	3230 ± 145
GX-6106	Shell, Spisula, broken and reworked, south of Tween Waters Inn, Captiva, depth 3 to 5 ft., 26° 30.5' N, 82° 11.3 W.	1885 ± 125
GX-6107	Shell, Chione, same as above.	1015 ± 145

GX-6120	Shell, Spisula, at pond, abandoned airstrip, Captiva, depth 3 ft., 26° 31.7' N, 82° 11.4' W.	1290 ± 125
GX-6121	Shell, Spisula, Foster Point, North Captiva, depth 8.5 ft., 26° 34.9' N, 82° 12.5' W.	1320 ± 145
GX-6122	Shell, Spisula, north end Buck Island, depth 2.5 ft., 26° 30.9 N, 82° 10.8' W.	995 ± 115
GX-6123	Shell, Chione, west of Tarpon Bay, Sanibel, depth 2 ft., 26° 26.5' N, 82° 5.8' W.	3010 ± 130
Gak-4020	Shell, Spisula, low ridge just south of Periwinkle Drive, Sanibel, depth 2 ft., 26° 27' N, 82° 03' W.	380 ± 75
Gak-4021	Shell, Dinocardium, same	460 ± 80
Gak-4022	Shell, Chione, canal to Tarpon Bay, Sanibel, depth 2.5 ft., 26° 27' N, 82° 4.9' W.	2150 ± 90
Gak-4023	Shell, Chione, worn, same as above.	2660 ± 75
Gak-4024	Shell, Chione, Wulfert Rd., Sanibel, depth 3.5 t., 26° 28' N, 82° 9.2' W.	1560 ± 90

```
C     ************************************************************
C     *                                                          *
C     *                    *** LAGOON  TIDES ***                 *
C     *                                                          *
C     *      THIS PROGRAM HAS BEEN DEVELOPED TO CALCULATE: 1/ THE*
C     *    TIDAL RESPONSE OF PINE ISLAND SOUND DUE TO THE ASTRONOMICAL
C     *    TIDES IN THE GULF OF MEXICO, AND              2/ THE*
C     *    RESULTING FLOWS AND THE AVERAGE VELOCITY OF EACH FLOW
C     *    THROUGH EACH OF THE INLETS WHICH CONNECT PINE ISLAND SOUND
C     *    TO THE GULF OF MEXICO.(IE.BLIND PASS,REDFISH PASS,CAPTIVA
C     *    PASS,AND THE NORTHERN AND SOUTHERN MODEL BOUNDARIES OF PINE
C     *    ISLAND SOUND).                                        *
C     *                                                          *
C     *      PINE ISLAND SOUND IS DIVIDED UP INTO 9 SEGMENTS,CALLED
C     *    "BOXES",WITHIN WHICH THE HYDRAULIC PARAMETERS ARE CONSIDER-
C     *    ED TO BE CONSTANT.THE TIDAL VARIATION WITHIN THE SOUND IS
C     *    DETERMINED BY CALCULATING THE FLOWS FROM ONE BOX INTO
C     *    ANOTHER (RESULTING FROM THE FLOWS THROUGH EACH INLET) WHICH
C     *    GIVE RISE TO CHANGES IN TIDAL ELEVATION.GULF TIDAL VARIA-
C     *    TIONS,REFERENCED TO THE TIDE AT INLET NO.11,ARE GIVEN
C     *    AT THE OUTSIDE OF EACH INLET,AND SO THE FLOWS THROUGH THE
C     *    INLETS ARE THEN CALCULATED BY KNOWING THE DIFFERENCE IN
C     *    WATER ELEVATION ACROSS THE INLET.
C     *      THE MODEL USES THE VERTICALLY INTEGRATED,SEMI-LINEARIZED
C     *    ONE-DIMENSIONAL EQUATION OF MOTION AND THE ONE-DIMENSIONAL
C     *    EQUATION OF CONTINUITY,BOTH IN FINITE DIFFERENCE FORM,TO
C     *    TO CALCULATE THE FLOWS INTO EACH BOX(SUBROUTINE "QCALC")
C     *    AND THE RESULTING CHANGES IN TIDAL ELEVATION(SUBROUTINE
C     *    "ETACAL"),RESPECTIVELY.THESE EQUATIONS ARE COMBINED TOGETHER
C     *    TO CALCULATE THE FLOWS THROUGH THE INLETS.
C     *                                                          *
C     *      A LIST OF SYMBOLS USED WITHIN THE PROGRAM,THEIR
C     *    DEFINITION AND THE CORRECT UNITS (WHERE APPLICABLE) IS AS
C     *    FOLLOWS:
C     *                      ** LIST OF SYMBOLS **               *
C     *                                                          *
C     *    L(I)     -:AVE. LENGTH OF EACH BOX          _ M '    *
C     *    W(I)     -:AVE.WIDTH OF EACH BOX            _ M '    *
C     *    D(I)     -:AVE. DEPTH OF EACH BOX           _ M '    *
C     *    TAU(I)   -:AVE.WIND STRESS ACTING ON THE WATER       *
C     *               SURFACE OF EACH BOX              _ N/M**2 '*
C     *    QF(I)    -:AVE. FRESH WATER INFLOW PER UNIT LENGTH    *
C     *               INTO EACH BOX                    _M**3/SEC/M'*
C     *    LI(I)    -:EQUIVALENT LENGTH OF EACH INLET  _ M '    *
C     *    WI(I)    -:EQUIVALENT WIDTH OF EACH INLET   _ M '    *
C     *    DI(IR)    -:EQUIVALENT DEPTH OF EACH INLET  _ M '    *
C     *     AC(I)    -:EQUIVALENT CROSS SECTIONAL AREA OF EACH   *
C     *                 INLET                           _ M**2 '*
```

```
C     *     KEN(I)  -:ENTRANCE LOSS COEFF. FOR EACH INLET                    *
C     *     KEX(I)  -:EXIT LOSS COEFF. FOR EACH INLET                        *
C     *     F(I)    -:DARCY-WEISBACH FRICTION FACTOR FOR                     *
C     *               EACH INLET                                             *
C     *     TA(I)   -:TIDAL AMPLITUDE AT THE OUTSIDE END OF                  *
C     *               EACH INLET                          - M .              *
C     *     RHO     -:MASS DENSITY OF AIR                 - KG/M**3 .        *
C     *     G       -:GRAVITATIONAL CONSTANT              - M/SEC**2 .       *
C     *     T       -:TIME                                - SECS .           *
C     *     DELTAT  -:TIME INCREMENT                      - SECS .           *
C     *     TOTTIM  -:TOTAL TIME LENGTH OF MODEL TEST RUN - HOURS .          *
C     *     NT      -:NUMBER OF TIME STEPS USED IN EVALUATION                *
C     *               OF TIDAL RESPONSE                                      *
C     *     ETA(I)  -:TIDAL VARIATION ABOVE M.S.L. IN EACH BOX               *
C     *               AND IN INLET SECTIONS               - M .              *
C     *     Q(I)    -:AVE. FLOWS INTO EACH BOX OR THROUGH                    *
C     *               EACH INLET                          - M**3/SEC .       *
C     *     V(I)    -:AVE. VELOCITY OF EACH FLOW THROUGH                     *
C     *               EACH INLET                          - M/SEC .          *
C     *                                                                      *
C     *                                                                      *
C     ************************************************************************
C
C
      DIMENSION W(9),WI(23),QF(9),D(9),DI(23),F(23),TA(23),ETA(24),Q(24)
     $,V(23),AC(23),TAU(9),TID12(900),TID3(900),TID5(900),TID18(900),
     $FLOW11(865),FLOW14(865),FLOW17(865),FLOW20(865)
      DIMENSION ETA12(865),ETA15(865),ETA18(865),ETA21(865),ETA24(865)
      REAL L(9),LI(23),KEN(23),KEX(23),PI,PERIOD
      DO 5 I=1,23
5     F(I)=0.05
      READ(5,101) (L(I),W(I),D(I),QF(I),TAU(I),F(I),I=1,9)
      READ(5,102) (LI(I),WI(I),DI(I),KEN(I),KEX(I),F(I),TA(I),I=11,23,3)
      READ(5,103) TOTTIM,DELTAT
      WRITE(6,104)
      WRITE(6,105) (I,L(I),W(I),D(I),QF(I),TAU(I),I=1,9)
      WRITE(6,106)
      WRITE(6,107)
      WRITE(6,108) (I,LI(I),WI(I),DI(I),KEN(I),KEX(I),F(I),TA(I),I=11,23
     $,3)
      WRITE(6,106)
      WRITE(6,109) TOTTIM
      WRITE(6,110) DELTAT
C
      NTMAX=TOTTIM*3600.0/DELTAT
      CALL TIDCAL(ETA12,ETA15,ETA18,ETA21,ETA24)
```

```
      NCOUNT=0
      DO 10   I=1,24
      ETA(I)=0.0
10    Q(I)=0.0
      DO 30   NT=1,NTMAX
         T=(NT-1)*DELTAT
         ETA(12)=ETA12(NT)
         ETA(15)=ETA15(NT)
         ETA(18)=ETA18(NT)
         ETA(21)=ETA21(NT)
         ETA(24)=ETA24(NT)
         CALL QCALC(L,W,D,QF,LI,WI,DI,KEN,KEX,F,ETA,Q,V,AC,TAU,DELTAT)
         CALL ETACAL(Q,L,W,DELTAT,QF,ETA)
         IF(NT.LT.72) GO TO 30
         TID12(NT)=ETA(12)
         TID3(NT)=ETA(3)
         TID5(NT)=ETA(5)
         TID18(NT)=ETA(18)
         FLOW11(NT)=V(11)
         FLOW14(NT)=V(14)
         FLOW17(NT)=V(17)
         FLOW20(NT)=V(20)
         NCOUNT=NCOUNT+1
         IF(NT.GE.298) GO TO 30
         IF(NCOUNT-2) 30,15,15
15       NCOUNT=0
         TIME=T/3600.0
         WRITE(6,106)
         WRITE(6,111) NT,TIME
         WRITE(6,112)
         K=10
         DO 20 M=1,5
         J=K+M
         WRITE(6,113) M,Q(M),ETA(M),J,Q(J),V(J)
            K=K+2
20       CONTINUE
         DO 25 MM=6,9
         WRITE(6,113) MM,Q(MM),ETA(MM)
25       CONTINUE
30    CONTINUE
      CALL TIMES2 (1,864,12.0,4.0,TID12,TID3,12.0,864,1)
      CALL TIMES2 (1,864,12.0,4.0,TID18,TID5,12.0,864,1)
      CALL TIMES3(1,864,12.0,4.0,FLOW11,FLOW14,12.0,864,1)
      CALL TIMES3(1,864,12.0,4.0,FLOW17,FLOW20,12.0,864,1)
C
1.1   FORMAT(6F8.2)
102   FORMAT(3F8.2,4F7.3)
103   FORMAT(2F6.2)
```

```
104   FORMAT('1',T60,'LAGOON  DATA'//T10,'BOX NUMBER',T29,'AVE. LENGTH',
     $T50,'AVE. WIDTH',T70,'AVE. DEPTH',T86,'FRESH WATER INFLOW',T106,
     $'WIND STRESS ON BOX'/T34,'(M)',T54,'(M)',T74,'(M)',T89,
     $'(M**3/SEC/M)',T111,'(N/M**2)')
105   FORMAT('0',T4,I2,T30,F8.2,T50,F8.2,T72,F6.2,T92,F6.2,T112,F6.2)
106   FORMAT(//)
107   FORMAT('0',T60,'INLET  DATA'//T4,'INLET NUMBER',T19,
     $'EFFECT. LENGTH',T35,'EFFECT. WIDTH',T51,'EFFECT. DEPTH',T67,
     $'ENTRANCE LOSS',T85,'EXIT LOSS',T99,'FRICTION FACTOR',T114,
     $'TIDAL AMPLITUDE'/T25,'(M)',T41,'(M)',T57,'(M)',T68,'COEFF.. KEN '
     $,T84,'COEFF.. KEX',T105,'F',T121,'(M)')
108   FORMAT('0',T9,I2,T22,F8.2,T38,F8.2,T55,F6.2,T71,F5.3,T87,F5.3,T103
     $,F6.3,T119,F6.3)
109   FORMAT('0',T5,'TOTAL TIME LENGTH OF MODEL TEST RUN = ',T44,F6.2,
     $T51,'(HOURS)')
110   FORMAT('0',T5,'TIME INCREMENT = ',T23,F6.2,T30,'(SECS)')
111   FORMAT('0',T5,'NUMBER OF THIS TIME STEP = ',T32,I5,T44,
     $'ELAPSED TIME = ',T60,F8.2,T69,'(HOURS)')
112   FORMAT('0',T26,'LAGOON TIDE OUTPUT',T86,'INLET FLOW OUTPUT'//T10,
     $'BOX NUMBER',T28,'FLOW INTO BOX',T45,'TIDAL VARIATION,ETA,',T69,
     $'INLET NUMBER',T86,'FLOW THROUGH INLET',T107,'AVERAGE VELOCITY'/
     $T30,'(M**3/SEC)',T49,'IN BOX  (M)',T90,'(M**3/SEC)',T107,
     $'THRO. INLET (M/SEC)')
113   FORMAT(1X,T5,2(9X,I2,9X,2(5X,F10.3,5X)))
      WRITE(6,114)
114   FORMAT('1')
      STOP
      END
```

```
C
C
C                          **********************************
C
      SUBROUTINE QCALC(L,W,D,QF,LI,WI,DI,KEN,KEX,F,ETA,Q,V,AC,TAU,DE_TAT
     $)
      DIMENSION W(9),D(9),QF(9),WI(23),DI(23),F(23),ETA(24),Q(24),V(23),
     $TAU(9),AC(23)
      REAL L(9),LI(23),KEN(23),KEX(23)
      G=9.807
      RHO=1.225
C
C   CALCULATION OF FLOWS THROUGH EACH INLET
C
      ETA(10)=ETA(1)
       ETA(13)=ETA(3)
      ETA(16)=ETA(5)
      ETA(19)=ETA(7)
      ETA(22)=ETA(9)
      DO 10  I=11,23,3
         AC(I)=WI(I)*(DI(I)+0.5*(ETA(I-1)+ETA(I+1)))
          IF(AC(I).EQ.0.0) GO TO 5
         R=AC(I)/(WI(I)+2.0*DI(I)+ETA(I-1)+ETA(I+1))
         AB=ETA(I-1)-ETA(I+1)
         IF(ABS(AB)-0.001) 8,8,9
8        Q(I)=0.0
         GO TO 10
9        SIGN=AB/ABS(AB)
         Q(I)=AC(I)*SQRT((2.0*G*ABS(AB))/(KEN(I)+KEX(I)+(F(I)*LI(I))/(4.
     $   0*R)))*SIGN
C  ***** REMOVE Q(14)=0.0 WHEN BLIND PASS IS OPENED ******
         V(I)=Q(I)/AC(I)
         GO TO 10
5        V(I)=0.0
10    CONTINUE
C
C   CALCULATION OF FLOWS INTO EACH BOX
C
      DO 20  J=2,9
         IF(W(J)-W(J-1)) 11,12,12
11       WW=W(J)
         GO TO 13
12       WW=W(J-1)
13       DELTAX=0.5*(L(J)+L(J-1))
         DA=D(J)+ETA(J)
         DB=D(J-1)+ETA(J-1)
         IF(DA.LT.0.0) DA=0.0
```


C-2

```
      IF(DB.LT.0.0) DB=0.0
      DAVE=DA*DB*(2.0*DELTAX/(L(J)*SQRT(DB)+L(J-1)*SQRT(DA)))**2
      WIDTH=0.5*(W(J)+W(J-1))
      ACAVE=DAVE*WIDTH
      QP=Q(J)
      IF(TAU(J).EQ.0.0) GO TO 18
      WIND=WIDTH/RHO*TAU(J)
      GO TO 19
18    WIND=0.0
19    IF(ACAVE.EQ.0.0) GO TO  21
      BOTTOM=WIDTH*F(J)*ABS(QP)*DELTAT/(8.0*(ACAVE)**2)
      GO TO 22
21    BOTTOM=0.0
22     Q(J)=(QP+WIND-ACAVE*G*(ETA(J)-ETA(J-1))*DELTAT/DELTAX)/(1.0+
     $   BOTTOM)
20   CONTINUE
     Q(1)=-(Q(11)+Q(2))
     RETURN
     END
```

```
C
C
C                          **********
C
C
      SUBROUTINE ETACAL(Q,L,W,DELTAT,QF,ETA)
      DIMENSION Q(24),W(9),QF(9),ETA(24)
      REAL L(9)
C
CC   CALCULATE THE TIDAL VARIATION IN EACH BOX
C
      DO 10  I=2,8
         ETAP=ETA(I)
         ETAF=QF(I)*DELTAT/W(I)
         ETA(I)=ETAP+(Q(I)-Q(I+1))*DELTAT/(L(I)*W(I))+ETAF
10    CONTINUE
      ETA(1)=ETA(1)-(Q(2)+Q(11))*DELTAT/(L(1)*W(1))+QF(1)*DELTAT/W(1)
      ETA(3)=ETA(3)-Q(14)*DELTAT/(L(3)*W(3))
      ETA(5)=ETA(5)-Q(17)*DELTAT/(L(5)*W(5))
      ETA(7)=ETA(7)-Q(20)*DELTAT/(L(7)*W(7))
      ETA(9)=ETA(9)-(Q(23)-Q(9))*DELTAT/(L(9)*W(9))+QF(9)*DELTAT/W(9)
      RETURN
      END
```

```
C
C
C                  ************************************
C                  ************************************
C
C
      SUBROUTINE TIDCAL(ETA12,ETA15,ETA18,ETA21,ETA24)
      DIMENSION ETA12(865),ETA15(865),ETA18(865),ETA21(865),ETA24(865),
     $AMP(16),ETA(16)
      REAL PERIOD(16),PHASE(16)
C     NH=NO.OF TIDAL HARMONIC CONSTITUENTS USED IN RECONSTRUCTION
      NH=16
C     M=NO.OF RECONSTRUCTED ETA VALUES TO BE PLOTTED.
      M=764
C     ISTV=NO.OF 5-MIN PTS TO BE SKIPPED BEFORE CALCULATING THE ETA
C     VALUES.
C     TLAG=TIME LAG OF TIDES WRT.'GULFTIDE'DATA SET.FOR STJAMES TIDE
C     (ETA12) AND FOR COYACOSTA TIDES(ETA24).TLAG=0.0 (MUST BE INCLUDED)
C     FOR BLIND PASS(ETA15),REDFISH PASS(ETA18) AND FOR CAPTIVA PASS
C     (ETA21) TIDES,TLAG=TIME DIFF.B/W THE ACTUAL TIDES AT THESE PASSES
C     AND THE TIDE MEASURED AT CAPTIVA PO.('GULFTIDE'). TLAG=+VE IF
C     TIDE LAGS GULFTIDE,&TLAG=-VE IF TIDE PRECEEDES GULFTIDE.
C
      DO 110 I=1,5
         READ(5,20) ISTV,AO,TLAG
20       FORMAT(I4,6X,F6.4,4X,F5.2)
         DO 30 K=1,NH
           READ(5,25) AAMP,APER,APHASE
25         FORMAT(F6.4,3X,F7.3,3X,F8.4)
           AMP(K)=AAMP
           PERIOD(K)=APER
30         PHASE(K)=APHASE
         LL=0
         MM=M+ISTV
         DO 100 LL=ISTV,MM
            L=LL-ISTV+1
           T=FLOAT(LL)-1.0
           TIME=T/12.0-TLAG
           ETASTO=0.0
           DO 40 J=1,NH
           ETA(J)=AMP(J)*COS(2.0*3.1416*TIME/PERIOD(J)-PHASE(J)*0.01745)
40         ETASTO=ETASTO+ETA(J)
           IF(I.EQ.5) GO TO 90
           IF(I.EQ.4) GO TO 80
           IF(I.EQ.3) GO TO 70
           IF(I.EQ.2) GO TO 60
           ETA12(L)=ETASTO+AO
           GO TO 100
```

```
      ETA15(L)=ETASTO+A0
   60 GO TO 100
      ETA18(L)=ETASTO+A0
   70 GO TO 100
      ETA21(L)=ETASTO+A0
   80 GO TO 100
      ETA24(L)=ETASTO+A0
   90 CONTINUE
  100 CONTINUE
  110 RETURN
      END
```

```
      SUBROUTINE TIMES2(IP,NP,SR,SCALE,DATA,DIGIT,SR2,NP2,IV)
C     ********************************************************************
CC    *                                                                  *
CC    * THIS SUBROUTINE WILL PLOT THE TIME SERIES ARRAYS FOR 2 ARRAYS    *
CC    * 'DATA' & 'DIGIT'.THE SCALES OF THE PLOT ARE SET FROM THE ARRAY   *
CC    * 'DATA',SO THE RANGE OF DATA VALUES IN 'DIGIT' MUST BE FAIRLY     *
CC    * SIMMILAR TO THE RANGE OF VALUES IN DATA.                         *
CC    *    NP-THE NUMBER OF POINTS TO BE PLOTTED                         *
CC    *    IP-THE INITIAL POINT IN THE TIME SERIES TO BE PLOTTED         *
CC    *    SR-THE SAMPLE RATE FOR THE TIME SERIES                        *
CC    *    SCALE-THE HOURS PER INCH OF PLOT                              *
C     ********************************************************************
      DIMENSION DATA(1),DIGIT(1),X(1825),Y(1805),T(1805),TT(1825)
      TMAX=FLOAT(NP-1)/SR
      TPLOT=SCALE*18.0
      NPLOT=INT(TMAX/TPLOT)+1
      NPPP=INT(TPLOT*SR)
      LP=IP+NP-1
      LP2=IP+NP2-1
      NPPP2=INT(SCALE*18.0*SR2)
      IF(NPPP2.GT.1801) GO TO 900
      IF(NPPP.GT.1801) GO TO 900
      XMAX=NPLOT*8.51
      CALL PLOTS(XMAX,21.,0,1.0,,0.)
C
CCC   FROM HERE TO STMT 300, WE SCALE THE ARRAY 'DATA' TO FIND
CCC   STARTV AND SCLVAL.
C
      DMAX=DATA(IP)
      DMIN=DATA(IP)
      DO 100 I=IP,LP
      DUM=DATA(I)
      IF(DUM.LT.DMIN) DMIN=DUM
      IF(DUM.GT.DMAX) DMAX=DUM
  100 CONTINUE
      SCLVAL=(DMAX-DMIN)/6.0
      DUM=1.0E-03
  150 IF(SCLVAL.LE.DUM) GO TO 200
      DUM=DUM*10.0
      GO TO 150
  200 SCLVAL=SCLVAL/DUM
      IF(SCLVAL.LE.0.2) SCLVAL=0.2
      IF(SCLVAL.LE.0.2) GO TO 250
      IF(SCLVAL.LE.0.4) SCLVAL=0.4
      IF(SCLVAL.LE.0.4) GO TO 250
      IF(SCLVAL.LE.0.5) SCLVAL=0.5
      IF(SCLVAL.LE.0.5) GO TO 250
```

```
      IF(SCLVAL.LE.0.8) SCLVAL=0.8
      IF(SCLVAL.LE.0.8) GO TO 250
      SCLVAL=1.0
  250 SCLVAL=SCLVAL*DUM
      STARTV=INT(DMIN/SCLVAL)*SCLVAL
      IF(DMIN.LT.0.0) STARTV=STARTV-SCLVAL
      DUM2=STARTV+6.0*SCLVAL
      IF(DUM2.GE.DMAX) GO TO 300
      SCLVAL=SCLVAL/DUM
      IF(SCLVAL.LE.0.2) GO TO 260
      IF(SCLVAL.LE.0.4) GO TO 262
      IF(SCLVAL.LE.0.5) GO TO 264
       F(SCLVAL.LE.0.8) GO TO 266
      CLVAL=0.2
      )UM=DUM*10.0
      GO TO 250
  260 SCLVAL=0.4
      GO TO 250
  262 SCLVAL=0.5
      GO TO 250
  264 SCLVAL=0.8
      GO TO 250
  266 SCLVAL=1.0
      GO TO 250
  300 CONTINUE
C
CCC   FROM HERE TO STMT 500 THE AXIES ARE DRAWN.
C
      CALL LINEWT(-1)
      DO 500 I=1,NPLOT
      ST=TPLOT*(I-1)
      XL=I*8.5
      CALL PLOT(XL,0.0,3)
      CALL PLOT(XL,21.,2.2)
      XL=XL-1.25
      YL=2.0
      CALL AXIS(XL,YL,'TIME-HOURS',-10,18.01,90.,ST,SCALE,20.)
      CALL AXIS(XL,YL,'TIDAL ELEVATION-METERS',22,6.01,190.,STARTV,
     $SCLVAL,20.)
  500 CONTINUE
C
CCC   FROM HERE TO STMT 600 ALL THE TIME SERIES ARE DRAWN.
C
      CALL PLOT(7.25,2.0,-3)
      K=IP
      JJ=0
      KK=IV
      MM=0
```

04 JULY 1979 LISTING OF HYDRODYNAMIC MODEL OF PINE IS. SOUND

```
      DO 600 I=1,NPLOT
      ST=TPLOT*(I-1)
      L=1
  450 X(L)=-DIGIT(KK)
      TT(L)=FLOAT(MM)/SR2-ST
      L=L+1
      KK=KK+1
      MM=MM+1
      IF(L.GT.NPPP2) GO TO 460
      IF(KK.GT.LP2) GO TO 460
      GO TO 450
  460 X(L)=-STARTV
      TT(L)=0.0
      L=L+1
      X(L)=SCLVAL
      TT(L)=SCALE
      L=L-2
      CALL LINE(X,TT,L,1,12,2)
      J=1
  550 Y(J)=-DATA(K)
      T(J)=FLOAT(JJ)/SR-ST
      J=J+1
      K=K+1
      JJ=JJ+1
      IF(J.GT.NPPP) GO TO 560
      IF(K.GT.LP) GO TO 560
      GO TO 550
  560 Y(J)=-STARTV
      T(J)=0.0
      J=J+1
      Y(J)=SCLVAL
      T(J)=SCALE
      J=J-2
      CALL LINE(Y,T,J,1,12,1)
      LWT=3
      DO 580 IL=1,24
      XL=-0.25*IL
      CALL PLOT(XL,0.0,3)
      CALL PLOT(XL,18.0,2,LWT)
      IF(LWT.EQ.3) LWT=-1
  580 LWT=LWT+2
      LWT=3
      DO 590 IL=1,72
      YL=0.25*IL
      CALL PLOT(0.0,YL,3)
      CALL PLOT(-6.0,YL,2,LWT)
      IF(LWT.EQ.3) LWT=-1
  590 LWT=LWT+2
```

04 JULY 1979 LISTING OF HYDRODYNAMIC MODEL OF FIVE IS. SOUND

```
      IF(ILT.NPLOT) CALL PLOT(8.5,0.0,-3)
  600 CONTINUE
      CALL PLOT(0.,0.,999)
      GO TO 999
  900 WRITE(6,901)
  901 FORMAT(' THE SCALE FACTOR IS TOO LARGE')
  999 CONTINUE
      RETURN
      END
```

APPENDIX B
Con't

*****the following are the two data subroutines called 'hamall' & capdat' the hydrodynamic models needs the data contained in these subroutines to model Pine Island Sound*****

```
/ladoad capdat
DAPDAT     FETCHED
/1
0000      1945.10 5417.72     1.00          0.0          0.00          0.010
0001      1864.90 5283.93     1.14          0.0          0.0           0.010
0002      2446.40 6885.63     1.27          0.0          0.0           0.010
0003      2606.80 7818.11     1.23          0.0          0.0           0.010
0004      3308.70 7841.15     1.63          0.0          0.0           0.010
0005      2687.10 7896.99     1.20          0.0          0.0           0.010
0006      3088.10 7721.25     0.90          0.0          0.0           0.010
0007      3048.00 7180.12     0.75          0.0          0.0           0.010
0008      2707.10 6180.78     1.10          0.0          0.0           0.010
0009      2065.2   3512.01    1.65         0.50         0.50          0.05   0.25
0010      3000.0     75.0     2.5          0.50         0.50          0.05   0.30
0011       540.0    220.0     5.34         0.50         0.50          0.05   0.30
0012      1350.0    625.0     4.72         0.50         0.50          0.05   0.30
0013      1824.6   5499.84    1.29         0.50         0.50          0.05   0.20
0014       72.0 300.0
```

APPENDIX B
Con't

***** the following are the two data subroutines called 'hamall' & 'capdat' the hydrodynamic models needs the data contained in these subroutines to model Pine Island Sound *****

```
/1 harmall
0000 8351      0.2398      -0.25
0001 0.1965    12.421      248.8228
0002 0.1626    12.000      283.8420
0003 0.2816    12.658      138.1712
0004 0.0653    23.934      178.6380
0005 0.0768    25.819      329.3757
0006 0.0629    24.066       57.4832
0007 0.1005    11.967      155.1988
0008 0.2775    12.626      355.9224
0009 0.0106    24.833      110.1599
0010 0.0096    23.099      339.0046
0011 0.0172    26.868      214.5224
0012 0.0122    12.191      257.4768
0013 0.0470   219.191       84.3383
0014 0.0419   327.869      323.7251
0015 0.0282   354.365      109.7659
0016 0.0209   661.230       44.3093
0017 3252      0.1756      -0.05
0018 0.1869    12.421       77.8219
0019 0.1001    12.000       99.6483
0020 0.0299    12.658      194.7250
0021 0.0528    23.934      185.8221
0022 0.1079    25.819      115.1912
0023 0.0601    24.066      132.1366
0024 0.1351    11.967      342.0671
0025 0.0157    12.626      145.0242
0026 0.0082    24.833      248.4851
0027 0.0088    23.099      238.9296
0028 0.0298    26.868      221.5013
0029 0.0461    12.191      140.3845
0030 0.0539   219.191       62.4574
0031 0.0578   327.869       81.6405
0032 0.0690   354.365      225.0921
0033 0.0161   661.230      193.1122
0034 3252      0.1756        0.45
0035 0.1869    12.421       77.8219
0036 0.1001    12.000       99.6483
0037 0.0299    12.658      194.7250
0038 0.0528    23.934      185.8221
0039 0.1079    25.819      115.1912
0040 0.0601    24.066      132.1366
0041 0.1351    11.967      342.0671
0042 0.0157    12.626      145.0242
0043 0.0082    24.833      248.4851
0044 0.0088    23.099      238.9296
0045 0.0298    26.868      221.5013
0046 0.0461    12.191      140.3845
0047 0.0539   219.191       62.4574
0048 0.0578   327.869       81.6405
0049 0.0690   354.365      225.0921
0050 0.0161   661.23       193.1122
0051 3252      0.1756        0.95
0052 0.1869    12.421       77.8219
0053 0.1001    12.000       99.6483
0054 0.0299    12.658      194.7250
0055 0.0528    23.934      185.8221
0056 0.1079    25.819      115.1912
0057 0.0601    24.066      132.1366
0058 0.1351    11.967      342.0671
0059 0.0157    12.626      145.0242
0060 0.0082    24.833      248.4851
0061 0.0088    23.099      238.9296
0062 0.0298    26.868      221.5013
0063 0.0461    12.191      140.3845
0064 0.0539   219.191       62.4574
0065 0.0578   327.869       81.6405
0066 0.0690   354.365      225.0921
0067 0.0161   661.230      193.1122
0068 3239      0.2369        0.15
0069 0.1156    12.421       98.5081
0070 0.0811    12.000       45.3995
0071 0.0573    12.685      288.5349
0072 0.0861    23.934      236.0377
0073 0.0820    25.819      125.0145
0074 0.0838    24.066      108.6996
0075 0.0441    11.967      268.5476
0076 0.0745    12.626      157.4006
0077 0.0086    24.833      295.8311
0078 0.0018    23.099       33.4601
0079 0.0157    26.868      219.2867
0080 0.0125    12.191      132.3917
0081 0.0553   219.191       64.0319
0082 0.0616   327.869      126.8128
0083 0.0598   354.365      267.9661
0084 0.0199   661.230      221.7917
0085 ****** the following are the two data sub-
0086         routines called 'hamall' & 'capdat' the
0087         hydrodynamic model needs the data con-
             tained in these subroutines to model
             Pine Island Sound ******
```

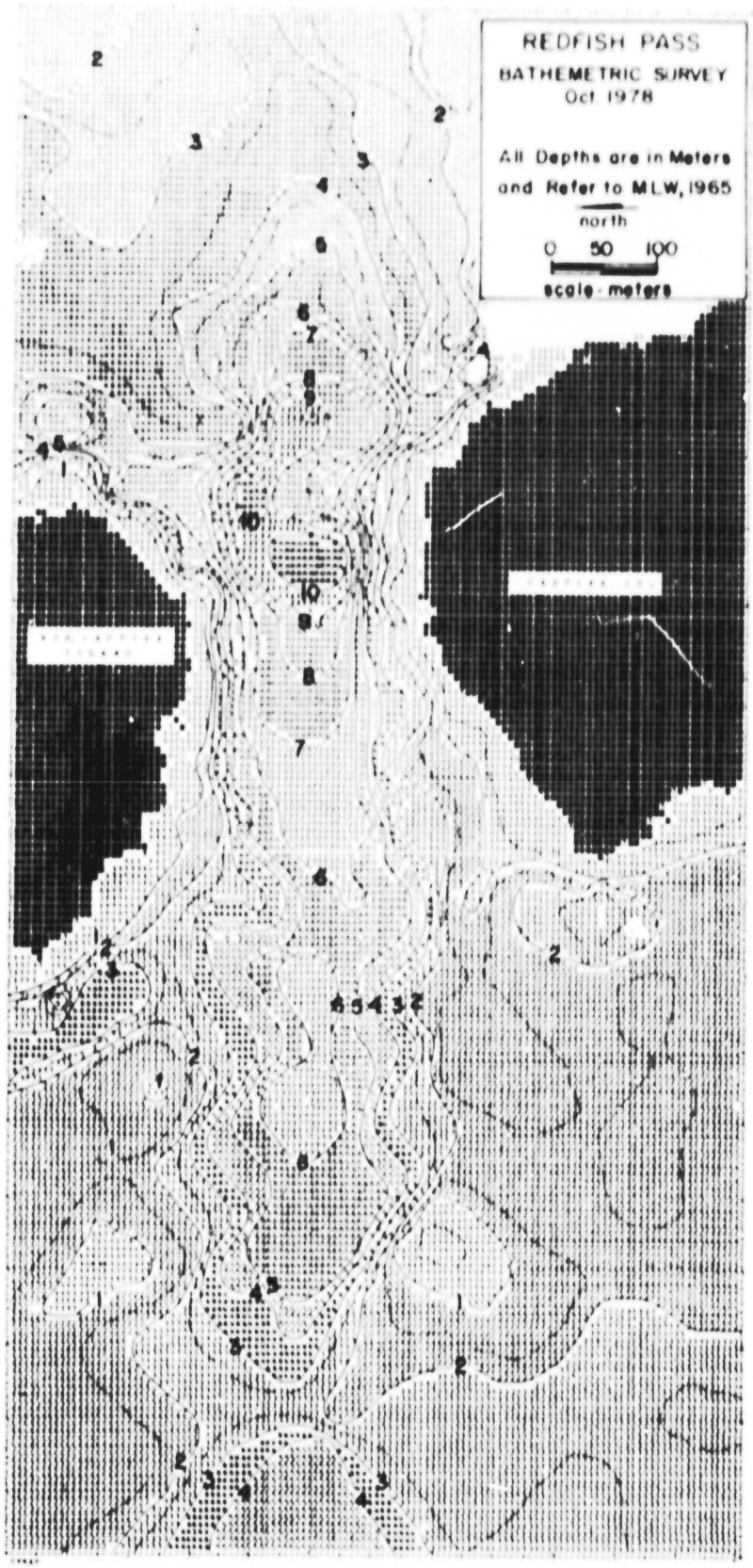

Appendix Figure C.1 SYMAP Two-Dimensional Map of Redfish Pass Bathymetry.

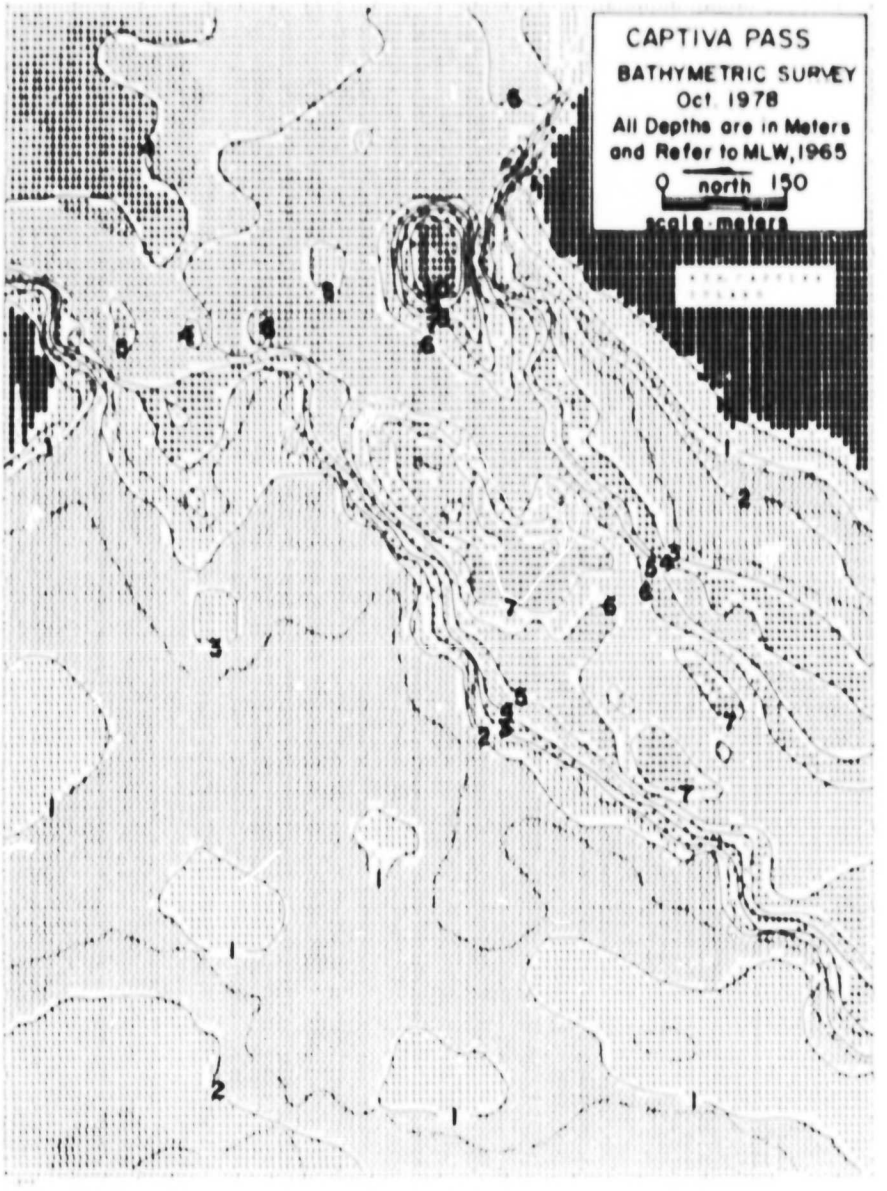

Appendix Figure C.2 SYMAP Two-Dimensional Map of Captiva Pass Bathymetry.

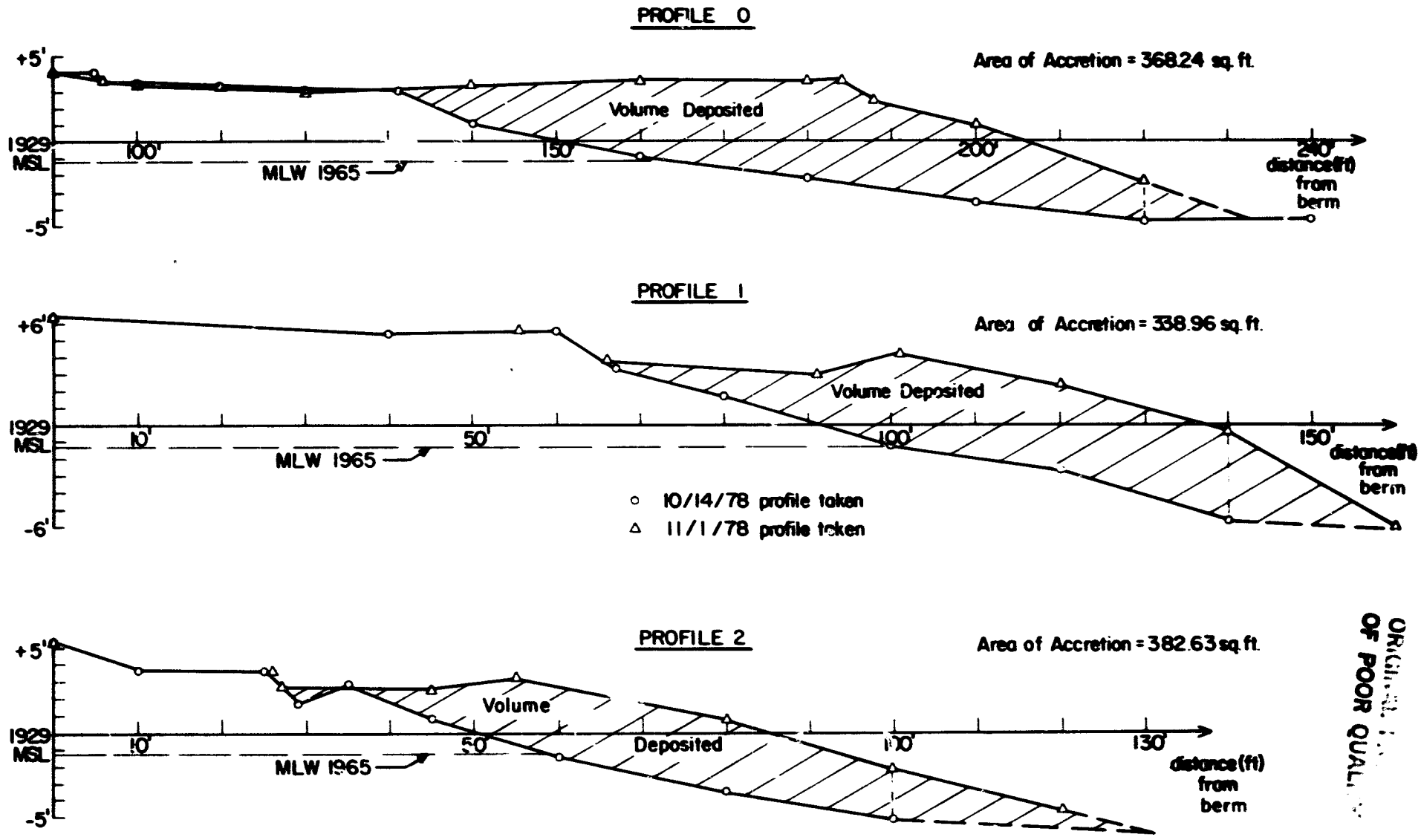

Appendix Figure D. Beach Profiles along the Southern End of Captiva Island.

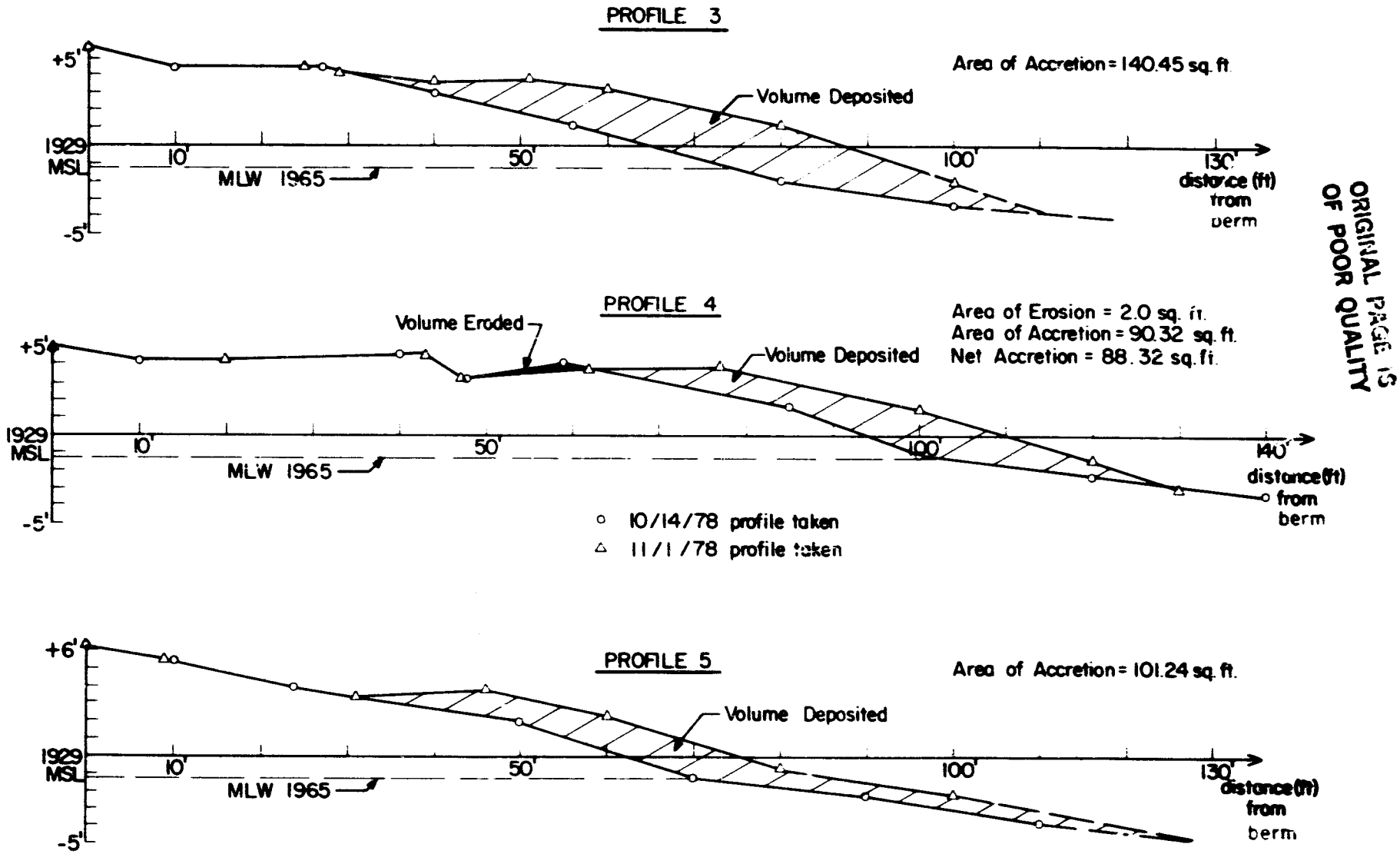

Appendix Figure D. continued

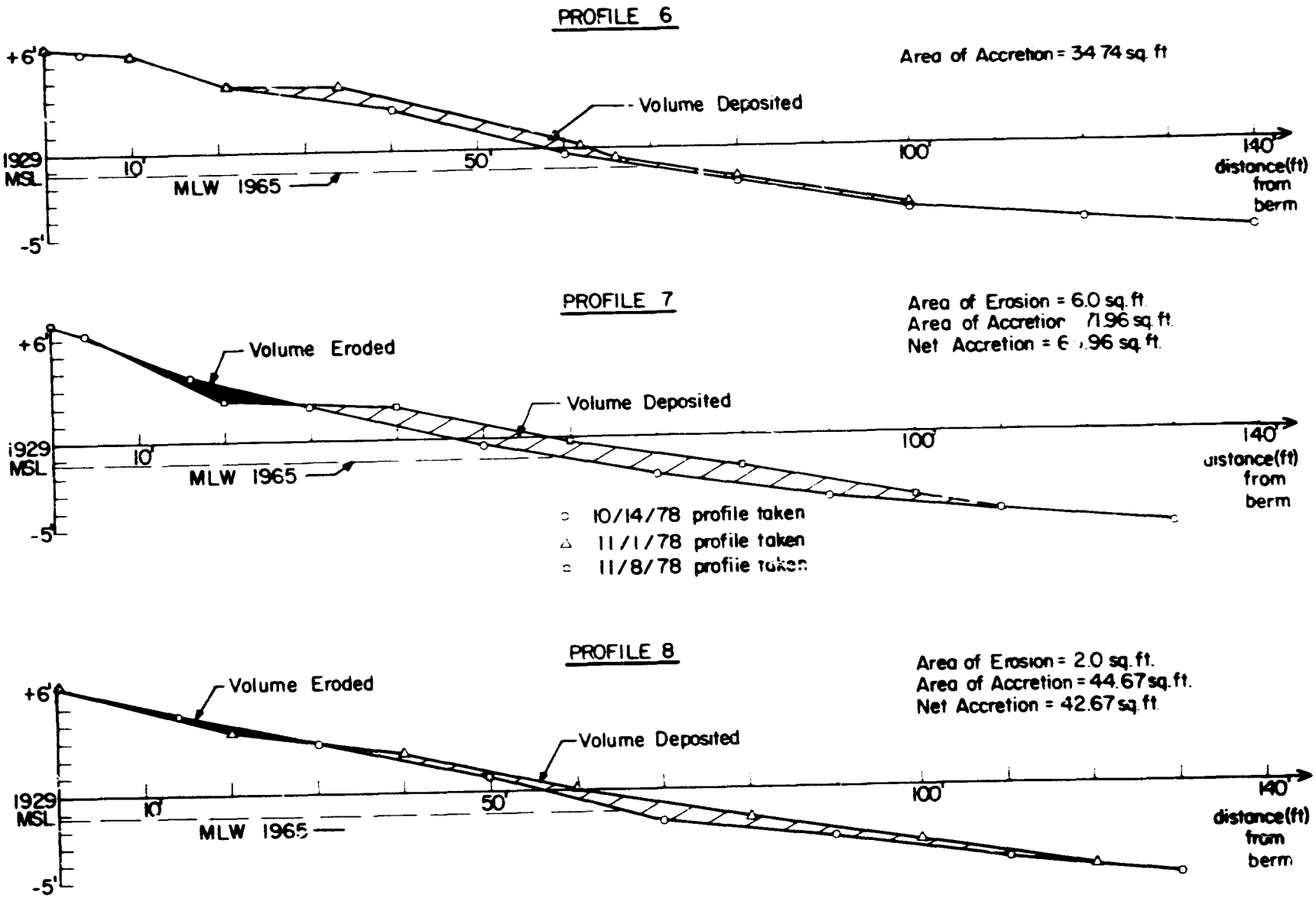

Appendix Figure D. continued

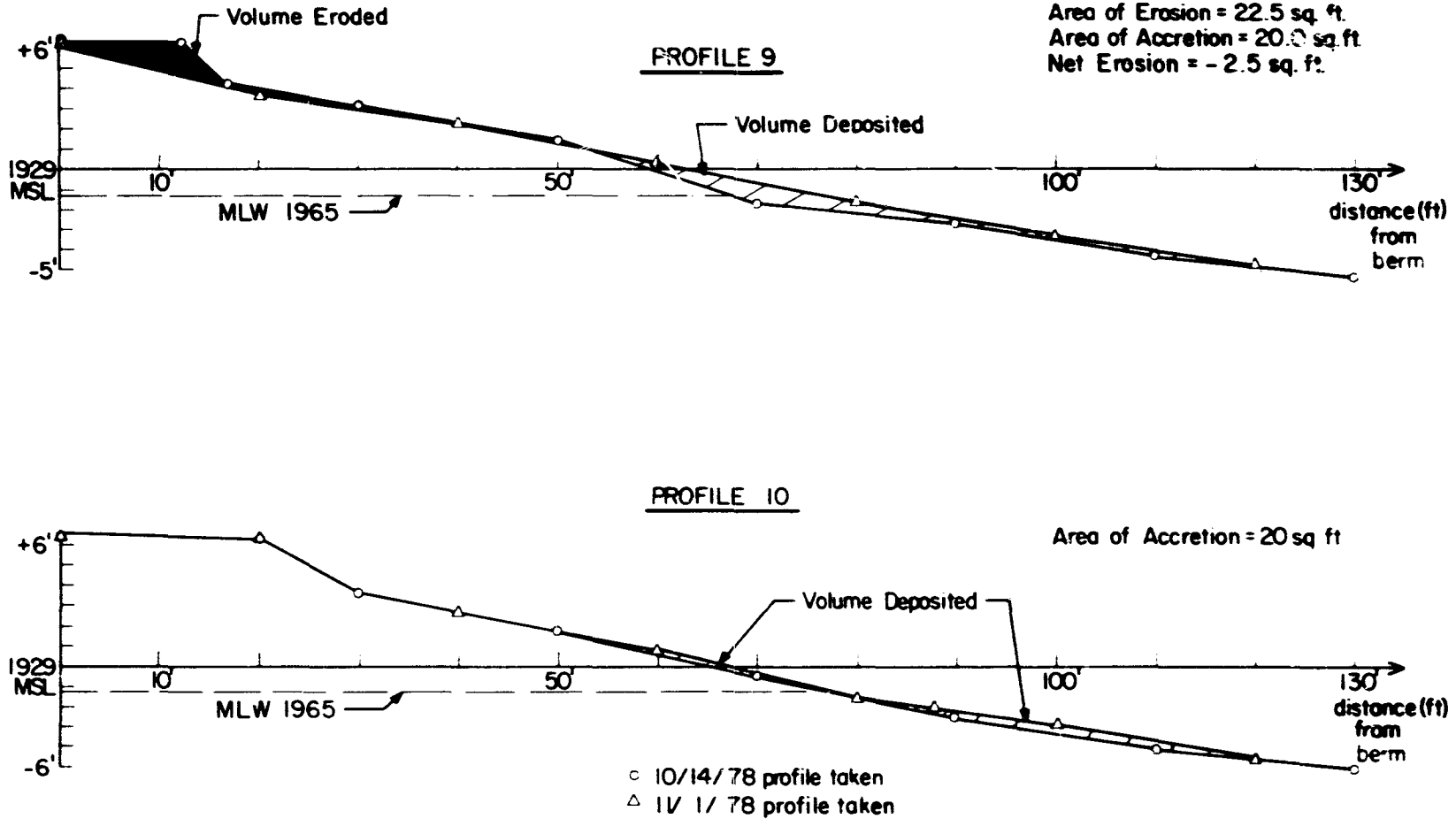

Appendix Figure D. continued

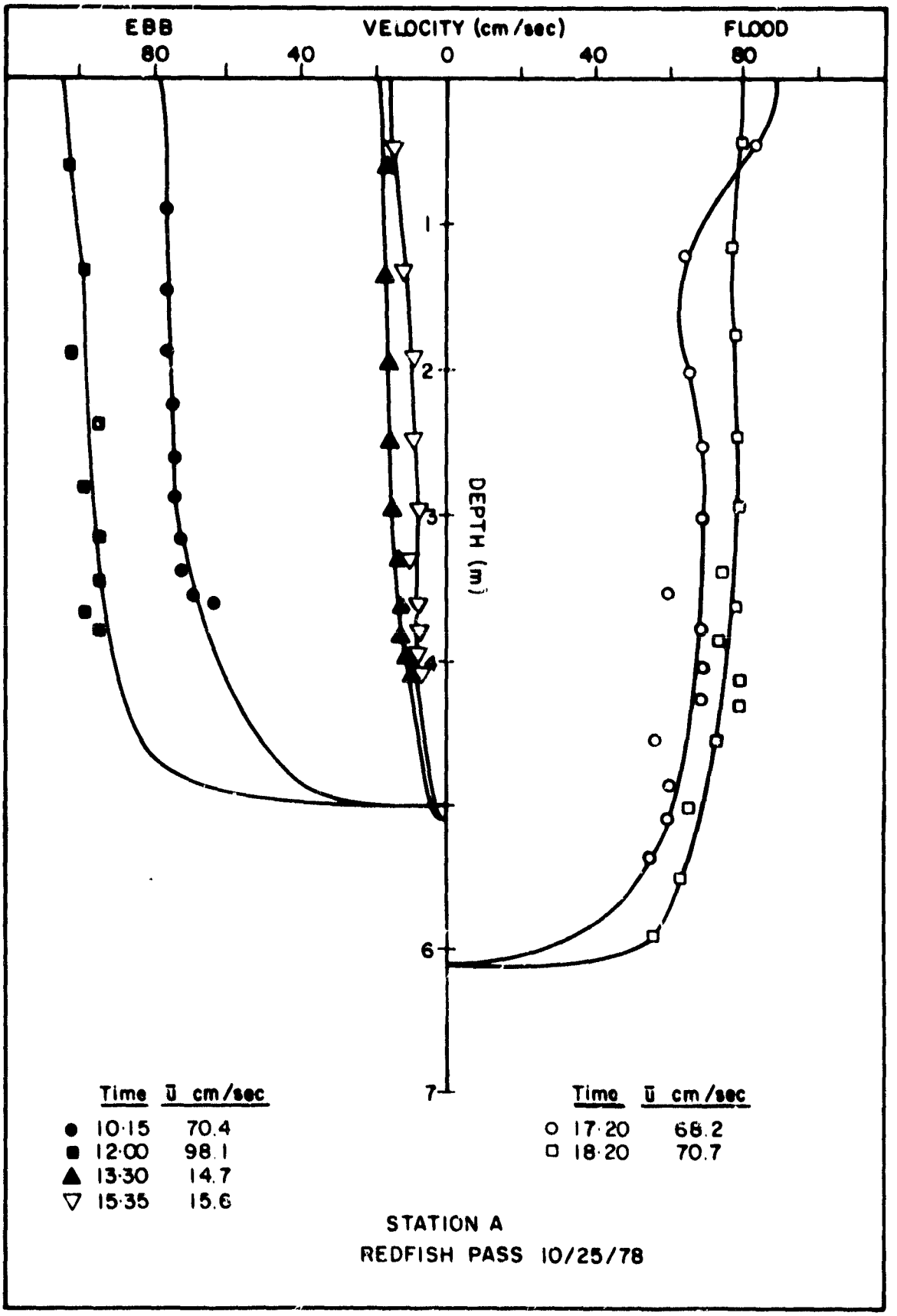

Appendix Figure E.1 Vertical Velocity Distribution for the Neap Tidal Condition at Station A, Redfish Pass, October 25, 1978.

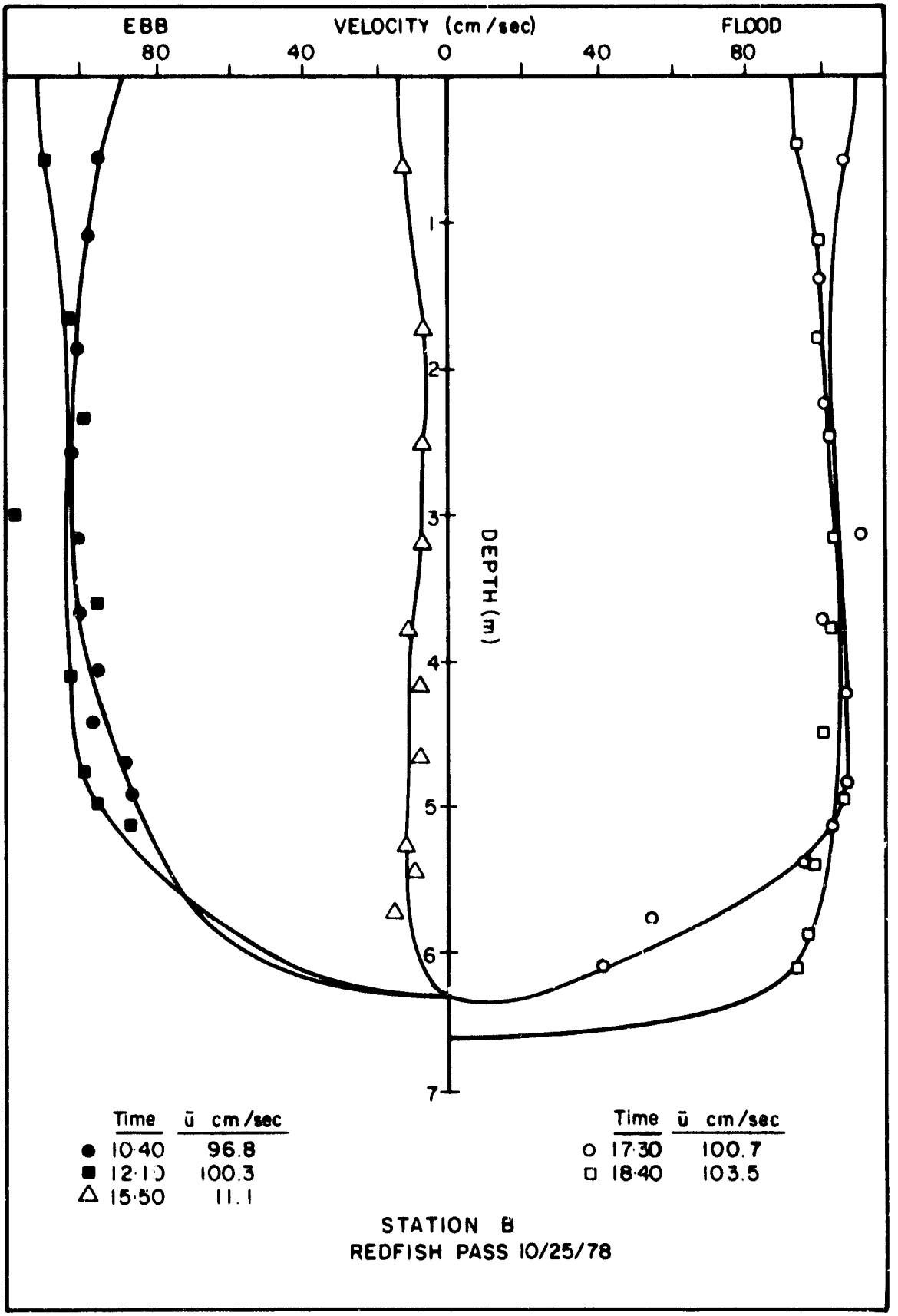

Appendix Figure E.2 Vertical Velocity Distribution for the Neap Tidal Condition at Station B, Redfish Pass, October 25, 1978.

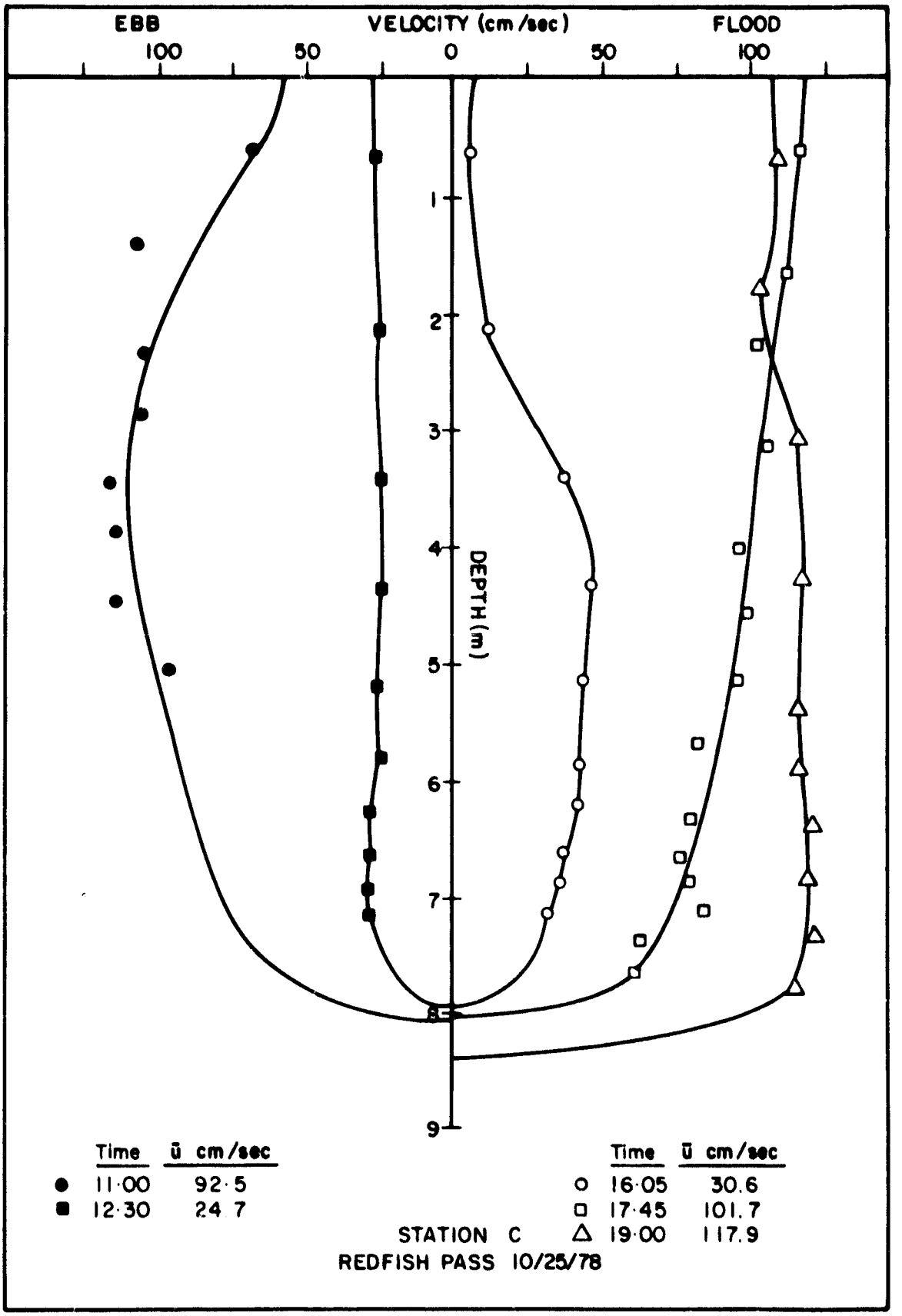

Appendix Figure E.3 Vertical Velocity Distribution for the Neap Tidal Condition at Station C, Redfish Pass, October 25, 1978

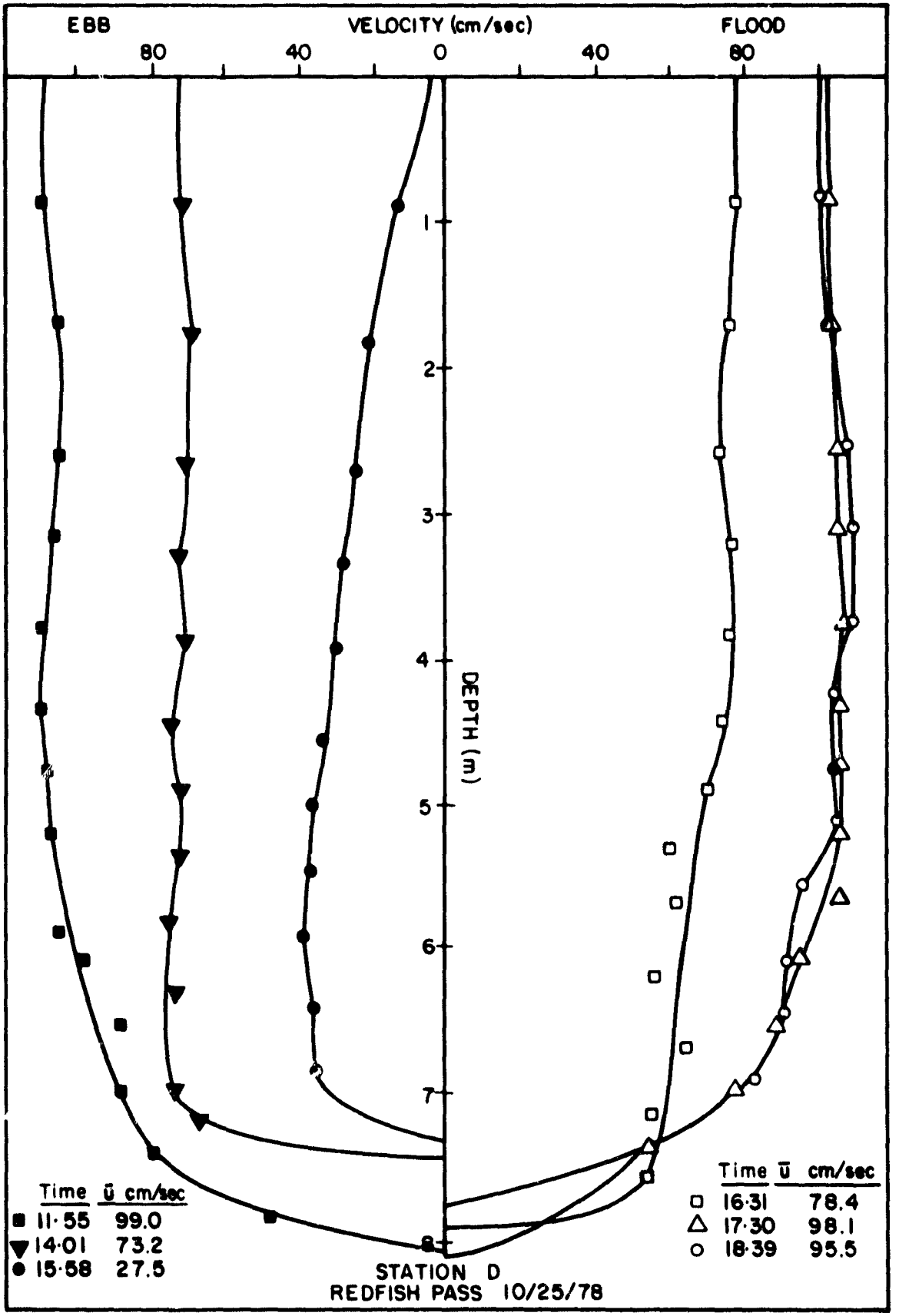

Appendix Figure E.4 Vertical Velocity Distribution for the Neap Tidal Condition at Station D, Redfish Pass, October 25, 1978.

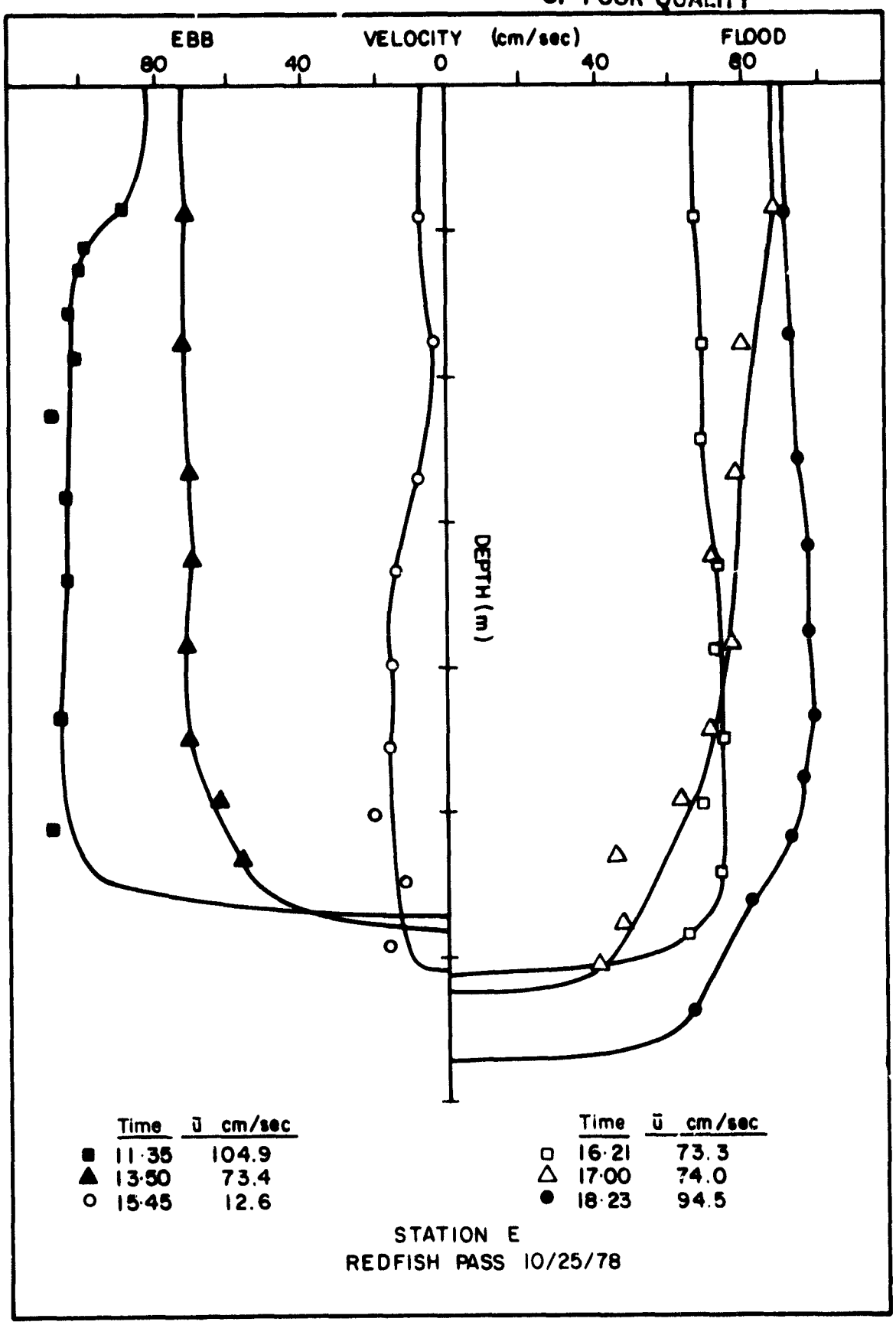

Appendix Figure E.5 Vertical Velocity Distribution for the Neap Tidal Condition at Station E, Redfish Pass, October 25, 1978.

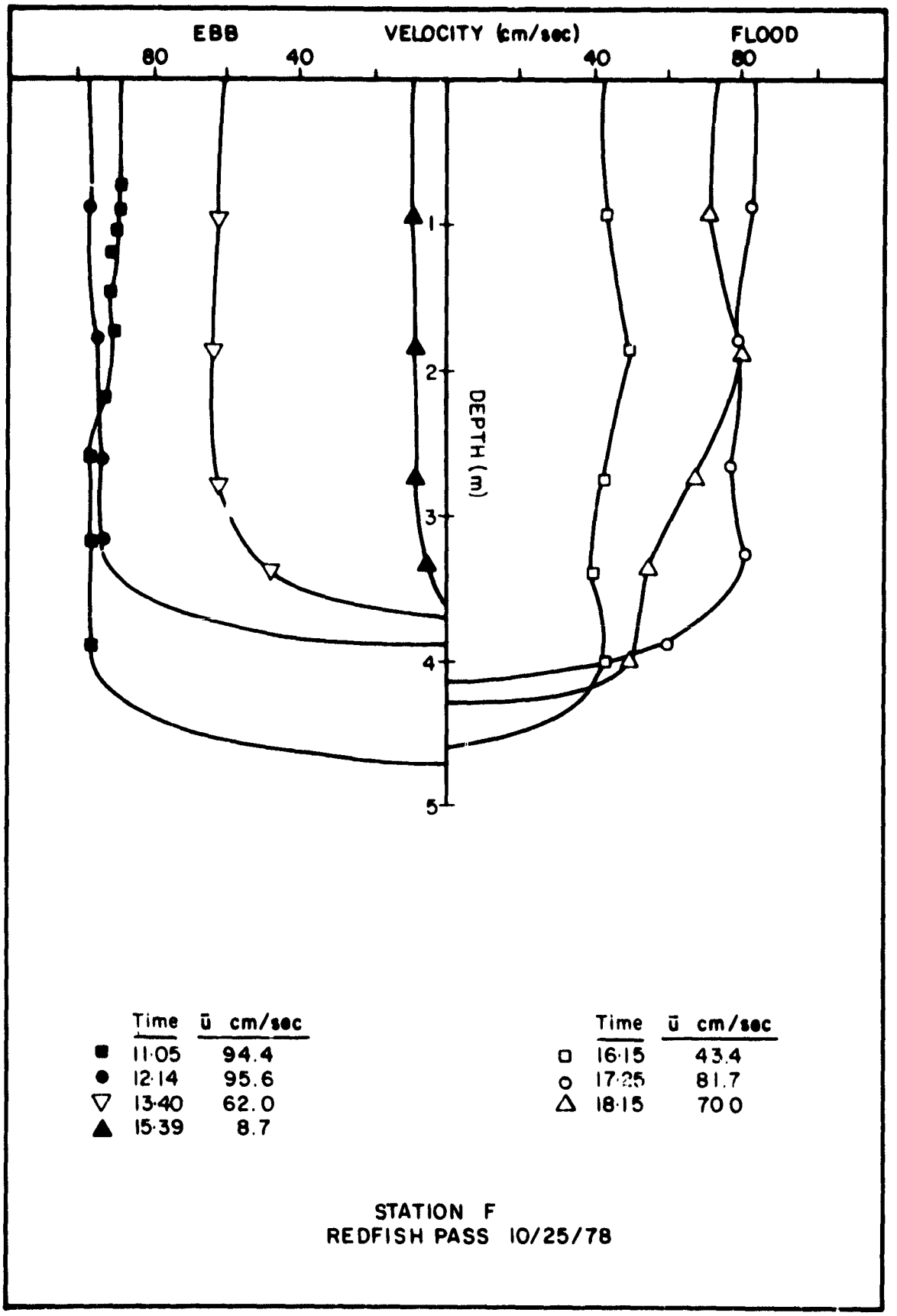

Appendix Figure E.6 Vertical Velocity Distribution for the Neap Tidal Condition at Station F, Redfish Pass, October 25, 1978.

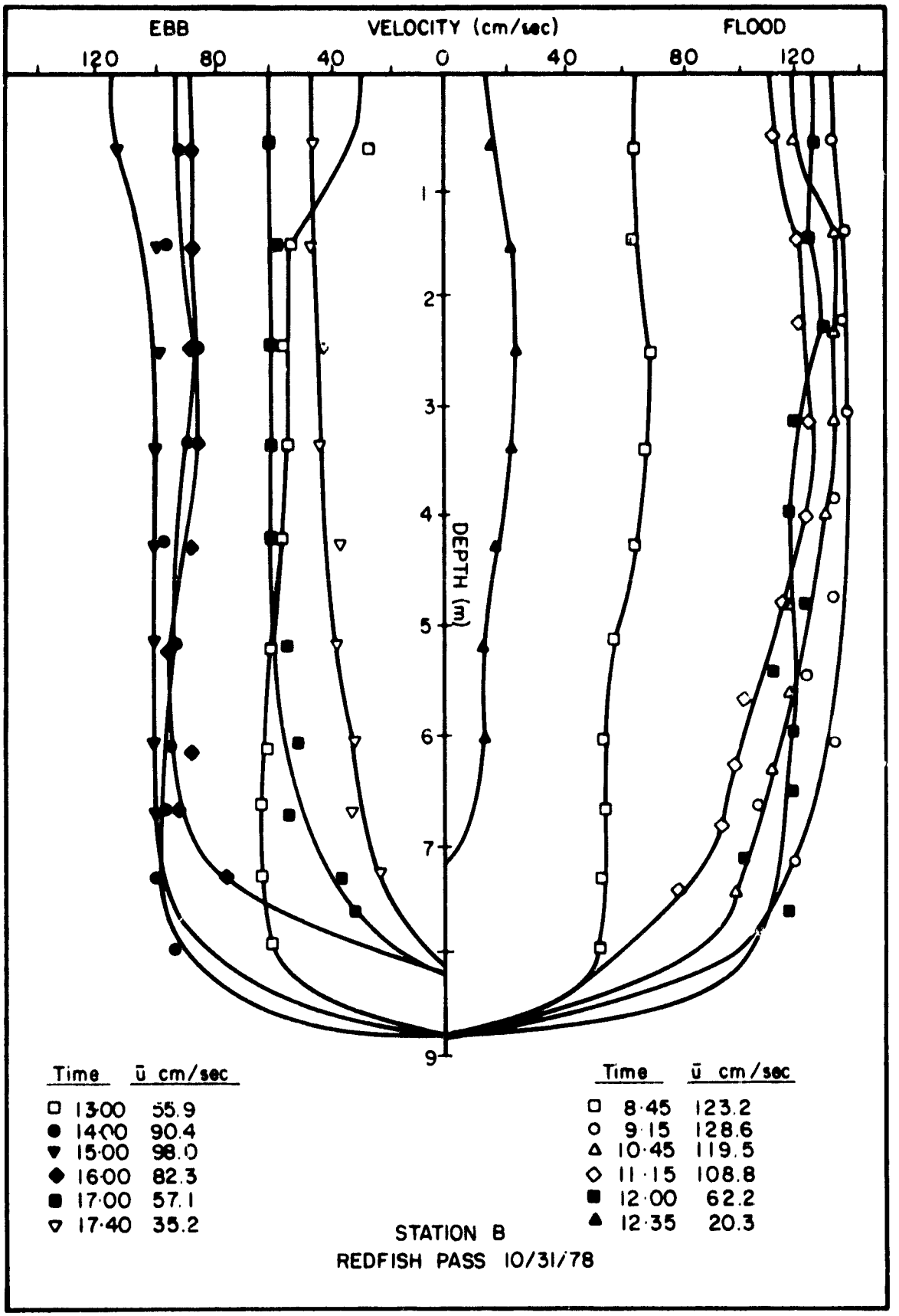

Appendix Figure E.7 Vertical Velocity Distribution for the Spring Tidal Condition at Station B, Redfish Pass, October 31, 1978.

ORIGINAL PAGE 13
OF POOR QUALITY

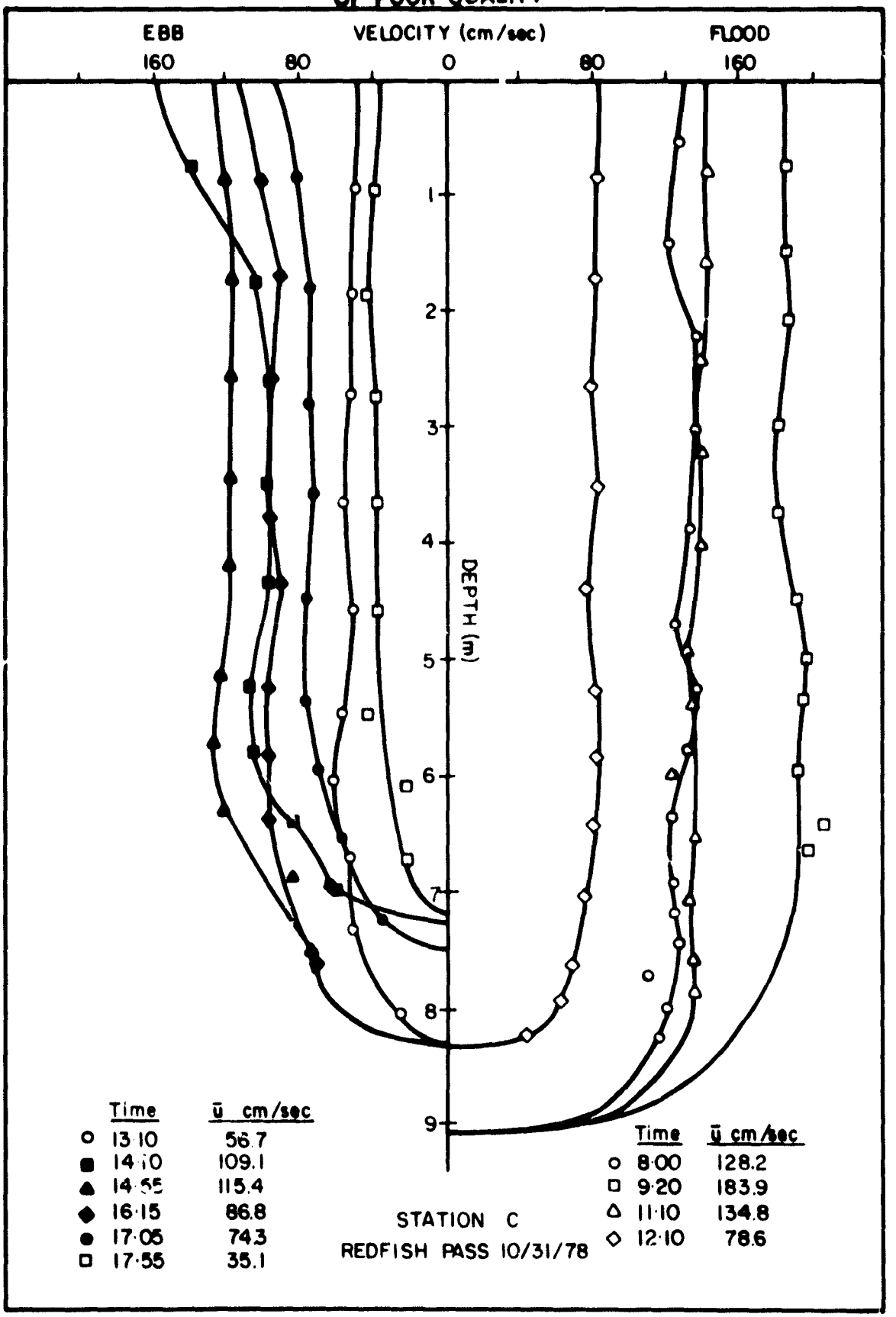

Appendix Figure E.8 Vertical Velocity Distribution for the Spring Tidal Condition at Station C, Redfish Pass, October 31, 1978.

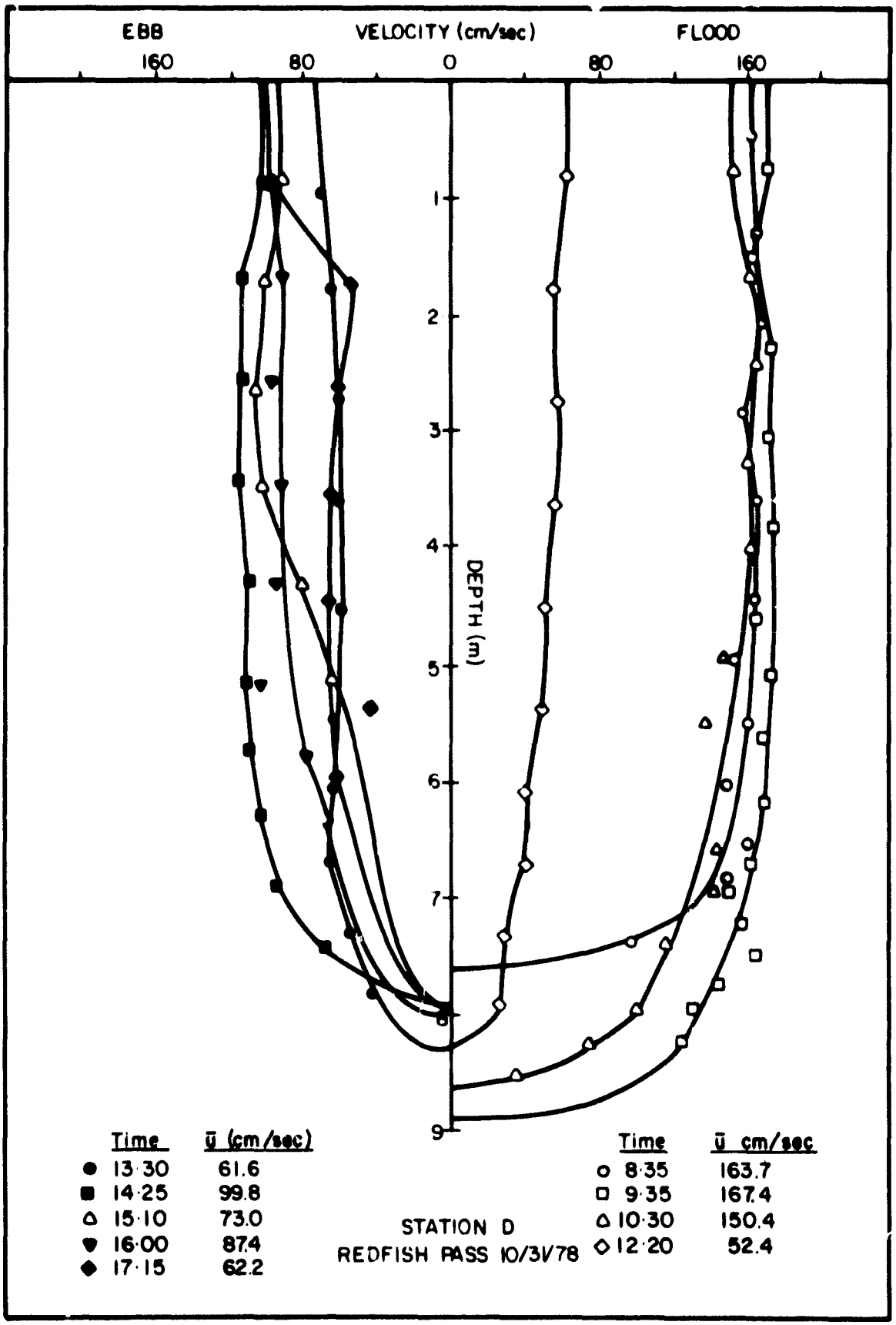

Appendix Figure E.9 Vertical Velocity Distribution for the Spring Tidal Condition at Station D, Redfish Pass, October 31, 1978.

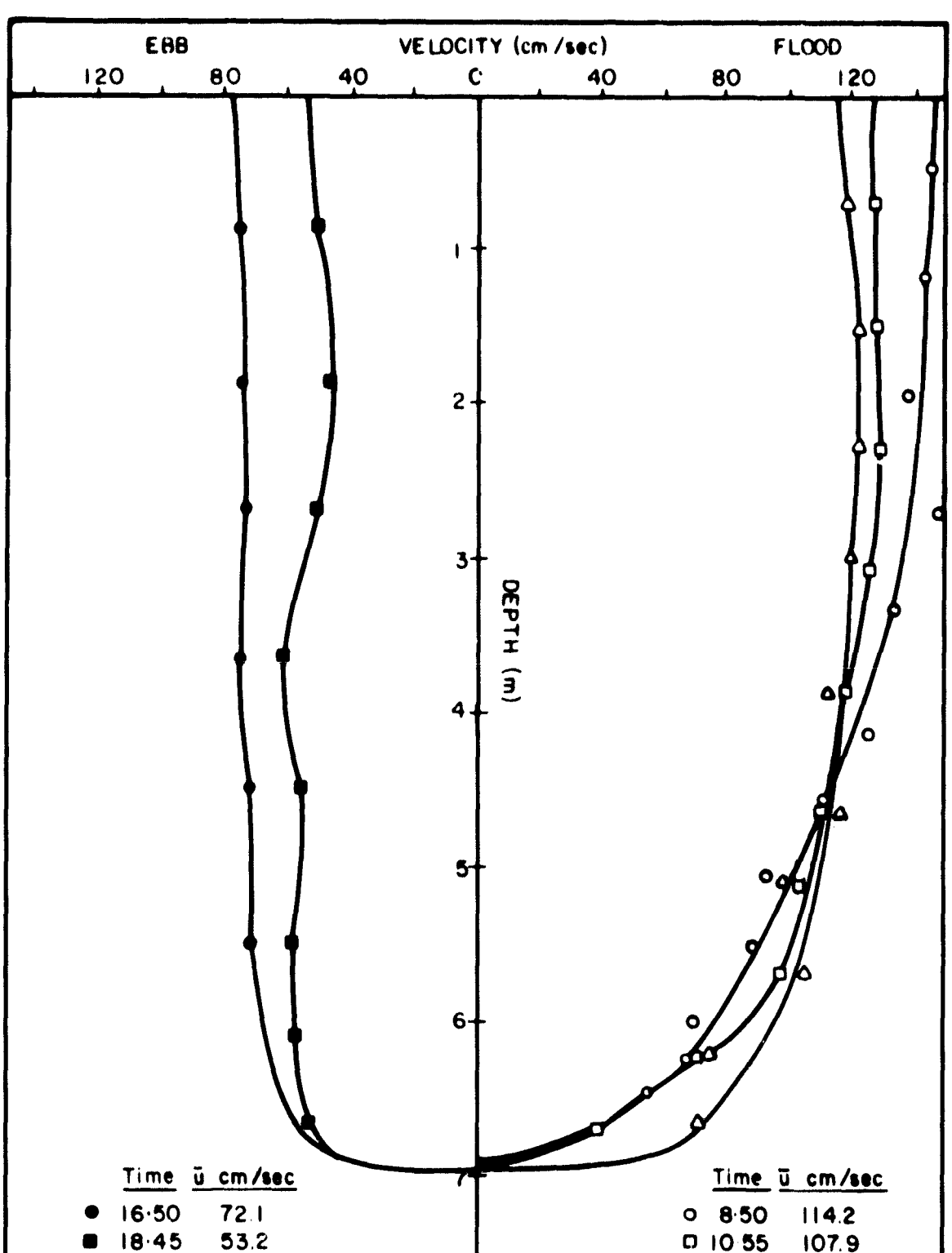

Appendix Figure E.10 Vertical Velocity Distribution for the Spring Tidal Condition at Station E, Redfish Pass, October 31, 1978.

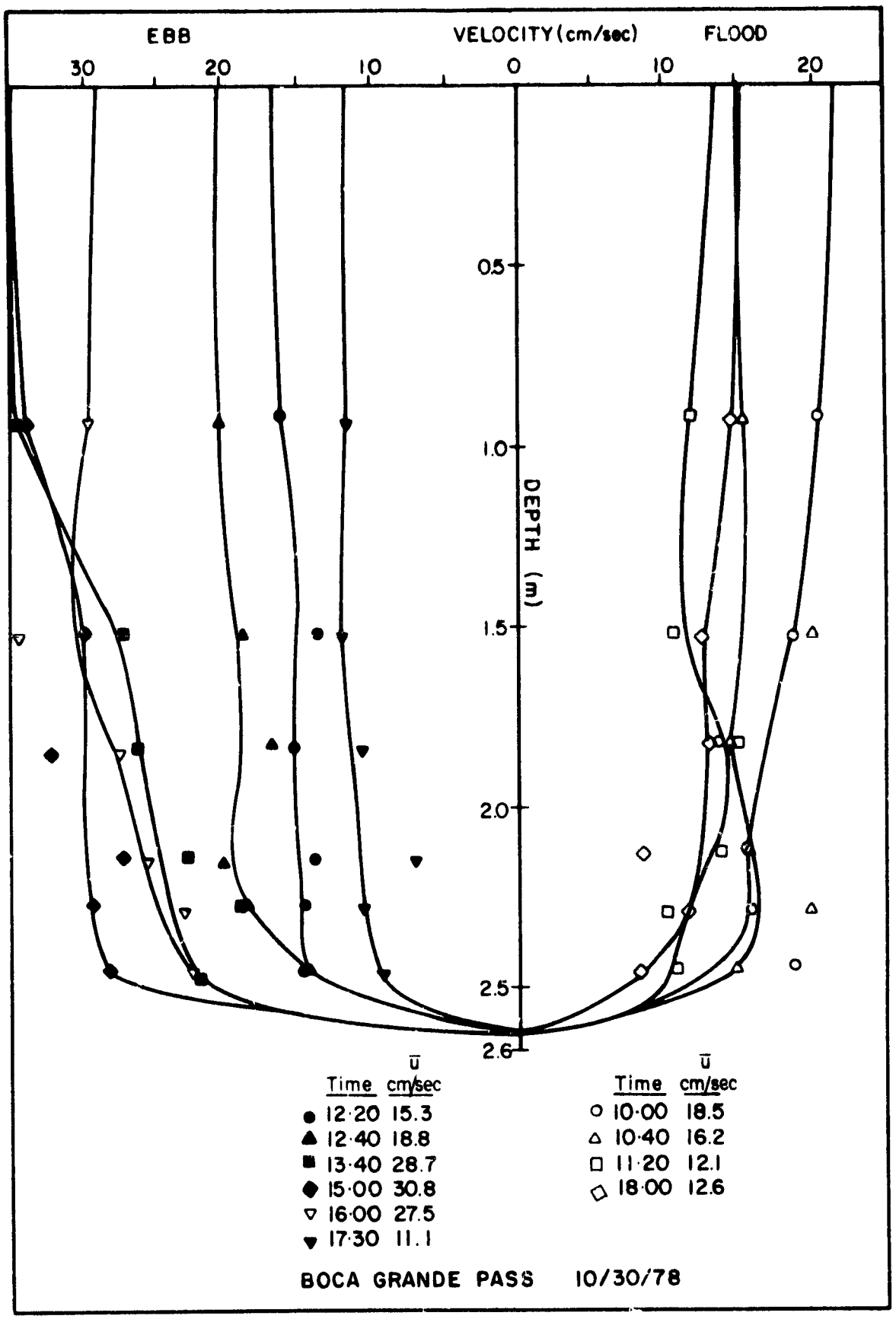

Appendix Figure E.11 Vertical Velocity Distribution for the Northern Model Boundary at Boca Grande Pass, October 30, 1978.

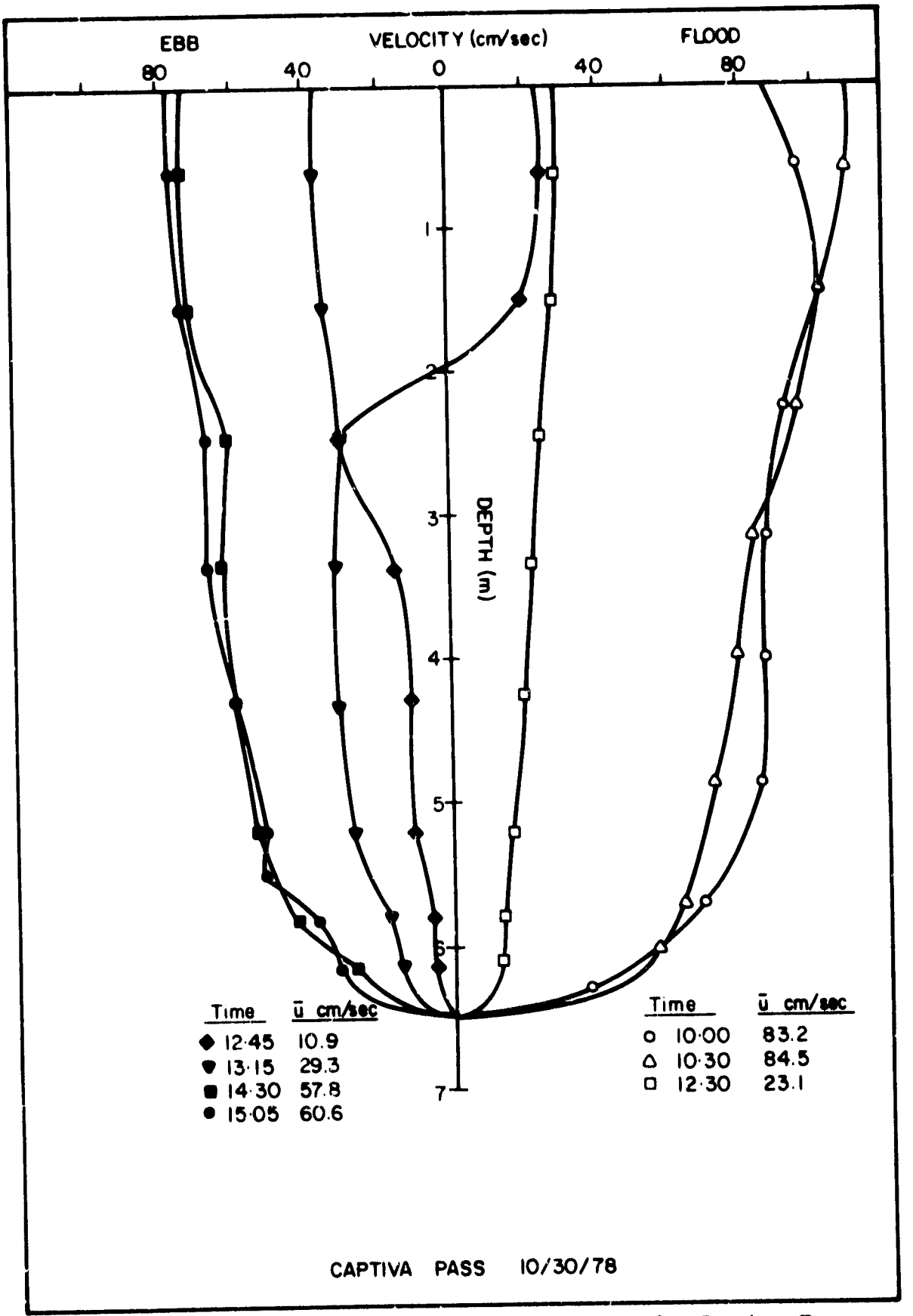

Appendix Figure E.12 Vertical Velocity Distribution for Captiva Pass, October 30, 1978.

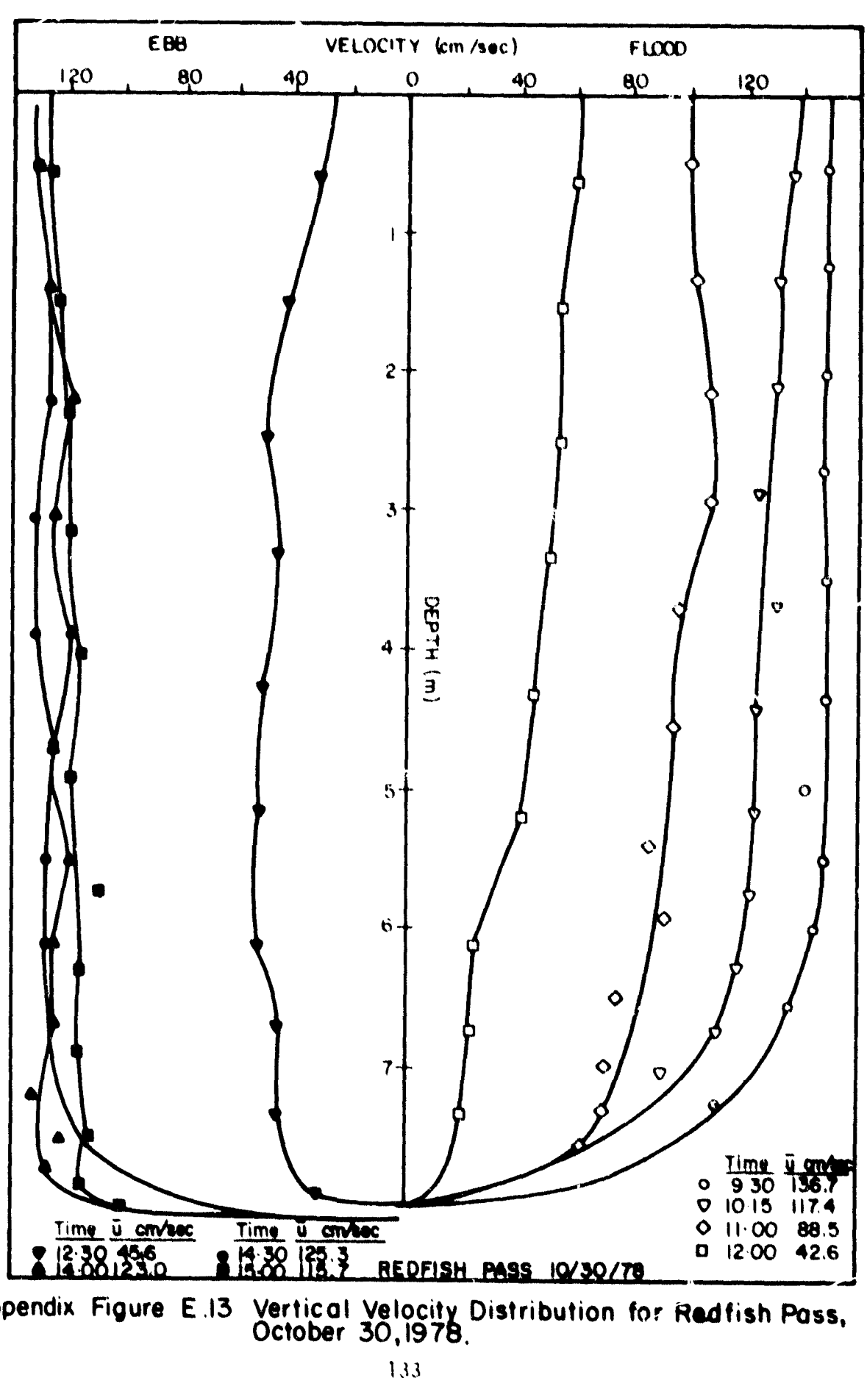

Appendix Figure E.13 Vertical Velocity Distribution for Redfish Pass, October 30, 1978.

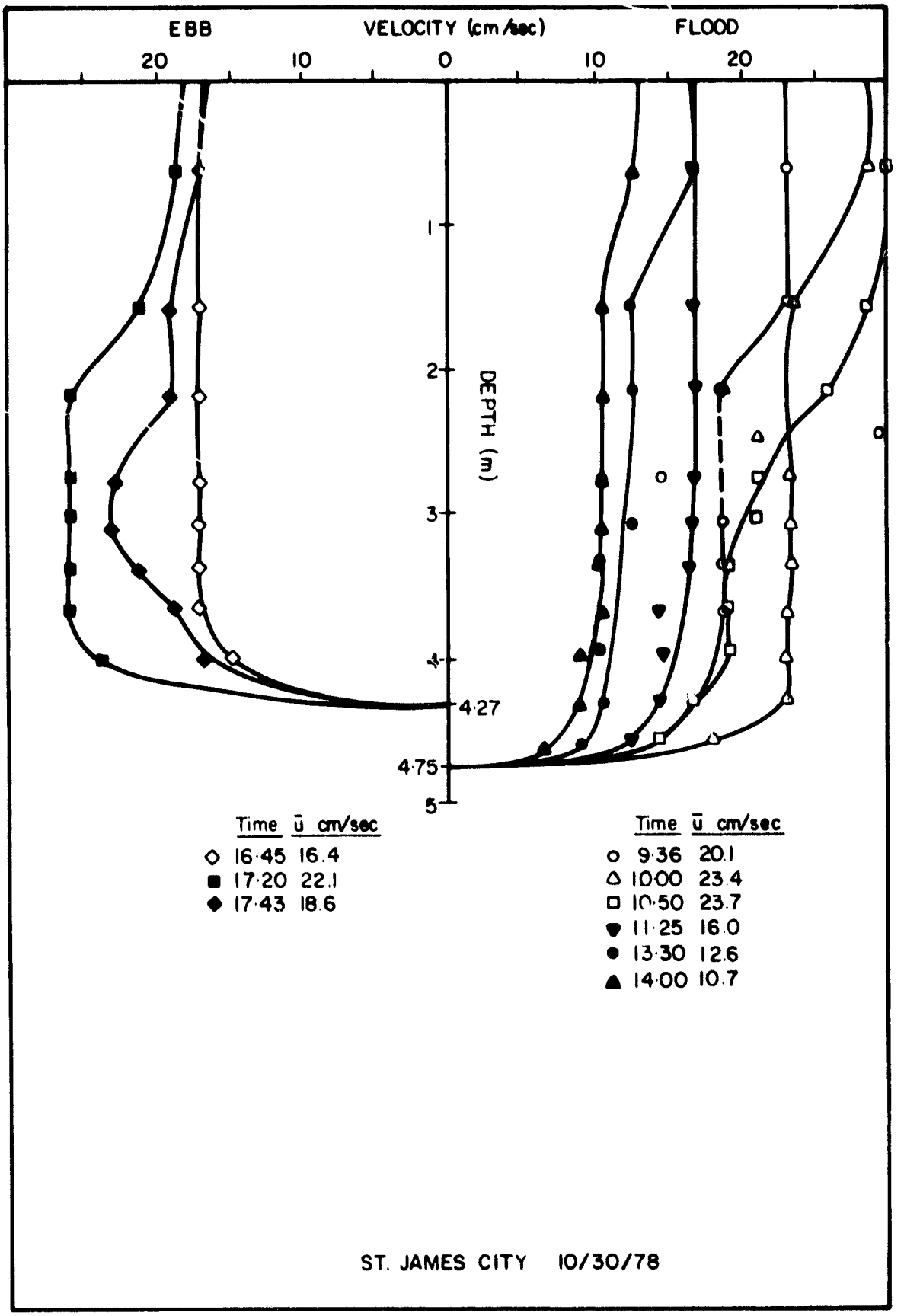

Appendix Figure E.14 Vertical Velocity Distribution for Southern Model Boundary at St. James City, October 30, 1978.